Precipitation Intensities For Design of Buried Municipal Stormwater Systems

by

Yi Wang

A Thesis
presented to
The University of Guelph

In partial fulfilment of requirements
for the degree of
Doctor of Philosophy
in
Engineering

Guelph, Ontario, Canada

ABSTRACT

Precipitation Intensities For Design of Buried Municipal Stormwater Systems

Yi Wang
University of Guelph, 2014

Advisor:
Professor Edward A. McBean

Extreme rainfall events are likely to be more frequent and intensive, as climate change occurs. For urban infrastructure, the design rainfall intensities may have changed, or involve considerable uncertainty in their characterization. Historical rainfall records for southern Ontario are analyzed to characterize design rainfall intensities, for purposes of determining rainfall intensities for use in municipal stormwater system design.

Using the L-moment diagram and the relative RMSE, the traditionally-used Gumbel distribution is confirmed as acceptable for modeling Annual Maximum Series (AMS) of rainfall records. However, the uncertainties involved in design rainfall intensities are commonly substantial, both in the Intensity–Duration–Frequency (IDF) curves provided by Environment Canada and in the estimates derived directly from historical records. The upper confidence limit of the design rainfall intensity expected value is demonstrated as an appropriate alternative to the use of the expected value in municipal stormwater system design, when the uncertainties involved are considerable.

A rainfall model using Partial Duration Series (PDS) is demonstrated to be suitable for events with recurrence intervals less than 10 years, compared to the model of AMS. The PDS model rainfall estimates are generally 2 to 5% greater than estimates from the AMS

model. To improve the design value estimates, partial duration series are analyzed using regional frequency analysis methods. For 10-year return storms, a 26% reduction in RMSE in the regional model was obtained, for the first time period (1960-1983), and a 35% decline for the second time period (1984-2007).

Following the splitting of rainfall records into two segments, all types of rainfall intensity models (AMS, PDS, and Regional) detect consistent changes in design rainfall intensities with statistical significance. Changes occur mostly in southern Ontario, along the coasts of Lake Erie and Lake Ontario from Windsor to Ottawa. Sensitivity analysis of changes identified with respect to the year of splitting suggests changes are occurring during the 1980s and 1990s; however, no consistent pattern is determined. At the end of this thesis, recommendations are summarized for assessment of the rainfall intensity estimates for stormwater system design.

ACKNOWLEDGEMENTS

Thanks to my supervisor Dr. Edward A. McBean for instructing and sponsoring my PhD study. Your confidence in me and my work is beyond unity — there are no type I errors.

Thanks to my committee members, Dr. O. Brian Allen, Dr. Andrea Bradford, and Dr. Juraj Cunderlik, for providing valuable feedback throughout this PhD program.

Thanks to my parents for bringing me into this world.

Table of Contents

List of Tables

List of Figures

Chapter 1

Introduction

1.1 Climate Change

1.1.1 Evidence of Global Warming

The IPCC fifth assessment report from work group I (IPCC WG1AR5) confirms that "warming in the climate system is unequivocal", with observational evidence of "warming of the atmosphere and the ocean, diminishing snow and ice, rising sea levels and increasing concentrations of greenhouse gases. Each of the last three decades has been successively warmer at the Earth's surface than any preceding decade since 1850." (IPCC, 2013)

Evidence of multi-decadal warming are listed in IPCC WG1AR5, such as an increase of about $0.72\,^{\circ}\mathrm{C}$ in the global mean surface temperature over the period of 1950-2012, and the increase of the maximum and minimum temperature over land since 1950. For average annual temperature in northern hemisphere, the period 1983-2012 was the warmest 30 years

in the last 800 years. The troposphere has globally warmed since the mid-20th century, and the upper ocean (above 700 m) has warmed from 1971 to 2010. (IPCC, 2013, TS 2.2)

1.1.2 Changes in Water Cycle and Total Rainfall

A water cycle describes the movement of water on, above, and below the surface of the Earth. Since the troposphere is getting warmer, and the saturated vapour pressure increases with temperature, the amount of water vapour in the atmosphere is expected to increase with climate warming. Therefore, as part of the water cycle, the precipitation process is suspected to change as well. Regional precipitation trends are reported in many studies, but when all land area is counted together, there is little change in the global mean land precipitation since 1900 (IPCC, 2013, TS TFE.1). The amount of precipitation is only a small fraction of total water vapour content of air, and the amount of heavy or extreme rainfall events is an even smaller fraction. As a consequence, the changes in heavy rainfall events show considerable spatial variability as well.

1.1.3 Evidence of Changes in Extremes

The IPCC WR1AR5 noted changes in daily precipitation extremes are occurring, with strong regional and sub-regional variations. Both increasing and decreasing trends are observed in precipitation extremes. Since the middle of the 20^{th} century, regional trends are occurring and varied between continents - increasing trends identified in North and South America, regional and seasonal variations found in Europe and Mediterranean, mixed re-

gional trends found in Asia and Oceania, and no significant trends found in Africa. Global assessment is currently not available for sub-daily trends of precipitation extremes; however, several regions have identified significant trends, and more increasing trends are discovered than decreasing trends. (IPCC, 2013, 2.6.2)

To clarify, the terms describing precipitation events in this study, "moderate extremes" or "heavy events" denote events with return periods of 5 or 10 years, and the "extremes" or "extreme events" denotes events with return periods of 25 years or longer.

1.2 Necessity of Assessing Design Rainfall Intensities

Changes in heavy rainfall events have impacts on urban stormwater systems. If increasing trends are predicted in the future, when heavy rainfall events will occur with greater frequency or intensity, the rainfall runoff volume and possibility of street flooding will increase as well. Therefore, design and assessment of stormwater management systems, adapted to future changes in heavy rainfall events, are of great importance.

One approach to design stormwater systems is the "event-based simulation", which simulates the scenarios when design storms of different return periods hit the design area. Design storms (hyetographs) are developed using the SCS method, the triangular hyetograph method, or the alternating block method. All three methods involve a design rainfall intensity value, which is estimated from the Intensity–Duration–Frequency (IDF) curve.

IDF curves are developed from regressions of rainfall intensity estimates for durations

from 5min to 24h and for return periods from 2y to 100y or even longer. These rainfall intensity estimates are derived from statistical models for historical rainfall records. The development of statistical models of the rainfall intensity assumes data values in the historical record are independent and identically distributed. The presence of trends in heavy rainfall events will violate these assumptions and increase uncertainties involved in the design rainfall intensity. Hence, the assessment of design rainfall intensities under climate change is necessary for stormwater system design.

1.3 Applications Using AMS Data and Related Uncertainties

Heavy rainfall events in rainfall records are extracted as data series to develop a rainfall intensity model. The series with all data values above a selected threshold is referred to as Partial Duration Series (PDS), and the group of all largest values from each year is referred to as Annual Maximum Series (AMS). The statistical model using PDS is referred to as the PDS model hereafter, and the model using AMS is referred to as the AMS model.

The development of the AMS model can substantially affect the precision of the rainfall intensity estimates, including the selection of the frequency distribution, the calculation of the distribution parameters, and estimates of distribution quantiles and confidence intervals. The Gumbel distribution has been widely used in relation to the AMS model. The Atmospheric Environment Service (AES, later renamed as the Meteorological Service of

Canada, MSC) of Environment Canada developed rainfall intensity models using AMS data and the Gumbel distribution (Hogg et al., 1989). The Ontario Ministry of Transportation (MTO) provides Intensity–Duration–Frequency (IDF) curves, using the Gumbel distribution as an extreme value probability density function. Given that the Gumbel distribution is a two-parameter distribution, this limits the performance when comparing to various three-parameter distributions, such as the Generalized Extreme Value (GEV) distribution, the Generalized Pareto (GPA) distribution, and the Pearson Type III (PE3) distribution. Of interest is to determine the most appropriate frequency distribution to model heavy rainfall intensities. Alternative methods for selecting frequency distributions include the Probability Plotting Correlation Coefficient (PPCC) method (after Filliben, 1975) and the goodness-of-fit measure introduced by Hosking and Wallis (1997).

Using either the MSC IDF curves or the AMS models developed in this thesis, the uncertainties involved in design rainfall intensity estimates are substantial since models necessarily rely upon limited rainfall records. The difference between the expected value and 95% confidence limits can be as large as 25% of the expected value of the rainfall intensity, which increases the risk of stormwater system failure to cope when assigning the expected value as the design rainfall intensity. The relationship between the uncertainty in rainfall intensity estimates and the record length needs to be characterized to find the circumstances under which a rainfall record can produce precise design rainfall intensity estimates.

1.4 PDS Model and Design Value Uncertainties

Rainfall intensity models typically employ AMS data to estimate the probability of a given value being exceeded. An AMS model focuses on the largest event in a year, ignoring the 2nd and 3rd largest values in the same year. The AMS model cannot model probabilities for situations when more than one rainfall event exceeds the predicted rainfall intensity in the same year, which indicates potential street flooding or basement inundations from an urban storm water management perspective. On the contrary, the rainfall intensity model using PDS data estimates the probability of a storm event exceeding the design rainfall intensity. However, the application of the PDS model has several barriers. There is no consensus about the selection of a rainfall intensity threshold to extract Partial Duration Series from historical rainfall records. The relationship between the recurrence interval of a given event and the non-exceedance probability of the event magnitude in the cumulative frequency distribution needs clarification. In the PDS model development, research is needed with respect to the sensitivity to missing values and rainfall intensity thresholds, and the selection of frequency distributions. The accuracy and precision of the PDS model estimates, in comparison with those from the AMS model, need to be assessed as well.

If use of a PDS model is appropriate for evaluating design rainfall intensities, the timeframe of the historical rainfall record needs to be examined as well. It follows that the use of the entire record, regardless of the length and which time period it is covering, is not always appropriate. For example, a very long record may involve temporal changes, since the climate when a rainfall record was recorded may include substantial differences from

the most recent climate. Therefore, an analysis of the design rainfall intensity changes versus the timeframe of the historical rainfall record used is needed. This can be examined by splitting the rainfall records into two approximately equal lengths of record to estimate design rainfall intensities separately, and then comparing to detect if changes are evident. The time of splitting may be enumerated over a range of years, to identify the sensitivity of design rainfall intensity changes in response to the split year.

1.5 Use Regional Frequency Analysis to Improve Design Value Accuracy

For design rainfall intensity estimates where substantial uncertainties exist (i.e. large magnitude of the confidence interval) due to either climate changing effects or limited rainfall records, grouping of adjacent rainfall stations and using regional frequency analyses, is an alternative to reduce uncertainties. In the aforementioned study of rainfall intensity changes using the PDS model, rainfall records are split into two segments. The design rainfall intensity estimates may involve considerable uncertainty due to limited record length, which leads to the merit of application of regional frequency analysis.

The regional frequency analysis technique identifies groups of rain gauges that share statistical similarity, develops a regional frequency distribution model, and calculates the design rainfall intensity at each rain gauge using the regional frequency distribution curve and a scale factor particular to individual rain gauges. This method was introduced in

Hosking and Wallis (1997) and only uses annual maximum series. Therefore, the original algorithms need to be modified to cope with the partial duration series.

There is need to assess the improvement in relation to the uncertainties involved in the design rainfall estimates from the regional frequency analysis approach compared with the PDS model, which only uses rainfall records from the given rain gauge. As well, the changes in design rainfall intensities identified from the regional frequency analysis, need to be compared with the changes identified from the PDS model approach, to review the consistency of the two approaches, and to confirm if changes are occurring in the study area.

1.6 Study Objectives

This study uses rainfall records from climate stations in the Province of Ontario to examine the issues and techniques introduced above. The principal research objective is to improve the understanding of design rainfall intensities pertinent to municipal stormwater system design. As a paper-based thesis, the major research questions are discussed in each of the following chapters and papers.

Chapter 2 is a supplementary chapter introducing data availability and data screening. This chapter is added to facilitate the reproduction of results in this thesis in the future.

Chapter 3, entitled “Improving the Efficiency of Quantile Estimates to Identify Changes in Heavy Rainfall Events”, introduces the investigation of the use of the Gumbel distribu-

tion to model AMS data, and changes in design rainfall intensities identified from selected rain gauges in the Province of Ontario. This paper has been submitted to the *Canadian Journal of Civil Engineering* and is in review.

Chapter 4, entitled "Uncertainty Characterization of Rainfall Inputs Used in Design of Storm Sewer Infrastructure", shows the analyses of uncertainties involved in the AMS model and the related IDF curves. This paper has been accepted by the *Journal of Urban and Rural Water Systems Modeling*.

Chapter 5 is a paper entitled "Performance Comparisons of Partial Duration and Annual Maxima Series Models for Rainfall Frequency Analysis of Selected Rain Gauge records, Ontario, Canada". It gives a demonstration of the advantages of using partial duration series instead of annual maximum series in rainfall intensity modeling. It also introduces a complete procedure to develop the PDS model for selected rain gauges in southern Ontario is introduced. This paper has been submitted to *Hydrological Research* and is in review.

Chapter 6, entitled "Identification of Design Rainfall Changes Using Regional Frequency Analysis — A Case Study in Ontario, Canada", demonstrates the application of the regional frequency analysis approach using selected rain gauges in southern Ontario, and assesses the improvement in relation to the model uncertainties. This paper has been submitted to the *Journal of Hydrology* and is in review.

Chapter 7 discusses the sensitivity of changes in design rainfall intensities with respect to the split time point used for the historical rainfall record, using the PDS at-site model.

The last chapter concludes by specifying the contributions of this research, and suggests

future work.

1.7 Scope of Research

The research scope extends from the study of distribution fitting and quantile estimation to the identification of step changes and assessment of model uncertainties. This research is focused on statistical approaches only, and will not assess the physical mechanisms behind the changes identified in rainfall intensities.

The research scope is limited by the availability of rainfall records. Most rainfall records obtained are from 1960s until 2000s; therefore, any temporal trend or change that spreads beyond this range cannot be identified. As well, design rainfall for very long return periods, e.g. 100 years, cannot be accurately estimated based on a rainfall record of 40 years. Most rain gauges are located in southern Ontario, and the rain gauges in northern Ontario are sparse. It is inappropriate to develop conclusions about regional changes in northern Ontario. Rainfall records are the only meteorological data used in this research, and any relationships with other weather parameters, for example temperature and wind speed, are not considered.

Chapter 2

Data Preparation

2.1 Introduction

The data obtained from Environment Canada were primarily over the time period of 1960-2007, with record length ranging from 1 to 65 years, and an average of 13 years. The rainfall records include daily maximum rainfall amounts over durations of 5, 10, 15, 30min, and 1, 2, 6, 12h. The rainfall records between April and October are used, and individual, annual records missing more than 20% were excluded. These data are referred to as "EC data" to distinguish from data from other sources hereafter. A detailed introduction of data availability and data preparation processes is provided.

Another set of rainfall data referred to frequently in this research is the "Intensity–Duration–Frequency (IDF) Files" obtained from the Engineering Climate Datasets of the Meteorological Service of Canada (MSC) website, which is publicly available at the web-

page: http://climate.weather.gc.ca/prods_servs/engineering_e.html. These IDF files will be referred to as "MSC IDF files" or "MSC IDF data" hereafter and, if not indicated, the term "Data" or "Data file" only refers to the EC data, not the MSC IDF data.

2.2 Data Format

Data obtained from Environment Canada are the tipping bucket rain gauge records, the "Rate of Rainfall (DLY03)". Climate stations are assigned identifications consisting of seven digits of numbers and letters. For example, the Waterloo Wellington Airport climate station is assigned an ID of "6149387". The DLY03 data include the largest amount of precipitation in a variety of time durations on daily basis. The time durations are indicated with element numbers, as given in Table 2.1. The data also include flags to indicate freezing conditions or unadjusted values. Each line in the data record represents the daily maximum precipitation amount for each day of a month, for a given rainfall duration. It consists of 7 digits of Station ID, 4 digits of Year, 2 digits of Month, 3 digits of Element number, 1 space, and followed by 31 daily data. The daily datum consists of 5 digital integers, a leading sign field, and a following flag. For months with less than 31 days, the last few days are recorded as missing values (-99999). In total, a monthly data record has 233 digits.

The MSC IDF data files include text files and graphs for 133 climate stations in the Province of Ontario. The text file includes metadata of the climate station (e.g. identifica-

Table 2.1: Element Number, Units, and Description for DLY03 Weather Elements

Element	Units	Description
124	0.01	Adjustment Factor
125	0.1mm	5 Minutes
126	0.1mm	10 Minutes
127	0.1mm	15 Minutes
128	0.1mm	30 Minutes
129	0.1mm	1 Hours
130	0.1mm	2 Hours
131	0.1mm	6 Hours
132	0.1mm	12 Hours
160		Chart Change Hour (Local Standard Time)

*http://climate.weather.gc.ca/prods_servs/documentation_index_e.html

tion, coordinates, length of record, is composite data, etc.), the tables for annual maximum series, return period rainfall amounts and rates, and interpolation equations and statistics. The graph files include the quantile-quantile plot of the annual maximum series, the return level plots for different durations, and the IDF plot. The MSC IDF data files provide annual maximum series of daily maximum rainfall amount over durations of 5, 10, 15, 30min, and 1, 2, 6, 12h.

2.3 Data Coverage

The raw data file includes rainfall records for 270 climate stations. The metadata includes station names, coordinates, elevations, and start/end/total years. As shown in Fig. 2.1, the climate stations are not spatially, evenly distributed. Approximately, one-third of the stations are located in northern Ontario, one-third in the Toronto and Hamilton area, and the reminder of the climate stations are unevenly located from Windsor to Ottawa. In

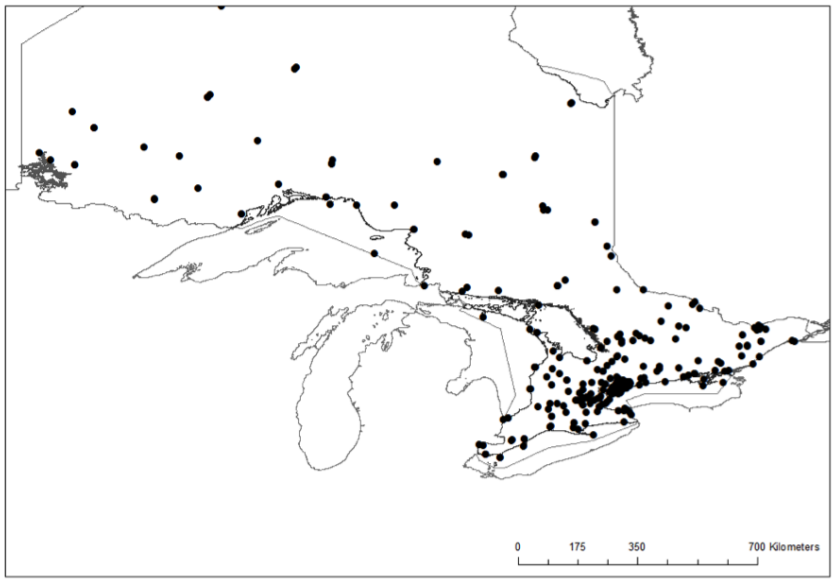

Figure 2.1: Spatial Coverage of Climate Stations in the Province of Ontario

Fig. 2.2, the number of climate stations that have rainfall records in a given year, regardless of missing values, is counted and plotted for the years from 1940 to 2010. The plot shows that the rainfall records started in 1960 (46 stations), reached a maximum of 125 stations in 1974, then decreased to 50 stations in 1996, and subsequently increased to 82 stations in 2006. From the temporal coverage of the rainfall records, the time span in this study is selected to be from 1960 to 2007. One exception is that the paper that studies the Gumbel distribution with annual maximum series also includes the 65 years of rainfall record at the Toronto climate station. Fig. 2.3 shows a histogram of the record length at all climate stations. One station located in Toronto has the longest rainfall record, 65 years from 1937 to 2002. Regardless of missing values, there are 16 stations having records longer than or equal to 40 years, and 27 stations having record lengths between 30 and 39 years. Spatially,

Figure 2.2: The Temporal Coverage of Climate Stations in the Province of Ontario

approximately two-thirds of the stations having records longer than or equal to 30 years are located in southern Ontario. Fig. 2.4 shows the number of records provided for each month at all climate stations. The number of records is counted as the number of data lines for each month in the data file, regardless of missing values in that month. The rainfall record availability from April to October is substantially higher than the availability of data from November to the next March.

2.4 Data Combination and Data Homogeneity

Further exploration of rain data finds situations when two or more climate stations have very close, or even identical coordinates, and most of these stations have rainfall

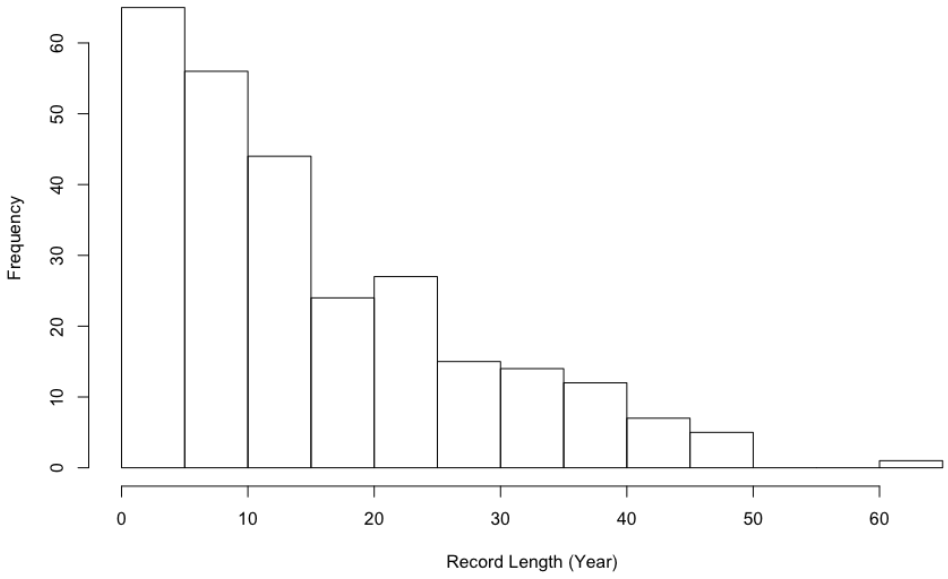

Figure 2.3: Histogram of Climate Station Record Lengths

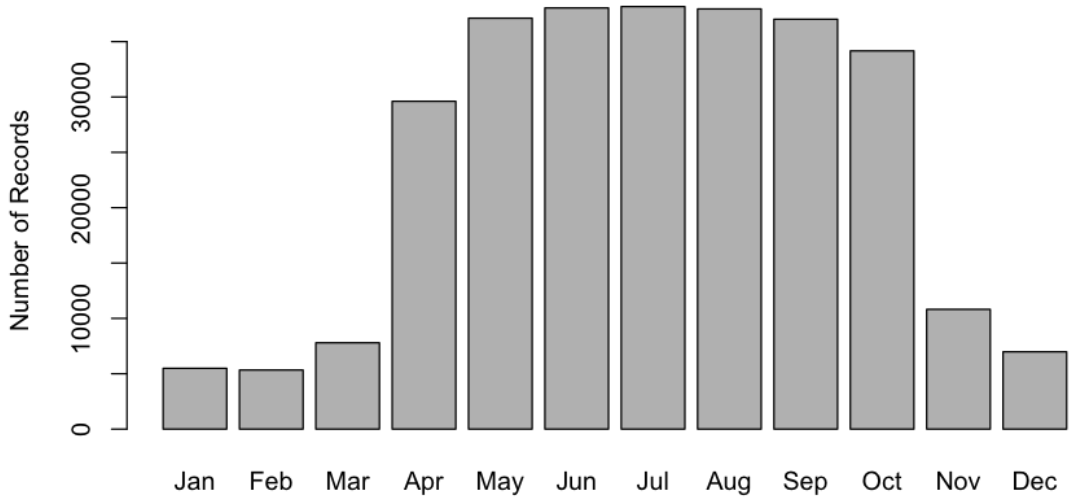

Figure 2.4: Total Number of Records in Each Month

records in consecutive order. This indicates the potential to combine rainfall records. The composite rainfall records are seen in the MSC IDF files as well. A list of climate stations combined in this study is given in Table 2.2, which includes climate stations that are marked as "Composite" in the MSC IDF files, and other climate stations that are geographically close. The identification used for a composite station is the same as the identification of the station with the latest record, with the same for the station names and coordinates. For example, the 1h rainfall record for the climate station named Chatham Waterworks (ID: 6131416) ended in May 23rd, 1983, and the rainfall record for the climate station named Chatham WPCP (ID: 6131415) started in Jun 1st, 1983. These two pieces of rainfall record are combined as one composite record and assigned an ID of 6131415 and a name of Chatham WPCP. The annual maximum series extracted from this composite rainfall record is compared with the annual maximum series provided in the MSC IDF files. The two data series are nearly identical, except the maximum value in 1983, which is 11.5 mm/h from the composite rainfall record, but marked as a missing value in the MSC IDF data file. The composite data from all 41 groups of climate stations are compared with MSC IDF data file, and they are almost identical, except the rainfall record at the Guelph stations for the time period before 1966. Two stations have rainfall records before 1966: Guelph Harrison Farm (ID: 6143077) from 1960 to 1966 and Guelph OAC (ID: 6143083) from 1962 to 1973. Neither of the annual maximum series extracted from these two stations is close to the annual maximum series from the MSC IDF file. Therefore, the rainfall data used in this research for the Guelph climate station for 1960-1966 is different from the MSC IDF file.

The comparison of the annual maximum series extracted from both the EC data and the MSC data files, examines data homogeneity as well. Data non-homogeneity can be introduced into rainfall records when a rain gauge is relocated, or the methodologies or equipment used to collect data are modified. The metadata provided by Environment Canada is not sufficient to conduct any test of homogeneity. However, the consistence between the two datasets provides confidence to assume data homogeneity.

Table 2.2: Climate Stations Selected to Combine Rainfall Records

Station ID	Start Year	End Year	Total Years
6020379	1966	1988	23
6020LPQ	2004	2006	3
6042755	1960	1973	14
6042715	1975	1981	7
6042716	1981	2006	25
6048261	1960	1994	35
6048268	2002	2006	4
6061358	1970	1975	6
6061361	1978	2006	25
6073960	1967	1999	32
6073980	2000	2006	7

6074209	1979	1995	17
6074211	1997	2006	10
6078290	1960	1969	10
6078285	2002	2006	5
6104025	1969	1996	28
6104027	1998	2007	10
6105976	1960	2001	42
6105978	2002	2007	6
6107835	1964	1982	19
6107836	1983	1989	7
6115820	1965	1992	28
6115811	1992	2004	9
611KBE0	1989	1995	7
6.11E+03	1997	2007	11
6122849	1969	1980	12
6122847	1997	2007	11
6127520	1962	1969	8
6127514	1970	2007	38
6131416	1965	1983	19
6131415	1983	2007	24

6131982	1962	1995	34
6131983	1997	2007	11
6133360	1966	2001	25
6133362	2002	2007	6
6137147	1960	1985	26
6137154	2003	2007	5
6137301	1960	1964	4
6137287	1971	2005	34
6137361	1960	1980	21
6137362	1980	2007	28
6139145	1963	1989	22
6139148	2002	2007	6
613FN58	1974	1994	21
613P001	2001	2007	6
6142285	1970	1993	19
6142286	2003	2007	5
6144475	1960	2002	43
6144478	2003	2007	5
6150700	1960	1975	16
6150689	1975	2007	33

6153300	1962	1996	35
6153301	1997	2007	11
6155186	1960	1965	6
6155187	1966	1975	10
6157831	1969	1990	22
6157832	1991	1994	4
6158080	1960	1975	16
6158084	1985	1992	8
6158350	1937	2002	65
6158355	2002	2007	6
61587PP	1966	1979	14
6158406	1980	1993	14
6155746	1964	1969	6
615N745	1970	1977	8
6012198	1960	1997	37
6012199	1999	2006	8
6014350	1971	1989	19
6014353	2004	2006	3
6048231	1999	2003	5
6048235	2004	2006	3

6075425	1967	2003	30
6075435	2004	2006	3
6111800	1973	1993	9
6111792	1997	2007	11
6112070	1962	1969	8
6112072	1977	2001	24
6122078	1961	1965	5
6122079	1965	1971	7
6145503	1962	1986	25
6145504	2003	2007	5
6143077	1960	1966	7
6143083	1962	1973	12
6143069	1975	1991	17
6143090	1997	2005	9

*The name and location of climate stations are listed in Table 8.1

Chapter 3

Improving the Efficiency of Quantile Estimates to Identify Changes in Heavy Rainfall Events

This paper investigates the use of the Gumbel distribution to model AMS data, and changes in design rainfall intensities identified from selected rain gauges in the Province of Ontario.

The frequency distributions are selected using the L-moment ratio diagrams and relative RMSE for estimates of given return periods. The distribution parameters are estimated using the L-moment method, and the design rainfall intensities and associated confidence intervals are estimated using the resampling method.

The design rainfall intensities for two time periods (pre1983 and post1984) are com-

pared to assess if changes have occurred over time. Rainfall records from several climate stations show statistically significant changes in design rainfall intensities.

This paper explains the methodology used to identify changes in rainfall intensity estimates by examining if two confidence intervals overlap. This methodology is used throughout all studies in this thesis, and is one of the most important theoretical bases and major contributions. This paper proves that changes in design rainfall intensities are evident, and suggests the necessity of assessing design rainfall intensities under climate change.

3.1 Abstract

To assess whether changes in heavy rainfall events are occurring over time, Annual Maximum (AM) records from 21 rainfall gauges in Ontario are examined using frequency analysis methods. Relative RMSE and related boxplots are used to characterize assessment for selecting distributions; the Gumbel distribution is verified as one of the most suitable distributions to provide accurate quantile estimates. Records were divided into two periods, and tested using the Mann-Kendall test and lag-1 autocorrelations to ensure that data in each period are identically distributed. The confidence intervals of design rainfalls for each return period (2, 5, 10, and 25-year) are derived by using resampling method, and compared at 90% confidence levels.

The changes in heavy rainfall intensities are tested at gauges across the Province of Ontario. Significant decreasing changes in heavy rainfall intensities are identified from

several gauges in central and southern Ontario. Increases in heavy rainfall intensities are identified in gauges at Sioux Lookout and Belleville.

3.2 Introduction

3.2.1 Background

Global warming is expected to lead to changes in extreme weather conditions such as intensive rainfall events, due to the increased energy in the atmosphere (Frei et al., 2006; Zhai et al., 1999; Fowler and Kilsby, 2003). If storms are increasing in intensity over time, the implications to water resources infrastructure and soil erosion may be substantial. As a consequence, it is important to assess changes (if any) in rainfall intensities from gauge measurements.

Assessment of potential evidence of climate change on rainfall patterns in Canada has been the subject of widespread investigation. Mladjic et al. (2011) compared the extreme precipitation event magnitudes of two time periods (1960–90 and 2041–70) in several regions across Canada to identify projected changes using regional frequency analysis and individual grid box analysis, separately. The results show that there are significant increases in event magnitudes for 7 out of 10 studied regions, including the Great Lakes region in the Province of Ontario. Mailhot et al. (2010) assessed the predicted future evolution of heavy precipitation, by comparing the historical and future grid box values (1850–2100). In Mailhot et al. (2010), the Canadian Global Climate Model (CGCM) was used to simulate future

daily precipitation to predict Annual Maximum series. These results show that future daily and multi-day events will be more intense and frequent for all regions across Canada except the Prairies. The time-of-change analysis indicates that the trend emerged during the period of 1985–2005, and this is supported by the finding that the number of grid boxes (approximately 340km$\times$340km, described in Fig 1. in Mailhot et al. (2010)) with significant trends is starting to increase during this period of time (1985–2005). Mailhot et al. (2007) assessed the stationarity of rainfall series in Quebec as the basis of the Intensity–Duration–Frequency (IDF) curve. Mailhot et al. (2007) compared the annual maximum series of observed precipitation record (1961–90) with that of Canadian Regional Climate Model (CRCM) simulations (2041–70) for durations of 2, 6, 12, and 24h. The results show that the current return periods for 2 and 6h events will be halved in future climate at a grid box level (45km$\times$45km resolution). Spatial correlation analysis showed that the spatial correlation would decrease in future climate, suggesting that annual extreme rainfall events may occur more frequently in convective weather patterns.

Changes in extreme rainfall have also been identified by others for the past several decades (Frich et al., 2002; Zhang et al., 2001; Vincent and Mekis, 2006)). Alexander et al. (2006) documented changes in precipitation in Canada between 1901 and 2003, and found statistically significant increases in several precipitation indices, including the max 1-day and 5-day precipitation, the very wet days, and the extreme wet days. Heavy events (less frequently than 5 times per year) in southeastern Canada (including Atlantic coast and Great Lakes-St. Lawrence area) are reported to be increasing over the period 1920–1970,

mostly during summer and autumn (April to October, after Stone et al., 2000)). Adamowski and Bougadis (2003) selected annual maximum records of 44 stations across the Province of Ontario, each with longer than 20 years of record and spanning from the 1970s to 1990s, to identify regional and local trends using the Mann-Kendall trend test. Positive trends are identified for gauges located in northern Ontario for storms of all durations, and for the central Ontario for storms longer than 15min. However, only four durations (5min, 10min, 2h, and 6h) in the northern Ontario were found to have significant trends. In the St. Lawrence region, rainfall intensities of all durations are decreasing, and decreasing trends of short duration storms (5, 10, and 15min) are significant. In the southern region, storms of 5 and 10 minutes duration are significantly decreasing, and storms of 2 hours duration are significantly increasing. Vasiljevic et al. (2012) analyzed partial duration series for 13 rain gauges in Ontario to identify trends in rainfall intensities related to urban stormwater designs. The results show that the storm intensities of 5-year return period have increased over the last 30 years at a rate of approximately two percent per year. For the Waterloo area, the storm intensities for both 5-year and 2-year return period have increased for durations shorter than 2 hours, with confidence of more than 80% (Vasiljevic et al., 2012).

Changes in heavy rainfall intensities are highly relevant to the design of urban infrastructure systems (Adamowski et al., 2010; Burn and Taleghani, 2013; Vasiljevic et al., 2012)). The events with return periods of 2 to 10 years are related to urban sewer infrastructure (e.g. swales, culverts, water detention ponds), and the 25 to 100 years events are related to major stormwater management system that consists of aboveground conveyance

routes (Chin, 2006, p479). Under changing climate conditions, rainfall rates for infrastructure design may be subject to change, and hence it is important to assess whether any changes are apparent in recent historical records as described below.

3.2.2 Study Objective

This paper examines changes in heavy rainfall events using annual maximum data series from 21 rainfall records that are longer than 40 years in Ontario by comparing the confidence intervals on the intensity of design rainfalls for various return periods and durations. Each record is divided into two periods (up to the end of 1983, pre-1983; from the beginning of 1984, post-1984) and checked with the Mann-Kendall test and lag-1 autocorrelations to ensure identically distributed data prior to developing a frequency distribution model. Confidence intervals of heavy rainfall event estimates are derived based on asymptotic theory, and the significance levels of this test are also determined to assess the degree to which heavy rainfall events in Ontario are changing.

3.3 Model Development

3.3.1 Assumptions of Independent and Identically Distributed Data

Data values at the same rain gauge are assumed to be independent since annual maximum series are extracted as one event within each year. In this study, only rainfall events occurring between April and October are considered; therefore, it is a good reason to be-

lieve that the annual maximum series are independent of each other. To make certain of the independence, the annual maximum series are tested of the lag-1 autocorrelation coefficients against 95% significant level critical values.

Mann-Kendall test (Mann, 1945; Kendall, 1978) is applied to assess whether data values in the same data series are identically distributed. The Mann-Kendall test is applied to each period of the record before commencing frequency analysis. The test is implemented in R project (R Core Team, 2013) using the package "Kendall" (McLeod, 2011).

3.3.2 Parameter and Quantile Estimation

The parameters for candidate distributions were estimated using Linear Moments (L-moment), a procedure which is reported to be most effective when dealing with hydrological extreme records (Hosking et al., 1985; Hosking and Wallis, 1987). Hosking and Wallis (1997) listed L-moments and parameter estimates for several frequency distributions commonly used in hydrologic modeling. The quantile functions of distributions are inverses of their Cumulative Distribution Function (CDF, $F(x)$) with parameters estimated from each dataset. For example, if $F(x) = \gamma (0 \leq \gamma \leq 1)$, then x is the γ-th quantile of variable x from the CDF. Stedinger et al. (1993) listed quantile functions for some widely used frequency distributions.

The CDF and quantile functions of Gumbel distribution are

$$F(x) = \exp(-\exp(-\frac{x-\xi}{\alpha})) \tag{3.1}$$

$$x(F) = \xi - \alpha \log(-\log(F)) \tag{3.2}$$

Where α and ξ are scale and location parameters respectively. Both x and ξ can be any real number, and α is greater than zero. Parameters are estimated by sample L-moments l_1 and l_2

$$\hat{\alpha} = \frac{l_2}{\log(2)}, \hat{\xi} = l_1 - \gamma\hat{\alpha} \tag{3.3}$$

Where $\gamma = 0.5772$ is Euler's constant. The sample l-moments l_1 and l_2 are defined as $l_1 = b_0$ and $l_2 = 2b_1 - b_0$, where b_0 and b_1 are estimator of the probability weighted moments defined as

$$b_r = n^{-1}\binom{n-1}{r}^{-1} \sum_{j=r+1}^{n} \binom{j-1}{r} x_{j:n} \tag{3.4}$$

In this study, sample l-moments and distribution parameters are estimated by using R package "lmom" (Hosking, 2013). Readers are referred to Hosking and Wallis (1997) for details of other probability distributions.

3.3.3 Confidence Limits of Quantile Estimates

Two methods are considered for deriving confidence limits of quantile estimates, the asymptotic method and the resampling method. The asymptotic method based on the central limit theorem requires large sample sizes, while the resampling method requires more computational effort.

When estimating the quantile of frequency distributions, the mean and variance as cal-

culated from the asymptotic distribution for large sample sizes (usually more than 50), are well approximated (Hosking et al., 1985; Hosking and Wallis, 1987); however, the asymptotic efficiency declines when the sample size is less than 50.

Resampling techniques, especially bootstrapping (Efron, 1979), are widely used in hydrologic research (e.g. Douglas et al., 2000; Burn and Hag Elnur, 2002; Adamowski and Bougadis, 2003) to estimate the confidence limits for quantile estimates when parametric methods are not applicable. A non-parametric method resamples the sample set (with or without replacement) and calculates the statistics being analyzed, hundreds or thousands of times, to construct an empirical distribution. The confidence limits of the statistics obtained from the original dataset are computed with this empirical distribution.

In this study, confidence limits for quantile estimates were computed using a resampling method. Rainfall records were resampled 200 times with replacement. For each of these resampled samples, quantiles of various return periods are estimated with the same distribution selected to describe the original sample. These 200 estimates are pooled together to estimate the 5% and 95% quantile as the lower and upper confidence limits.

3.3.4 Selecting Probability Distributions

How the data are statistically distributed affects the analysis of frequency. An improper selection of a probability distribution may lead to a large bias in estimates of extreme events. Often, the probability density function of extreme value data series is heavy-tailed (negative shape parameter, see Hosking and Wallis, 1987; Madsen et al., 1997), which

means the occurrence of extreme events is more frequent than if normally distributed. Therefore, preferences need to be given to probability distributions with better precision and accuracy in the tails of the distribution.

Hosking and Wallis (1997) introduced a series of methods for regional frequency analysis, including the L-moment ratio diagram, the goodness-of-fit measure, and the assessment of the accuracy of quantile estimates. The L-moment ratio diagram is used to select candidate distributions based on the 3rd and 4th sample L-moment ratios (t_3, t_4). In this diagram, L-moment ratios are plotted as points, with t_3 as the x-axis and t_4 as the y-axis. Two-parameter frequency distributions (e.g. Normal distribution) are also plotted as points since their t_3 and t_4 are fixed values. Three-parameter frequency distributions are plotted as curves, since the t_3 and t_4 will change as the shape parameter changes. Those distributions close to plotted points of samples will be selected as candidate distributions for further assessments.

Hosking and Wallis (1997) explain that the choice of a frequency distribution should be focused on the accuracy of quantile estimates in the upper tails when analyzing extreme events. It is argued finding a frequency distribution that is close to an observed sample does not guarantee that new observations in the future will match historical samples, especially when physical processes may subject to change.

One approach to select distributions by measures of goodness-of-fit is the Probability Plot Correlation Coefficient (PPCC) method (after Filliben, 1975). This procedure is applied to test the goodness-of-fit for extreme value distributions (Fill and Stedinger, 1995;

Burn and Taleghani, 2013). The extreme events lie in the upper tail of a frequency distribution and hence represent only a small portion, compared to the bulk of data, of the correlation coefficient between the data and the frequency distribution. Therefore, using PPCC measures will degrade the goodness-of-fit that would otherwise be obtained if only the upper tail of the frequency distribution was employed. As a result, the PPCC method is not applied in this research to select frequency distributions.

Hosking and Wallis (1997) introduced a "goodness-of-fit measure" to use as the basis for selecting the distribution for regional analyses. This approach assumes heavy rainfalls in a homogeneous region can be described by the same distribution apart from a scale factor. The goodness-of-fit measure will assess the similarity between the 4^{th} L-moment ratios of each candidate distribution and the regionally averaged 4^{th} L-moment ratios from rainfall records; however, it is not suitable for this study since heavy rainfalls from different gauges are not necessarily in a homogeneous region. The relative Root Mean Square Error (RMSE) is one of those measures suggested in Hosking and Wallis (1997) for assessing the accuracy of quantile estimates from a regional frequency analysis algorithm. However, it is capable of assessing the accuracy of quantile estimates with different candidate distributions as well. Using Monte Carlo simulation, M repetitions are drawn from candidate distributions with parameters estimated from the original sample sets, and all repetitions have the same size as the original sample set. The quantile estimate $Q^{[m]}(F)$ for non-exceedance probability F is calculated from the mth repetition. The relative RMSE of

quantile estimates over M repetitions is calculated as

$$R(F) = [M^{-1} \sum_{m=1}^{M} (\frac{Q^{[m]}(F) - Q(F)}{Q(F)})^2]^{1/2} \tag{3.5}$$

$Q(F)$ is the true value of the quantile at probability F, and represented by the quantile estimated with the original sample herein. To obtain the quantiles from the original sample, plotting positions are selected according to candidate distributions as per Stedinger et al. (1993), namely: Gringorten's plotting position ($\frac{i-0.44}{n+0.12}$) (Gringorten, 1963) was applied for Gumbel distribution; Cunnane's plotting position ($\frac{i-0.4}{n+0.2}$) (Cunnane, 1978) was used for three-parameter log-normal distribution, generalized extreme value distribution and generalized normal distribution; the Pearson Type III distribution uses Blom's plotting position ($\frac{i-0.375}{n+0.25}$) (Blom, 1958). The quantile at probability F is then interpolated with ordered observations and their plotting positions.

Makkonen (2006) criticized the usage of various plotting positions, and advocated that the Weibull formula ($p = \frac{i}{n+1}$) is the only correct plotting position. A Monte Carlo experiment is used herein to justify the usage of alternative plotting positions. For the Gumbel distribution as an example, with given parameters $[0, 1]$, 20 values are randomly generated, and the estimate of the 5-year event ($R = 5, p = 0.8$) is linearly interpolated between the two values with plotting positions closest to $p = 0.8$. One hundred replications of this resampling procedure show that, compared to the true 5-year quantile (1.499), Weibull's plotting position overestimates by 8.3% and the rest of the plotting positions all have bias

within 5%. This experiment is repeated 100 times, and the Weibull's plotting position averaged 6.9% overestimation, which is more than three times the bias of other plotting positions. The same experiment is conducted for the Pearson Type III distribution, with parameters $[0, 1, 0]$. Again, Weibull's plotting position averaged 5.28% overestimated while other plotting positions all have average bias within 2%. Therefore, this study will continue to use different plotting positions for different probability distributions.

To assess the performance between the records for all 21 gauges and the candidate distributions, the relative RMSE ($R(F)$) is developed into a series of boxplots, with each box depicting statistics (including mean, max, min, and interquartile range) of the relative RMSE of a specific duration, return period, and candidate distribution.

3.4 Application of the Frequency Distribution Model

3.4.1 Data description

Figure 3.1 shows the 21 selected rainfall stations in Ontario; they all have at least 40 years of rainfall records. Rainfall records are in the form of maximal rainfall amount over durations of 5, 10, 15, 30min, and 1, 2, 6, and 12h of each day. All of the records employed are recorded by tipping bucket rain gauges and have been corrected to the standard rain gauge. (Sandy Radecki, personal communication, 2013). According to Mekis and Hogg (1999), rainfall measurement methodologies have been modified several times. Rain gauges were changed to Type-B at most locations in 1970s, which replaced the previous

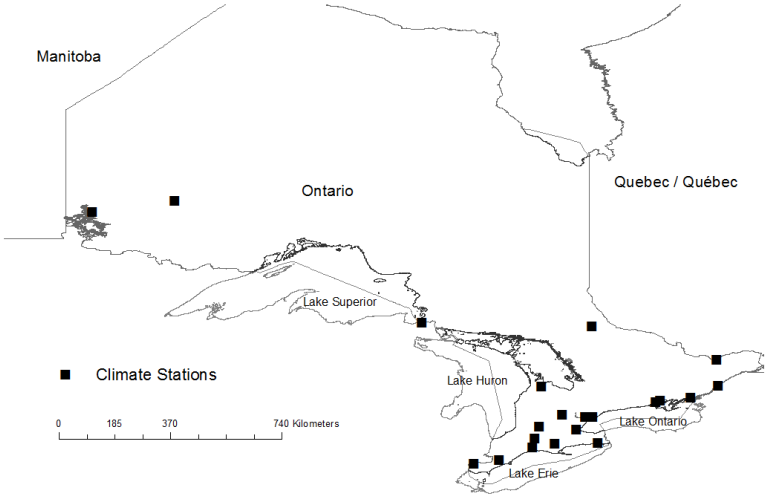

Figure 3.1: Location Map Showing 21 Climate Stations within Province of Ontario

Meteorological Service of Canada (MSC) gauge. The Type-B gauge was introduced to reduce systematic errors—adhesion of water to the gauge surface, evaporation, and splash out. Also around 1965, the inside container of MSC gauges was changed to soft plastic material from copper, which has different wetting characteristics. These modifications introduced non-homogeneity in rainfall records (Groisman and Legates, 1995; Karl et al., 1993, 1995). Goodison and Louie (1986) reported that compared to pit gauge measurements, MSC gauge measurements are 4% lower on average, and Type-B gauges measurements are 1% lower, at three test sites in Canada (particularly, -1.9% and -0.4% at Mt. Forest, Ontario). The presence of non-homogeneity in the rainfall record may lead to false significant changes detected from the record (Groisman and Legates, 1995). The correction approach from Goodison and Louie (1986) is not used since the metadata of rainfall records are not available. Based on the fact that all data are quality-controlled by Environment Canada, it

is reasonable to assume homogeneity in rainfall records employed herein.

As a consequence of instrument, location, and elevation changes, many station names and identifiers were changed. Simply combining records from two stations will result in risk of non-homogeneity; Mekis and Hogg (1999) applied a "simple ratio of observation" method to adjust combined records. The simple ratio of observation method is only applicable when two records have an overlapping period. In this study, stations of approximate or identical coordinates are considered as potential station groups to be combined. A close examination of rainfall records reveals that the successive record starts right after the preceding record ends for many stations. Therefore, it is impossible to adjust records based on the ratios calculated from overlapped observations. Hence, the quality controlled rainfall records were combined without adjustment where two or more stations are at identical or approximate location for this assessment.

In some circumstances, gaps in a record exist. Mekis and Hogg (1999) adjusted their dataset by filling missing data gaps with values generated from probability distributions consistent with the available data. The goal of filling missing data gaps is to ease the computing process by creating a continuous time series (Mekis and Hogg, 1999). Instead of filling gaps, this study acknowledges the presence of missing data. A threshold of 20% was employed to classify an annual record as having missing data, where the ratio of missing data is calculated based on the number of days with missing values between April 1st and Oct 31st. If in a year the missing ratio is more than 20%, the data for that year are not included in the subsequent assessments.

To evaluate whether a change in heavy rainfall events has occurred, each record was split into two parts at a fixed time (at the end of year 1983). The year 1983 is selected as it is close to the mid point of most rainfall records; and splitting all records at the same time point makes it possible to show spatial variability of changes between two time periods (pre-1983 and post-1984).

3.4.2 Test of Identically Distributed Assumptions

The assumption of identically distributed data in each period of a record is examined first, by means of the Mann-Kendall trend test. Records detected with significant trends include the annual maximum 10min rainfall record from the Windsor gauge in the 1st period, and the annual maximum 5, 15, 30, 60, 120min rainfall records from the Toronto Pearson Airport gauge in the 2nd period. As a result, the assumption of non-stationarity is violated; thus, these records are excluded from subsequent analyses.Further, the annual maximum 5min rainfall record at Delhi, Ontario has significant lag-1 autocorrelation, and is excluded. The 5 and 10min records at Toronto Lester B. Pearson Airport are excluded for the same reason. For other rainfall records, all assumptions have been verified before proceeding with frequency analysis.

3.4.3 Distribution selection

To identify candidate distributions, 3rd and 4th L-moment ratios of samples from rainfall records of all gauges are plotted in the L-moment ratio diagram (Fig 3.2). Each circle in

Fig 3.2 represents an L-moment ratio estimated from a rainfall record. The Logistic (L), Normal (N), Uniform (U), Exponential (E), Generalized Logistic (GLO), and Generalized Pareto (GPA) probability distributions are excluded because they deviate from the bulk of the circles. The candidate distributions include the Gumbel (GUM) distribution and three three-parameter distributions, namely the Generalized Extreme-Value (GEV) distribution, the Generalized Normal (GNO) distribution, and the Pearson type III (PE3) distribution. In addition, the three-parameter Log-Normal (LN3) distribution is close to the center of the circles in Fig 3.3 after log-transforming the original data. Therefore, LN3 is added to the candidate distribution set as well.

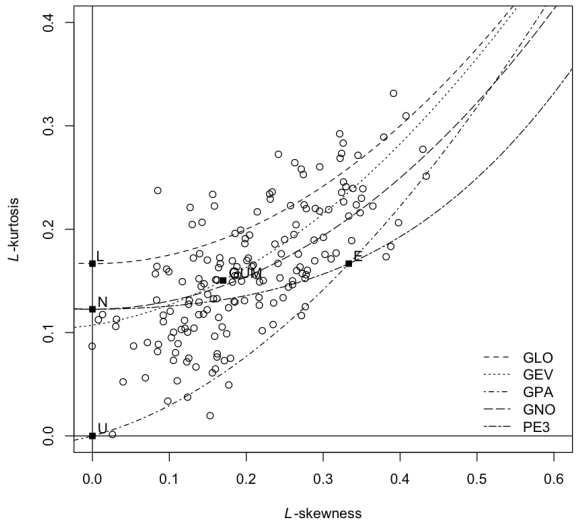

Figure 3.2: L-moment Ratio Diagram with Samples

*The solid boxes represent two-parameter distributions, such as Logistic (L), Normal (N), Uniform (U), Exponential (E), and Gumbel (GUM). The curves represent three-parameter distributions, such as Generalized Logistic (GLO), Generalized Extreme-Value (GEV), Generalized Pareto (GPA), Generalized Normal (GNO), and Pearson type III (PE3).

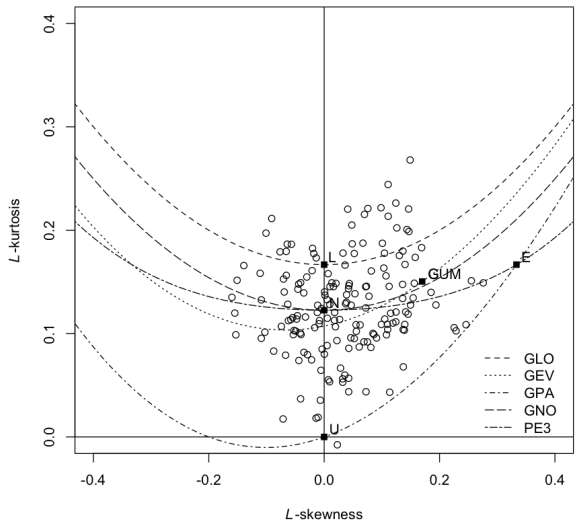

Figure 3.3: L-moment Ratio Diagram with Log-transformed Samples
*The solid boxes represent two-parameter distributions, such as Logistic (L), Normal (N), Uniform (U), Exponential (E), and Gumbel (GUM). The curves represent three-parameter distributions, such as Generalized Logistic (GLO), Generalized Extreme-Value (GEV), Generalized Pareto (GPA), Generalized Normal (GNO), and Pearson type III (PE3).

To assess the performance between the records for all 21 gauges and the candidate distributions, the relative RMSE ($R(F)$) is developed into a series of boxplots, as shown in Fig. 3.4. The four panels represent the results for return periods of 2, 5, 10, and 25-year respectively. In each panel, the dotted lines separate groups of boxes with respect to the time durations, and within each group, the five boxes represent the five distributions, namely GUM, LN3, GEV, GNO, and PE3 from left to right. Each box depicts statistics (including mean, max, min, and interquartile range) of the relative RMSE of a specific time duration, return period, and candidate distribution.

All candidate distributions show similar performance throughout the plots in Fig 3.4. The GUM shows larger dispersion than other candidates in the estimate of the 2-year event

over durations from 30min to 2h, but also shows lower mean errors in the estimates of 25-year events. All five candidates perform similarly for estimating the 5 and 10-year events. Considering the extra computational effort when applying three-parameter distributions, and the tradition of using GUM in rainfall frequency analysis (Chow et al., 1988, Ch14), the Gumbel distribution is selected as the frequency distribution to characterize the heavy rainfalls at all the gauges.

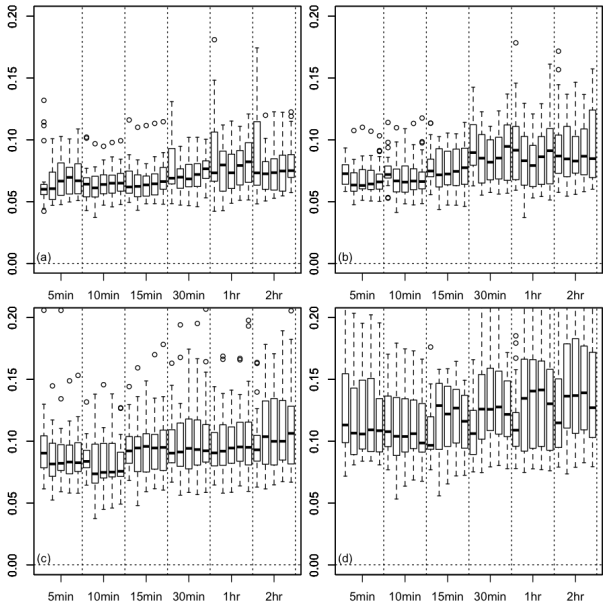

Figure 3.4: Boxplot of the Relative RMSE of the Candidate Distributions

* The four panels represent the results for return periods of 2, 5, 10, and 25-year respectively. In each panel, the dotted lines separate groups of boxes with respect to the time durations, and within each group, the five boxes represent the five distributions, namely GUM, LN3, GEV, GNO, and PE3 from left to right. Each box depicts statistics (including mean, max, min, and interquartile range) of the relative RMSE of a specific time duration, return period, and candidate distribution.

3.5 Identification of Quantile Changes by Comparing Confidence Intervals

To investigate if changes in heavy rainfall intensities have occurred, Confidence Intervals (CIs) of quantiles estimated from two segments of the data are compared at the same exceedance probability (e.g., 20% annual exceedance or 5-year return period). Vasiljevic et al. (2012) first introduced this method, but the CIs were calculated following Yevjevich's method (Yevjevich, 1972, pp. 211), which is not precise. In this research, the confidence intervals are estimated with resampling methods, which yields more precise estimates. The rationale of using a confidence interval comparison method rather than a Student's t-test is explained below.

For demonstration, two sample sets are denoted as $\{x_1\}$ and $\{x_2\}$, each with a sample size of n, and the means and standard deviations of the two sample sets are $\bar{x}_1, \bar{x}_2$, s_1, and s_2. The quantiles with non-exceedance probability p are denoted as x_{1p} and x_{2p}, and the corresponding standard deviations are s_{1p} and s_{2p}. The objective is to test the significance of difference between two quantiles.

For the Student's t-test of means, if two means are significantly different, then:

$$t^* = \frac{\bar{x}_1 - \bar{x}_2}{\sqrt{\frac{s_1^2}{n} + \frac{s_2^2}{n}}} > t_{\frac{\alpha}{2}} \tag{3.6}$$

$$\bar{x}_1 - \bar{x}_2 > t_{\frac{\alpha}{2}} \sqrt{\frac{s_1^2}{n} + \frac{s_2^2}{n}} \tag{3.7}$$

The statistic t^* is compared with the critical value t_c, which is the $1 - \frac{\alpha}{2}$ percentile (two-sided test) of t distribution with degrees of freedom $n - 1$.

The confidence intervals for group means are $\bar{x}_1 \pm t_{\frac{\alpha}{2}} \frac{s_1}{\sqrt{n}}$ and $\bar{x}_2 \pm t_{\frac{\alpha}{2}} \frac{s_2}{\sqrt{n}}$. If there is no overlap between confidence intervals, then:

$$\bar{x}_1 - t_{\frac{\alpha}{2}} \frac{s_1}{\sqrt{n}} > \bar{x}_2 + t_{\frac{\alpha}{2}} \frac{s_2}{\sqrt{n}} \tag{3.8}$$

$$\bar{x}_1 - \bar{x}_2 > t_{\frac{\alpha}{2}} (\frac{s_1}{\sqrt{n}} + \frac{s_2}{\sqrt{n}}) \tag{3.9}$$

With the knowledge that $(\frac{s_1}{\sqrt{n}} + \frac{s_2}{\sqrt{n}}) \geq \sqrt{\frac{s_1^2}{n} + \frac{s_2^2}{n}}$ is always true, then if Eq 3.9 is the case, Eq 3.7 also holds. In other words, if two statistics have non-overlapped confidence intervals, they are necessarily significantly different, with significance at least that used to construct confidence intervals.

Similarly, the t test statistic for quantiles is $t^* = \frac{x_{1p} - x_{2p}}{\sqrt{s_{1p}^2 + s_{2p}^2}}$; however, several issues hindered the use of the t test. The relationship between standard deviations of quantile (s_{1p} or s_{2p}) and sample ($\{x_1\}$ or $\{x_2\}$) is not as certain as that of the sample mean. For the sample mean, the Standard Error of the Mean (SE) is computed as the sample standard deviation divided by the squared root of the sample size (e.g. $SE_1 = \frac{s_1}{\sqrt{n}}$). For a sample

quantile, there is no straightforward relationship. The standard deviation of a quantile may vary with the shape of the population distribution and the non-exceedance probability of the quantile. Use of asymptotic equations is only plausible when the sample size is larger than 50, as in the preceding discussion.

It is difficult to calculate degrees of freedom of the constructed test statistic for the quantile estimate. When testing the sample mean, the test statistic t^* (using the t-test, for example) is directly calculated from samples, and the degrees of freedom is $n-1$. However, the quantile (x_{1p} or x_{2p}) is indirectly calculated with distribution parameters estimated from samples, plus the standard deviation of quantile is estimated by a resampling method. It is impossible to explicitly relate the samples to the test statistic, and therefore, determining the degrees of freedom of the test statistic is challenging.

The use of the t-test to compare two sample quantiles is hindered since it is difficult to explicitly derive the quantile standard deviation and degrees of freedom. The comparison of confidence intervals is used as a compromise method to identify changes in quantiles. Using a resampling method to obtain M quantile estimates from each period of record, denoted as $\{x_{1p1}, x_{1p2}, \cdots, x_{1pM}\}$ and $\{x_{2p1}, x_{2p2}, \cdots, x_{2pM}\}$, the confidence intervals are represented as the interval between the $\frac{\alpha}{2}$ and $1 - \frac{\alpha}{2}$ percentile in each series. If these two confidence intervals do not overlap, these two quantiles are necessarily significantly different, at a significance level less than α.

It is acknowledged that this method is not a statistical test, but a substitutive method to identify significant difference. It is acknowledged that a significant difference may exist

when confidence intervals overlap, and for non-overlapped confidence intervals, the actual significance level is less than α.

For a special case when the standard deviation of the two quantiles are equal, and the sample sizes are large enough to use normal score to replace t score, it is possible to determine the significance level. In this case, $s_{1p} = s_{2p}$, and the Equation 3.9 is changed to

$$\bar{x}_{1p} - \bar{x}_{2p} > t_{\frac{\alpha}{2}}(s_{1p} + s_{2p}) = t_{\frac{\alpha}{2}}\sqrt{2}\sqrt{s_{1p}^2 + s_{2p}^2} = t_{\frac{\alpha'}{2}}\sqrt{s_{1p}^2 + s_{2p}^2} \tag{3.10}$$

where α' is the actual significant level for the comparison of confidence intervals, and $t_{\frac{\alpha'}{2}} = \sqrt{2}t_{\frac{\alpha}{2}}$. Using normal table, if $\alpha = 0.1$, then $\alpha' = 0.02$, and if $\alpha = 0.05$, then $\alpha' = 0.006$. The assumption of the equality between the standard deviations of estimated quantiles, and the use of normal score instead of t score are difficult to be tested. This study will continue to use the significance level of α and address that the actual significance level is less than α.

3.6 Results

The annual maximum 5min rainfall record at Windsor, plotted in Fig 3.5, is taken as an example to illustrate the confidence intervals comparison. After testing the stationarity in both periods of record ($p_1 = 0.186, p_2 = 0.581$, two-sided test), the Gumbel distribution parameters are estimated for each period. Further, the confidence intervals ($1 - \alpha = 0.9$) of 2 to 25-year quantiles are calculated with the resampling method. The quantiles and corre-

sponding confidence intervals are listed in Table 3.1. The results show that the confidence intervals for events of all return periods do not overlap, indicating changes have occurred in these design rainfall. These two periods of record, along with quantiles and confidence intervals, are also plotted in Fig 3.6, indicating the rainfall intensities are decreasing (at the nominal level of $\alpha = 0.1$).

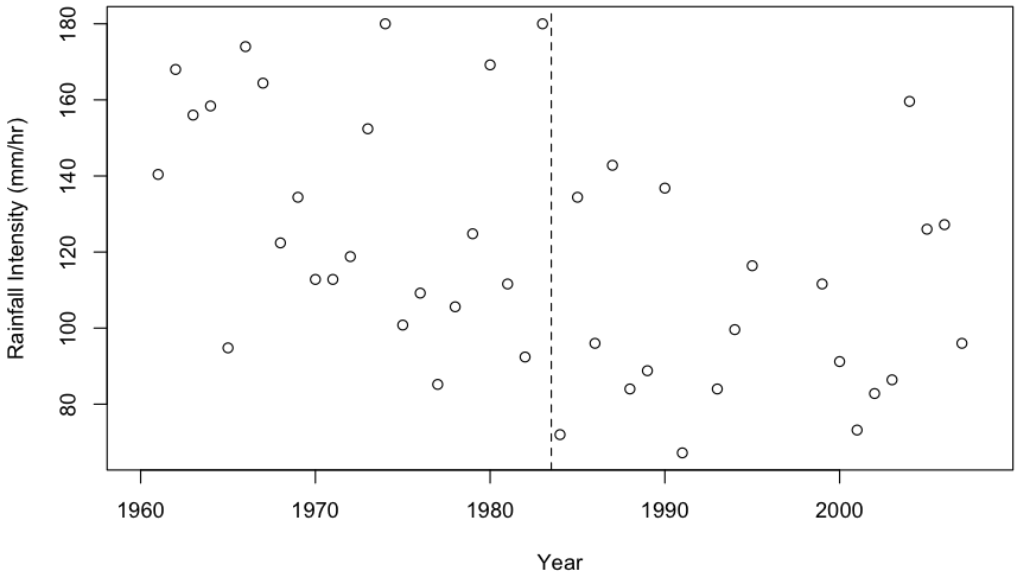

Figure 3.5: Annual Maximum Rainfall record for 5 min Duration at Windsor, ON

Table 3.1: Quantiles and Confidence Intervals for 5min duration record at Windsor (mm/h)

Return Period	1st Period			2nd Period		
	Upper Limit	Quantile	Lower Limit	Upper Limit	Quantile	Lower Limit
2-year	139.25	127.97	119.21	107.27	99.17	91.72
5-year	167.43	157.23	144.34	133.73	124.07	110.82
10-year	186.79	176.61	161.14	152.12	140.56	123.16
25-year	211.70	201.09	181.34	175.17	161.39	138.89

Table 3.2 summarizes the results of the CIs comparison test. The arrows and hyphens

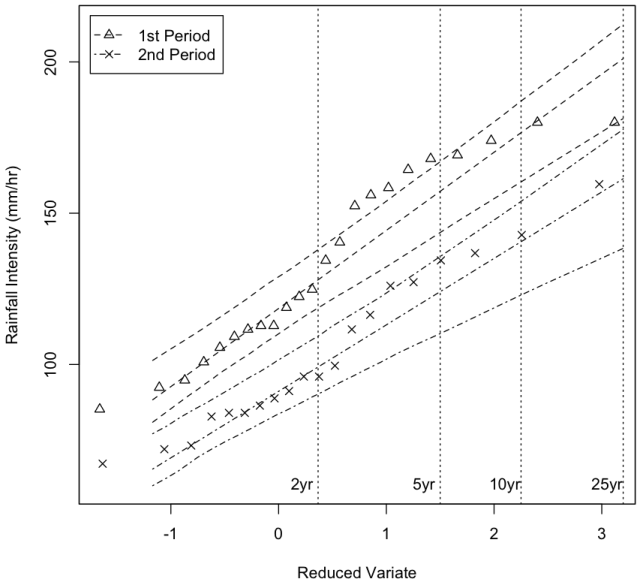

Figure 3.6: Confidence Interval Comparisons for 5min Rainfall Record at Windsor, ON

in cells represent the results of CI comparison of 2, 5, 10, and 25-year events. An up-arrow indicates an increase in rainfall intensity occurred in the 2nd period of record, and a down-arrow indicates a decrease in rainfall intensity. A hyphen means the CIs are not identified as significantly (at $\alpha < 0.1$ significant level) different. For example, the 2$^{\text{nd}}$ cell in the 13$^{\text{th}}$ row, which represents the results of CI comparison of the 5min record at Windsor, shows all down arrows ($\downarrow\downarrow\downarrow\downarrow$), indicating the quantiles for 2, 5, 10 and 25-year events are all decreased.

The results show that 2-year rainfall event magnitude at the Sioux Lookout rain gauge in northern Ontario has significantly increased after 1984, while the rest of the rain gauges in northern Ontario show no changes. In eastern Ontario, only the Belleville gauge (out of five gauges) demonstrates increases in heavy rainfall intensities. In central and south-western Ontario, most changes are recognized as significantly decreased. Four gauges, at

Windsor, Chatham, St. Thomas, and Toronto, identified significant decreases in magnitudes of rainfall events of various return periods. The Delhi gauge identified significant increases in heavy rainfall events over durations of 30min and 1h, as the only exception in this geographical area. Due to the low spatial density of rain gauges, it is difficult to conclude spatial trends of changes; nevertheless, the results provide an indication of regional changes in heavy rainfall magnitudes before/after year 1983.

3.7 Discussion

The changes in heavy rainfall intensities identified in this research are compared with evidence provided in the literature. Adamowski and Bougadis (2003) observed significant decreasing trends in short duration heavy rainfalls in southern Ontario, during the time period of 1970s to 1990s, which is consistent with the results presented in this research. However, the decrease in rainfall intensities in the St. Lawrence region identified by Adamowski and Bougadis (2003) was not observed in this research. Notice that the test of trends in rainfall records and test of rainfall intensity changes, as probability distribution quantiles are not identical. It is reasonable to observe inconsistencies between these two types of tests. Mailhot et al. (2010) conclude that change of extreme rainfall will emerge during the time period of 1985–2005. The claim of Mailhot et al. (2010) is supported in this research with many observations of changes in extreme rainfall that took place after 1983.

The results in Vasiljevic et al. (2012) show increases in 30 and 60min duration 5-year rainfall in southern Ontario, between the time periods of 1970–1984 and 1985–2003. This evidence is inconsistent with findings in this research. This inconsistency is due to: a) several heavy events took place during the 1960s, which are not included in the research of Vasiljevic et al. (2012); however, these events result in greater estimates of extreme rainfall intensities in the first time period in this research; b) Vasiljevic et al. (2012) use partial duration series to identify changes in extreme rainfall intensities; while, this research uses annual maximum series; c) this research uses 90% confidence level while Vasiljevic et al. (2012) uses 80%. That will result in a shorter confidence intervals, which identifies more cases of significant differences between quantiles estimates. A greater confidence level in quantile estimates will yield more conservative results, as shown in Table 3.2.

3.8 Conclusion

From the results of the distribution selection, five candidate distributions can all provide similarly accurate quantile estimates for annual maximum rainfall data. It is also shown that, for selected distributions, the boxplots of relative RMSE can provide a means of fitting to specific events over all durations and all gauges, and it is more focused on the accuracy of event estimates (e.g. events of 2 to 25-year return periods). The boxplot is capable of comparing all alternative distributions, by putting the boxes side-by-side and comparing central tendencies and dispersions. This is more visual than listing a table of correlation

coefficients.

The changes in extreme rainfall intensities in Ontario are identified, demonstrating that some gauges in central and southern Ontario have experienced decreases in heavy rainfall pre/post-1983. Increases in heavy rainfall are identified in gauges at Sioux Lookout and Belleville; however, there is not sufficient information to characterize regional changes in Ontario when using annual maximum series.

Table 3.2: Results of 90% Confidence Interval Comparison Test

ID	5min	10min	15min	30min	1h	2h
6034075	----	----	----	----	----	----
6037775	----	----	----	----	----	↑---
6057592	----	----	----	----	----	----
6085700	----	----	----	----	----	----
6100971	----	----	----	----	----	----
6104175	----	----	----	----	----	----
6105978	----	----	----	----	----	----
6116132	----	----	----	----	----	----
6131415	----	----	----	--↓↓	--↓↓	----
6131983	/	/	----	-↑↑↑	---↑	----
6136606	----	----	----	----	----	----
6137362	-↓↓↓	----	----	----	----	----
6139525	↓↓↓↓	/	↓↓↓↓	↓↓--	↓---	----
6142400	----	----	----	----	----	----
6144478	----	----	----	----	----	----
6148105	----	----	----	----	----	----
6150689	----	↑---	↑↑--	----	↑↑--	--↑-
6153301	/	----	----	----	----	----
6158355	-↓↓↓	-↓↓↓	----	----	----	----
6158733	/	----	/	/	/	/
6158875	----	----	----	----	----	----

*The arrows and hyphens in cells represent the results of CI comparison of 2, 5, 10, and 25-year events (from left to right). An up-arrow indicates an increase of rainfall intensity occurred in the 2nd period of record, and a down-arrow indicates a decrease of rainfall intensity. A hyphen means no significant change ($\alpha = 0.1$) is shown or, in other words, the CIs are not significantly different. Cells with slashes represent records that are not stationary.

*The name and location of climate stations are listed in Table 8.1

Table 3.3: Results of 80% Confidence Interval Comparison Test

ID	5min	10min	15min	30min	1h	2h
6034075	----	----	----	----	----	----
6037775	----	----	----	----	↑---	↑↑--
6057592	---↓	----	----	----	----	----
6085700	----	----	----	----	----	----
6100971	----	----	----	----	----	----
6104175	----	----	----	----	----	----
6105978	----	----	----	↓---	↓---	----
6116132	----	----	----	----	----	----
6131415	----	----	----	-↓↓↓	--↓↓	----
6131983	/	----	---↑	-↑↑↑	-↑↑↑	----
6136606	----	----	----	----	----	----
6137362	-↓↓↓	---↓	----	----	----	----
6139525	↓↓↓↓	/	↓↓↓↓	↓↓↓↓	↓---	↓---
6142400	----	----	----	----	----	----
6144478	----	----	----	---↓	----	----
6148105	----	----	----	----	----	----
6150689	↑↑--	↑↑--	↑↑↑-	↑---	↑↑--	↑↑↑↑
6153301	/	/	----	--↓-	-↓↓↓	----
6158355	↓↓↓↓	-↓↓↓	-↓↓↓	----	----	----
6158733	/	----	/	/	/	/
6158875	----	----	----	----	----	----

Chapter 4

Uncertainty Characterization of Rainfall Inputs Used in Design of Storm Sewer Infrastructure

Chapter 3 shows that changes in design rainfall intensities are evident. However, the comparison of the confidence intervals is highly related to the extent of the confidence intervals, i.e. the uncertainties associated with the statistical models. Therefore, this paper analyzes the uncertainties involved in the AMS model and related IDF curves. The climate stations used in this paper are the same as in chapter 3.

Two sources of IDF curves are discussed in this paper, the MSC IDF data file and the online search tool provided by the Ministry of Transportation Ontario (MTO). One amendment to this paper is that this paper was written in early 2013 and criticized MTO

IDF for not providing uncertainty information, while MTO updated their tools to provide uncertainty information in late 2013. This paper points out that the uncertainty associated in the IDF curves could be substantial, and needs assessment before being applied to the stormwater system design.

The uncertainties associated with estimates from the statistical models are analyzed in relation to the time period of the rainfall record. The paper shows that the extent of the confidence interval is linearly related to the log-transformed length of rainfall record. In the Province of Ontario, the circumstance is that most climate stations do not have sufficient length of rainfall record to generate rainfall intensities with a desirable level of uncertainty.

This paper demonstrates the necessity of assessing, and provided insight in the quantification of uncertainties in the design rainfall intensities.

4.1 Abstract

Intensity–Duration–Frequency (IDF) curves from which design rainfall magnitudes are developed, are constructed using rainfall predictions associated with different return periods and durations. However, the degree of confidence for estimates of rainfall rates as input for the design of stormwater infrastructure is influenced by the length and character of historical precipitation records. Relationships are assessed between the length of the period of historical record of rainfalls and uncertainties of predictions for different confidence levels, using both analytical and resampling methods. The uncertainty in IDF curve regression is

also analysed.

The correlation between the log-transformed lengths of the record and the ratios of the standard deviations of predictions are determined to be high, allowing a linear regression model to be developed to characterize the 95% confidence intervals. Based on 20 rain gauges in Ontario, it is estimated that to achieve a 95% confidence interval as small as 10% of the predictions, at least 49, 62, and 73 years of records are needed for 5, 10, and 25-year recurrence events respectively. Considering that record lengths of rain gauges are mostly < 50years, the challenges to accurately estimate the event magnitudes are substantial. This underscores the importance of considering uncertainties when using design rainfall rates based on available records.

Further, an example of non-linear regression between the IDF estimates and confidence intervals and rainfall durations shows the possibility of underestimating design rainfall intensities. This raises awareness of uncertainties when selecting design rainfall rates.

4.2 Introduction

Rainfall is one of the most important inputs in stormwater infrastructure design, to determine the conveyance capacity needed for the stormwater system. The rainfall input may be a rainfall event obtained from the historical record characterized from several decades of historical events, or a storm generated from the IDF curves, combined with a selected rainfall distribution (e.g. a triangular distribution).

Uncertainty of a design rainfall arises since the rainfall intensities are not known with certainty; there is a range of values. This range is typically represented as a confidence interval. Thus, it is important to consider the confidence intervals as well as the design rainfall intensities. Use of the upper confidence limit is more conservative in stormwater design, although this approach may increase the cost due to the extra capacity needed for conveying the predicted stormwater flows. When dealing with uncertainties, the selected design rainfall intensity should be a balance between cost and risk of being more frequently exceeded; a smaller range of uncertainty is helpful to ensure the design performs as intended.

For Ontario, IDF curves are available from two sources: the IDF database from the Ontario Ministry of Transportation (MTO) and the IDF data file from Environment Canada (EC). MTO's IDF database provides estimated rainfall depth and intensities, and the regression coefficient values for the equations. MTO's IDF curves are remarkably localized—they are available at locations that don't have rainfall gauges, which implies spatial interpolation has been employed. However, the MTO's IDF curves are not provided with information on uncertainties.

The EC IDF data files contain more information in comparison with the MTO's IDF database, although EC IDFs are only at locations at which there are rain gauges. EC IDF data files include the Quantile–Quantile plot for distribution fit, and event estimate graphs, based on historical records at a rainfall gauge. The annual maximal rainfall intensities over various durations are also provided, together with the estimates of events for return periods from 2-year through 100-year. The confidence intervals for the event estimates are

also supplied, at the confidence level of 95%, two-sided. The regression coefficients for each of these IDF curves are also available. With the data provided, users are immediately advised about the magnitudes of the uncertainties, and capable of fitting rainfall records with alternative probability distributions and quantifying the uncertainties.

An issue is raised when examining the confidence intervals related to storm durations. EC's IDF curves provide confidence intervals for durations of 5 min, 10 min, 15 min and 30 min and for 1 h, 2 h, 6 h, 12 h and 24 h. However, the design rainfall for stormwater system design could be over any duration $\leq$ 2 h, depending upon the hydrologic characteristics (e.g. time of concentration) of the catchment. The confidence limits are needed to compare with expected values, to be confident of the design rainfall selected. Therefore, interpolation or regression of the confidence intervals is necessary, in addition to the regression of the expected values of design rainfall intensities.

The intensities and confidence intervals used for IDF regression are usually estimated by parametric methods, including fitting a probability distribution to extreme rainfall data series, and estimation of the extreme event intensities for selected exceedance frequencies. Uncertainties are introduced into estimated intensities generated from both modelling error and sampling error involved in parametric methods, and further introduced into IDF curves and design rainfalls.

The uncertainties in design rainfalls sometimes could be very large. As an example, Figure 4.1 illustrates the IDF curves for Waterloo, Ontario. The cautionary note in the upper right corner indicates the large range of the confidence intervals. The 10 years return

period event of 1h duration rainfall is estimated to be $45.1mm/h$ as an expected value, with a 95% confidence interval of $\pm 9.9mm/h$, which is almost $\pm 20\%$ of the expected value. Consequently, designers are looking at a design rainfall intensity which could be anywhere from $35.2mm/h$ to $55mm/h$, reflecting the 95% confidence interval. In response, one pos-

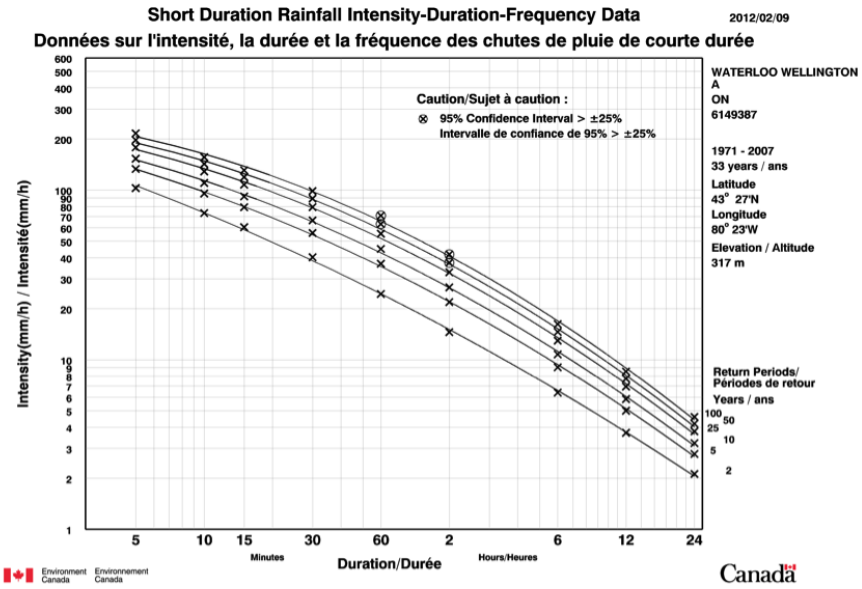

Figure 4.1: IDF Curves for Waterloo, Ontario. (Publicly available from Environment Canada)

sibility is to have a longer record, which would reduce the uncertainties in design rainfall estimates by reducing sampling error; the length of the rainfall record needed to achieve a specified degree of certainty in design rainfall estimate should be determined as well. However, a lengthy record may contain temporal trends or step changes. It is not always appropriate to use the longest record, as the current climate storms are suspected to be different from decades or hundreds of years ago.

Of interest is to develop the relationships between the width of confidence intervals

for design rainfall versus the length of the rainfall record, to quantify the length of record needed to achieve specific uncertainty or to determine the magnitude of the uncertainties given the available historical period of record. Further, this paper develops the relationships between the design rainfall confidence limits and the rainfall durations of the same return period, to provide the confidence limits for selection of the design rainfall for a given design storm duration.

4.3 Literature Review

The uncertainties in extreme rainfall event estimation have been analyzed in research to investigate the impact of climate change (Fowler and Kilsby, 2003; García-Ruiz et al., 2000; Coles et al., 2003) and to estimate the impact of uncertain input to stormwater system design (Aronica et al., 2005; Semadeni-Davies et al., 2008). However, the relationship between uncertainties in the estimation of extreme event intensities and record length have not been comprehensively investigated. Rauch and de Toffol (2006) investigated six rainfall series in Austria to assess the length of the rainfall series required to estimate extreme rainfall and associated uncertainties, of 1-year return period events with 15 min duration. The rainfall intensities are estimated based on segments of the historical record, with the lengths of 1, 10, and 20 years. In Rauch and de Toffol (2006), a correlation is observed between the magnitude of uncertainties (expressed as the ratio between the width of the 90% confidence interval and the expected value using the entire record) and the length of

segments of the historical record. It is suggested to use ≥ 10 years record to estimate a 1-year event. Use of the longest available record is not always recommended, as increasing record length might be influenced by temporal trends. Rauch and de Toffol (2006) only tested the 1-year return period rainfall over 15 min duration, which cannot demonstrate all the characteristics of all extreme rainfall events; this relationship between uncertainties in the estimation of extreme event intensities and the record length needs to be thoroughly investigated.

4.4 Methodologies

The uncertainty of design rainfall in this research is represented as the confidence interval at the confidence level of 95%. There are two methods to describe the relationships between the length of the rainfall record and the confidence intervals: the analytical method and the resampling method. In both methods, the sample sets are fitted with the Gumbel distribution using L-moments (Hosking and Wallis, 1997, Chapter 2). In the analytical method, the variance of the rainfall estimate is calculated by the asymptotic method (after Stedinger et al., 1993).

$$Var(\hat{x}_p) = \frac{\alpha^2[(1.1128 - \frac{0.9066}{n}) - (0.4574 - \frac{1.1722}{n})y + (0.8046 - \frac{0.1855}{n})y^2]}{n-1} \qquad (4.1)$$

where $y = -\ln(-\ln(\frac{1}{T}))$ is the reduced variant for the Gumbel distribution; T is the return period in years. α is the scale parameter for the Gumbel distribution. n is the sample size.

The confidence interval is:

$$CI = \hat{x}_p \pm z\sqrt{Var(\hat{x}_p)} \tag{4.2}$$

where z is the normal score for a given significance level.

The rainfall intensity is estimated by the inverse of the cumulative distribution function of the Gumbel distribution, Equation 4.3, with scale (α) and location (ξ) parameters, for non-exceedance probability p

$$\hat{x}_p = \xi - \alpha \ln - \ln p = \xi + \alpha y \tag{4.3}$$

In this research, the uncertainty is characterized as a percentage of the width of the confidence interval compared to the expected value.

$$\frac{CI - \hat{x}_p}{\hat{x}_p} = \pm z\frac{\sqrt{Var\hat{x}_p}}{\hat{x}_p} = f(n, y; \xi, \alpha) \times 100\% \tag{4.4}$$

Note that the percentage is a function of the sample size (n) and the reduced variant (y), which is a function of the return period (T). Therefore, for a specified return period, the magnitude of uncertainty is only determined by the sample size, which equals the length of the record when using annual maxima. With the analytical method, the relationship between the record length and the uncertainties can be computed using Equation 4.4.

With the resampling method, the relationship is characterized 100 times using similar

procedures to those used in the analytical method based on resampled datasets. First, 5000 values are synthesized using the Gumbel distribution to form a large dataset (A). Second, 100 values are randomly selected from this dataset A, to construct an annual maximum rainfall record (B) over 100 years. Third, the first 10 values in this record B are assumed as a sample set (C) (a sample size <10 is expected to have large sampling error, defined as the variance of the sample). Fourth, the sample set C is fitted with the Gumbel distribution to calculate the percentage of the 95% confidence interval compared with the event estimates for return periods of 2, 5, 10, and 25-year. The third step is repeated by including the next value from the record B into the sample set C until the sample size reaches 100. Subsequently, the percentages are plotted against the log-transformed size of the sample set C taken from the record B. Finally, steps two through four are repeated 100 times, with results as plotted in Figure 4.2, and compared with the curve developed by the analytical method.

The relationship between the log-transformed record length and the percentages of the confidence intervals is depicted in Figure 4.2 (the solid black curve is the analytical method of Equation 4.4). The figure demonstrates that the relationship is approximately linear, especially for the segment between 20 and 100 years of record. The 100 trials of the resampling methods are also drawn in Figure 4.2 (the dashed grey curves), and compare favourably with the analytical method (the solid black curve).

In Figure 4.2, the resampled curves (the grey curves) scatter over a large range when the record length is <20 years, and are in immediate proximity to the analytical curve as

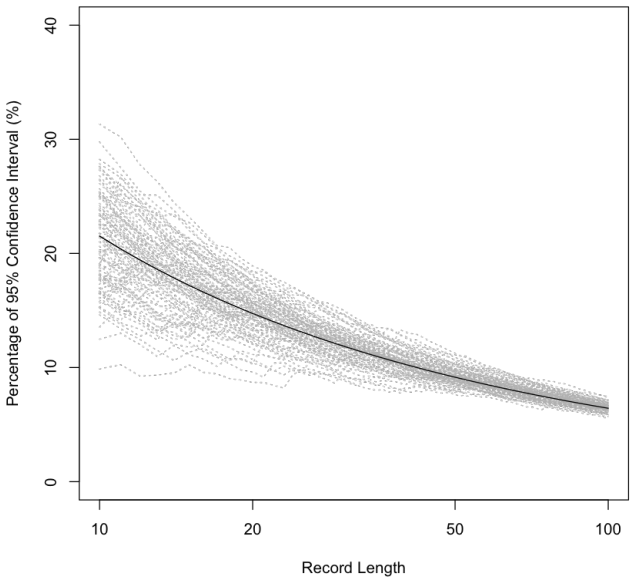

Figure 4.2: Analytical and Resampling Methods for the Relationships between the Record Length and the Uncertainties for Wvents of 10-year Return Period

the record length increases. In addition, the resampled curves are distributed evenly around the analytical curve. Therefore, these resample curves are valid as good estimates of the relationships between uncertainties and record lengths. For 100 repetitions, the resampled curves show considerable density close to the analytical curve, and the relationship is obvious. There is no necessity of more repetitions to make it denser.

Steps three and four in the resampling method are used to draw the relationships between record length and uncertainties in the historical record (used as data set B). A least squares linear regression is applied to model this relationship, and extrapolated to get the minimum record length needed to achieve a specific percentage of uncertainty.

To verify the minimum record length, a bootstrap method was applied to the historical record. In the bootstrap method, the historical record is assigned as the population (dataset

A), and the dataset B is randomly selected (with replacement for 50 or 100 repetitions) with length calculated from the linear regression model. The dataset B is directly used to fit to the Gumbel distribution and estimate the confidence intervals, and the percentage of the width of the confidence interval against the expected value is calculated as well. The mean of the percentages in each repetition is compared to the desired percentage to check the minimum record length estimate.

The nonlinear regression of IDF curves and their confidence intervals are developed, and compared with the linear regression available from EC's IDF files. The non-linear equation used for the IDF curves is

$$I = a(t + c)^b \tag{4.5}$$

where I is the design rainfall intensity in mm/hr, a, b, c are coefficients to be optimized by the least-squares method, and t is rainfall duration in hours.

Further, the regression functions for the upper and lower confidence limits are developed using Equation 4.5, by substituting the intensity with the upper or lower limits, I_{Upper} and I_{Lower}.

4.5 Data Description

Twenty-one rainfall gauges with lengthy records (30 years or longer) are used in this research, with location and length as listed in Table 4.1. These records include daily max-

imal rainfall amount over durations of 5, 10, 15, and 30 min and for 1, 2, 6, 12, and 24 h. Rainfall rates recorded between April 1st and October 31st are used to emphasize summer storm characteristics, and a yearly record will be excluded if missing more than 20% of data for the seven months record of a year. Annual maximum data series are extracted and utilized in the analysis of relationships between the record length and the uncertainties of rainfall estimates. The non-linear regression analysis of the design rainfall estimates and confidence intervals uses data in the EC IDF data files.

4.6 Results and Discussion

The 1 h duration historical record at Kingston is analyzed as an example. As shown in Figure 4.3, the relationship for the 25-year event fluctuates when the record length increases from 10 to 20 years, but the percentages are gradually reduced to 13% when using the entire record of 45 years.

The linear regression for the percentage (r) of 95% confidence intervals and the length of the record (l) is expressed in Equation [6], based on the segment of curve from 20 to 45 years.

$$r = 45.66 - 8.64 \log l \tag{4.6}$$

The slope and the correlation coefficient are both significant at $p < 0.001$.

Using Equation 4.6, the minimal length of the record for Kingston needed to achieve a

Table 4.1: Record Lengths and Percentages of Uncertainty of Rainfall Gauges in Ontario

ID	Years	Record Length Needed $			Actual Percentage #		
		5-year	10-year	25-year	5-year	10-year	25-year
6158355	65	53	67	81	9	10.4	11.9
6137362	43	59	81	99	10.5	12.2	14.1
6139525	43	44	51	59	10.5	12.2	14.2
6150689	41	41	57	74	10.1	11.8	13.8
6105978	42	41	53	65	9.7	11.4	13.4
6144478	46	48	61	74	10.3	11.9	13.8
6142400	42	59	69	78	13.2	14.8	16.7
6104175	45	40	51	62	9.5	11.1	13.0
6158733	46	50	65	79	10.2	11.8	13.7
6153301	39	27	42	59	8.7	10.5	12.5
6057592	37	53	66	79	11.5	13.4	15.4
6131983	39	43	50	57	11.1	12.8	14.9
6131415	35	82	116	136	11.7	13.6	15.7
6116132	30	48	54	61	15.5	17.4	19.6
6037775	33	136	148	151	12.9	14.9	17.1
6085700	34	48	60	71	11.6	13.5	15.7
6148105	33	59	68	77	13.8	15.7	17.9
6100971	34	59	70	81	12.7	14.6	16.8
6034075	33	44	50	57	13.6	15.5	17.7
6136606	31	38	45	53	11.7	13.7	16.0
6158875	32	43	49	56	12.9	14.8	17.1

*The name and location of climate stations are listed in Table 8.1

$ This is the record length needed to achieve a 95% confidence interval whose width is 10% of the predictions.

This is the percentage of the width of a 95% confidence interval to the predictions when using all available rainfall records.

* The percentages of the 95% confidence interval for all events at Sioux Lookout A do not decrease as record length increases. This results in a very flat linear regression and the slope equal to zero is not rejected. Thus, very large record lengths are calculated by extrapolation.

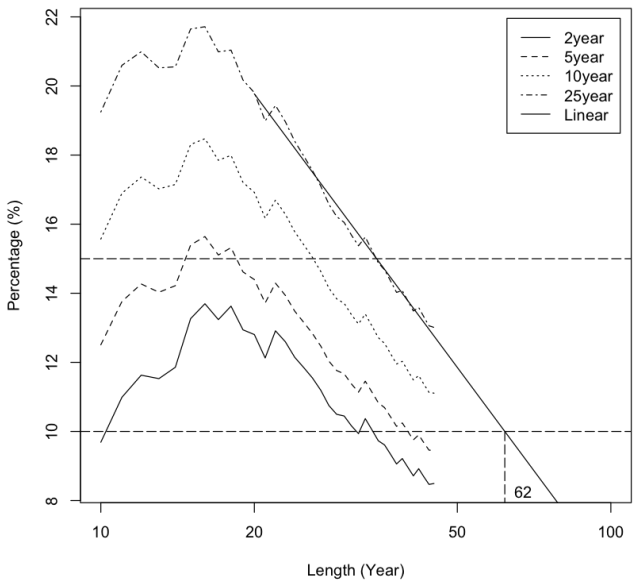

Figure 4.3: Relationship at Kingston between the Percentage of the 95% Confidence Interval and the Record Length.

95% confidence interval as small as $\pm 10\%$ of the prediction is $exp(\frac{45.66-10}{8.64})$, or 62 years.

The bootstrap method is used to check this estimate of record length. Fifty and 100 sets of 62 values are randomly selected from the historical record, with replacement, and fitted to the Gumbel distribution. The 25 y event intensity is estimated using Equation 4.3 for each set of values. The mean, variance, and 95% confidence limits are estimated based on these 50 and 100 estimates, assuming the normal distribution. The percentage of the magnitude of the confidence interval to compare to the mean is obtained from Equation 4.4. This bootstrap method gives a percentage of 10.7% for 50 sets of values, and 9.4% for 100 sets of values. Hence, good agreement is observed between the analytical method and the resampling method, indicating that the assessment of the required record length as 62 years is valid.

Table 4.1 lists information about the 21 rain gauges, including the record length available and the percentage of 95% confidence interval compared to predictions based on the entire record (one hour duration). The lengths needed to achieve the 95% confidence interval as low as 10% of the predictions for 5, 10, and 25-year events separately, are listed therein. Excluding the gauge at Sioux Lookout A (at which gauge the slope of the linear regression function is not rejected as equaling zero, one possible reason is that more outliers or other kinds of wild data are included as expanding the record length), it is calculated that the average length of record needed to achieve a 95% confidence interval as low as 10% of the prediction is 49, 62, and 73 years for return periods of 5, 10, and 25-year respectively. Considering that the average record length is 40 years for the remaining 20 gauges, it is strongly recommended to consider the uncertainties of rainfall intensity estimates when selecting design rainfall from these IDF curves, because otherwise the design rainfall is at risk of being significantly underestimated.

Table 4.2: Five-Year Event Estimates and 95% Confidence Intervals at Waterloo

Duration	Intensity (mm/h)	95% Confidence Interval
5 min	153.3	±24.1
10 min	110.4	±17.7
15 min	91.9	±15
30 min	66.4	±12.5
1 h	45.1	±9.9
2 h	26.7	±5.8
6 h	10.8	±2.1
12 h	5.9	±1
24 h	3.2	±0.5

The 5-year event IDF curve at Waterloo is employed as an example to explain the im-

portance of using confidence intervals as well as expected values. The expected values and 95% confidence intervals are obtained from EC's IDF files, and listed below in Table 4.2. The EC regression equation is shown in Equation 4.7 as a benchmark, which is a linear regression between the intensities (I) and the log of durations (t) in hours.

$$I = 30t^{-0.691} \tag{4.7}$$

The non-linear regression using Equation 4.5 becomes,

$$I = 36.6(t + 0.07)^{-0.685} \tag{4.8}$$

Both of these equations are plotted in Figure 4.4, and demonstrate the expected values and 95% confidence intervals for events over nine durations of storms.

In Figure 4.4, the EC regression equation (Equation 4.7) is close to the lower confidence limit of rainfall events at durations of 30 min, 1 h, and 2 h. Therefore, if a hydrologic model uses design rainfall over 90 min duration, it is in fact using an intensity that is close to the lower confidence limit. Further, there is a 95% chance that this event will be exceeded more frequently than once every 5 years on average. The non-linear regression equation is not perfectly fitted to data beyond 2 h duration. This should not be a concern, since the time of concentration in urban stormwater system design are usually less than 2 hours.

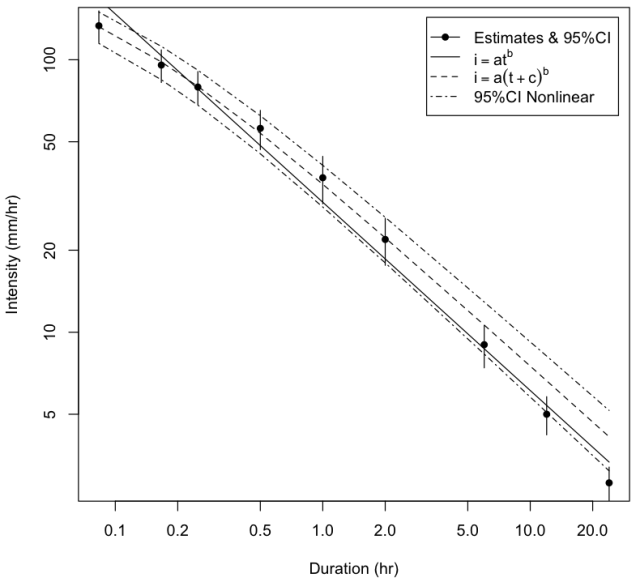

Figure 4.4: IDF Curve for 5-Year Event at Waterloo

4.7 Conclusion

A linear relationship is observed and modeled between the uncertainties (in the form of the percentage of the 95% confidence intervals, compared with the expected values) and the record length. Using this linear relationship, it is possible to quantify the record length needed to achieve a specified uncertainty; for example, the width of a 95% confidence interval that is $<$10% of the expected value. With the record lengths quantified, modelers are better aware of uncertainties in rainfall intensities estimated from records with limited durations.

The uncertainties of extreme event predictions are constrained by the length of the historical record. It is difficult to provide a confident estimate of the 100-year event based on a record of 40 or 50 years. This situation is a very common circumstance for Ontario.

Stormwater infrastructure design is, in fact, dealing with heavy rainfall intensities involving a very large extent of uncertainties. Using the expected value does not incorporate the uncertainty in the estimation of the rainfall intensities which are used for design of stormwater infrastructure.

The design rainfall intensities obtained from the IDF curve regression equations may be exceeded more frequently than the design return period. Modelers should compare these intensities with the corresponding confidence intervals to decide which of the intensities (the upper confidence limit or the interpolated expected value) should be used in modeling.

Chapter 5

Performance Comparisons of Partial Duration and Annual Maxima Series Models for Rainfall Frequency Analysis of Selected Rain Gauge records, Ontario, Canada

This paper demonstrates the advantages of using Partial Duration Series (PDS) instead of Annual Maximum Series (AMS) in rainfall intensity modeling, and a complete procedure to develop the PDS model for selected rain gauges in southern Ontario. This paper uses the same set of climate stations as the two preceding papers.

This paper explains the theoretical difference between the event-based model and the annual-based model, and clarifies the relationship between the recurrence interval of a given event and the non-exceedance probability in the cumulative frequency distribution. These are important theoretical bases and major contributions in this thesis.

This paper introduces approaches for developing PDS models (the PDS-E in this paper), including the selection of thresholds, the sensitivity to missing values, the selection of frequency distributions, and quantile and confidence interval estimates. This paper shows that the PDS model produces larger rainfall intensity estimates than the AMS model, and is more pertinent for stormwater infrastructure design of frequent rainfall events. The paper shows that the uncertainties associated with the PDS model is considerable and needs improvement.

5.1 Abstract

To assess the advantages of rainfall frequency models based on Partial Duration Series (PDS) in comparison with models based on Annual Maximum Series (AMS), rainfall records from 21 rainfall gauges in Ontario are examined. A procedure to develop the PDS Event-based model (PDS-E) is derived, showing sensitivities to missing values, selection of thresholds, and quantile and confidence limit estimates.

The true values of 2 and 5-year return period design rainfall intensities are 10% and 3% greater in PDS than in AMS data on average, which indicates the necessity of using

PDS data and the event-based model for frequent event modeling, instead of the annual-based model. The accuracy of PDS-E estimates of design rainfall is sensitive to the exceedance threshold; and for an elevated threshold, which improves the model accuracy, the PDS-E estimates of 1h duration and 5-year return period events is 3.5% greater than AMS model estimates. Nevertheless, the 2-year return period design rainfall estimates are mostly greater for the PDS-E than in AMS model.

The PDS-E is demonstrated to be more pertinent for stormwater infrastructure design of frequent rainfall events. The exceedance threshold needs to be assessed with respect to sensitivity of accuracy of estimate and extent of uncertainty, and the model accuracy needs further improvement.

5.2 Introduction

Predictions of design rainfall intensities are critical inputs for design of urban stormwater systems. Traditionally, the Annual Maximum Series (AMS) has been used for generating Intensity–Duration–Frequency (IDF) curves and ultimately, to determine the design capacity of infrastructure for stormwater management. However, another data series pertinent to frequency analysis is the Partial Duration Series (PDS).

A PDS is a data series extracted from the historical record by selecting rainfall events exceeding a certain threshold (x_T) with corresponding time of occurrence. The PDS data series are also referred to as Peaks–Over–Threshold (POT). The magnitude of exceedance

of PDS is usually modeled either by Exponential distribution (EP) or Generalized Pareto distribution (GPA); and the arrival rates (the number of exceedances in each year) are modeled as a Poisson process, or negative binomial distribution; and the length of time between exceedances are commonly modeled by the Exponential distribution as well.

The PDS model (models generated using PDS data) has rarely been used in practice for design of stormwater management systems, although the PDS of flood records have been analyzed to estimate flood frequency and event magnitudes. Todorovic and Zelenhasic (1970) developed models of flood count (the number of flood occurrences in each time interval) and flood magnitudes based on flood records for the Susquehanna River. Later, Todorovic and Rousselle (1971) expanded this model to include seasonal differences, and achieved fairly good agreement between observed and theoretical results. Cunnane (1979) judged the validity of the Poisson process on data from gauges in Great Britain, and concluded that when all data are considered jointly, the number of occurrences in each year does not follow the Poisson process. Madsen et al. (1994) modeled the total rainfall depth and the maximum 10min rainfall intensity of individual storms with PDS based on rainfall records in Denmark. Madsen et al. (1995) further developed a regional Bayesian approach to provide estimates of T-year events (events which will be exceeded in one year amongst every T years on average) with less uncertainty compared to estimates using only at-site data, and also provided estimates at non-monitored sites. Trefry et al. (2005) also applied a PDS/GPA model for regional rainfall frequency analysis for the State of Michigan, and used the predictions for events with recurrence intervals of less than 10 years.

For frequent events (recurrence interval less than 10 years), Laurenson (1987) argued that AMS recurrence interval could be misleading, and suggested using PDS and recurrence interval (same magnitude as return period) concepts. By using AMS, the recurrence interval is the average period between years in which a given value is exceeded, regardless of the number of exceedances in any one year. However, when using PDS, recurrence interval is the average period between individual exceedances within a given period of time. Laurenson (1987) agreed that the annual exceedance probability is the reciprocal of the recurrence interval of the AMS, although the reciprocal of PDS recurrence interval is "not the probability of anything". Therefore, Laurenson (1987) did not apply conventional probability analyses on PDS, and required that the probability of exceedances must be "within a given period of time" — such as the probability of a given value being exceeded in a year.

The AMS model (statistical model generated with AMS data) predicts the return period between years in which a given rainfall intensity is exceeded; or conversely, predicts the rainfall intensity that will be exceeded with a given return period on average (or a given annual exceedance probability, dimensionless). The AMS model is not concerned with the number of exceedances within a year, which is reasonable when modeling extreme events (e.g. 100-year return period storm) but misleading when dealing with frequent events. Laurenson (1987) selected a 10-year return period as a dividing line between extreme events and frequent events. Hereafter, AMS model is also called the annual-based model.

The PDS model predicts the return period between exceedances of a given rainfall intensity, or the rainfall intensity that will be exceeded with a given return period on average.

The PDS model is a probability model of the exceedance magnitudes, although the probability needs to be adjusted according to the number of events in PDS and the number of years in the rainfall record being used. The PDS model can characterize frequent events, even when the return period is shorter than one year. The PDS model is hereafter called Event-based model, or PDS-E, since it is related to the occurrence frequency of a given event. If the arrival rate of events is modeled together with the PDS model to map to annual exceedance probability, it is an annual-based model similar to the AMS model, and is referred to as PDS annual-based model, or PDS-A.

If PDS and AMS data extracted from the same rainfall record are sorted in descending order, the PDS have values greater than, or equal to, the value at the same rank in the AMS, because the PDS may include heavy events excluded in the AMS. With the same given rainfall intensity, there may be more events in the PDS exceeding this intensity than in the AMS; thus, the recurrence interval of exceedances of the given intensity in the PDS is shorter than or at least equal to the recurrence interval in the AMS (they are only equal when the PDS and the AMS have the same number of storms greater than the given intensity). Conversely, for the same recurrence interval, the given rainfall intensity in the PDS is greater than or equal to that in the AMS. The "given rainfall intensity" is estimated with statistical models and referred to as the design rainfall in municipal infrastructure design. Correspondingly, the true value of the PDS-E estimate is greater than or equal to that of the AMS model estimate, for the same return period.

Besides the greater true value of design rainfall and shorter recurrence interval, there

are advantages arguing for use of PDS-E. Firstly, the flexibility of a PDS-E makes the model versatile to deal with different frequency analysis tasks. Selecting a higher threshold to extract PDS from rainfall record would allow better fitting of a distribution for extreme events, and a lower threshold could reduce sampling variances. Secondly, the PDS model can be adjusted for circumstances of missing data, compared to the AMS model. In the AMS model, it is not necessarily reliable to take the recorded maximal event as the maximum of a year, when there are many missing values in a year. However, in the PDS model, any event that has intensity greater than the threshold would be utilized in developing the data series, regardless of how many values are missing in that year (although it is acknowledged that it is difficult to conduct any statistical analysis if there are too many missing values).

A threshold is required to extract PDS, and there is no general consensus with respect to how the threshold should be selected (Ashkar and Rousselle, 1983a, 1987). Rainfall events in PDS are required to be independent and identically distributed.

The PDS-A, as an annual-based model, estimates a true value smaller than that of the PDS-E model. The PDS-A involves more sources of uncertainty since fitting the arrival rate to the Poisson distribution introduces model errors. Cunnane (1973) compared the variances of predictions given by both an AMS model and a PDS-A, and points out that the PDS-A requires a sample set at least 1.65 times that of the AMS model to achieve the same accuracy. This conclusion, especially the scale of 1.65, is referred to in studies such as Tavares and Silva (1983); Rosbjerg (1985); Buishand (1989); Wang (1991).

5.3 Study Objective

To demonstrate the advantages of the PDS event-based model, this paper theoretically proves, for a given return period, the true value of the design rainfall for PDS-E is greater than that for AMS or PDS-A. It also clarifies the relationship between the return period and non-exceedance probability in statistical distribution modeling. Further, based on rainfall records of 21 rainfall stations in the Province of Ontario, this paper introduces the details of establishing the PDS-E, including sensitivity analysis to missing values, methodologies to select thresholds, probability distribution fitting, and estimation of quantiles and variances. The PDS-E estimates of design rainfall are compared with the AMS model in relation to model precision and accuracy.

5.4 Event-Based Model and Annual-Based Model

5.4.1 Event-based Model and Return Period

As introduced in Laurenson (1987), the return period of partial duration series is the average period of time between exceedances; while, the return period of annual series is the average period of time between years in which the given event is exceeded. In annual series the number of events is always equal to the number of years in rainfall records. Therefore, the reciprocal of the return period (1 year in T years return period) is a dimensionless value and equals the exceedance probability of the design rainfall intensity in the Cumulative Distribution Function (CDF) of the annual series. A problem arises when using partial

duration series. The reciprocal of the return period has dimension (1 event in T years), and the exceedance probability of the event intensity is related to the number of events in the partial series, which is further related to the arbitrary threshold used to extract partial series. To solve this problem, the average arrival rate (λ) is used to convert the reciprocal of the return period to a dimensionless value and be related to the exceedance probability in the CDF. It is explained more precisely as follows.

Denote a PDS extracted by threshold x_T from N years of rainfall records as $\{x_1, x_2, \cdots, x_n\}$, which has a true CDF of $F_P(x)$. The average annual arrival rate λ is estimated by n/N (events per year). In PDS, the exceedance probability of an intensity x is described as $Pr\{x_i \geq x\} = 1 - F_P(x)$.

The exceedance probability for intensity ${x_T}'({x_T}' > x_T)$ is $1 - F_P({x_T}') = \frac{n'}{n} = \frac{n'/N}{n/N} = \frac{\lambda'}{\lambda}$ (dimensionless), where n' is the number of values in PDS exceeding ${x_T}'$. The reciprocal of the return period, T_p, for given intensity (${x_T}'$) is

$$\frac{1}{T_p} = \lambda' = \lambda[1 - F_p({x_T}')] \text{ (Events per year)} \tag{5.1}$$

Then the reciprocal of return period and the exceedance probability are related in PDS. Further, the non-exceedance probability of a given value is $F_P({x_T}') = 1 - 1/\lambda T_p$.

5.4.2 Annual-Based Model and Return Period

For the AMS model, the return period (T_a) and the exceedance probability are directly related as Equation 5.2

$$\frac{1}{T_a} = 1 - F_A(x_T) \text{ Dimemsionless} \tag{5.2}$$

where $F_A(x)$ is the CDF of the AMS data. The non-exceedance probability of a given value is $F_A(x_T) = 1 - 1/T_a$.

For the PDS-A model, to model the number of occurrences of exceedances in any year, the Poisson distribution with parameter λ'' is used as in Equation 5.3.

$$P(\kappa; \lambda'') = e^{-\lambda''}\lambda''/\kappa!, \kappa = 0, 1, 2 \cdots \tag{5.3}$$

The parameter λ'' is estimated as the average arrival rate of exceedances of the design value in PDS-A. The probability of having no arrivals in a year is $P(0; \lambda'') = e^{-\lambda''}$.

Thus, the annual exceedance probability for the T_a-year return period is calculated as given in Equation 5.4.

$$1 - e^{-\lambda''} = 1/T_a \tag{5.4}$$

To find the design value (x''_T) and exceedance probability ($1 - F_P(x''_T)$) in PDS-A, the λ'' in Equation 5.4 is isolated and substituted into Equation 5.1 as λ', which is as given in

Equation 5.5.

$$\lambda[1 - F_p(x''_T)] = \frac{1}{T_p} = \lambda' = \lambda'' = -\ln 1 - \frac{1}{T_a} = \ln \frac{T_a}{T_a - 1} \tag{5.5}$$

And the non-exceedance probability of a given value is $F_P(x''_T) = 1 - \frac{1}{\lambda} \ln(\frac{T_a}{T_a - 1})$.

To summarize, given a return period T, the non-exceedance probability in CDF of PDS-E is $1 - 1/\lambda T$, of AMS model is $1 - 1/T$, and of PDS-A is $1 - \frac{1}{\lambda} \ln(\frac{T}{T-1})$.

5.4.3 Difference in the True Value of the Design Rainfall

The true value of the design rainfall is interpolated between two observations having probability plotting positions closest to the non-exceedance probability. The ranks of values being interpolated in AMS model and in PDS-E are the same, while the values in PDS-E are greater than or equal to those in AMS model, as aforementioned. Therefore the true value of the design rainfall in PDS-E is greater than or equal to that of the AMS model.

Given the fact that $1/T > \ln(T/(T-1))$, the non-exceedance probability of PDS-E is constantly greater than that of PDS-A. Using the same PDS data, the true value of the design rainfall of PDS-E is greater than that of the PDS-A.

The relationship between true values of the design rainfall of the AMS model and the PDS-A is determined by two factors: the extra heavy events in PDS data results in larger ranked values, and the smaller non-exceedance probability in PDS-A that results in smaller interpolation. These two counter-acting factors vary from case to case, and make the incon-

sistent relationships between true values of the design rainfall of AMS model and PDS-E, as per Fig. 5.1. Consequently, the widespread impression that the PDS annual-based model should give greater predictions than the AMS model is incorrect.

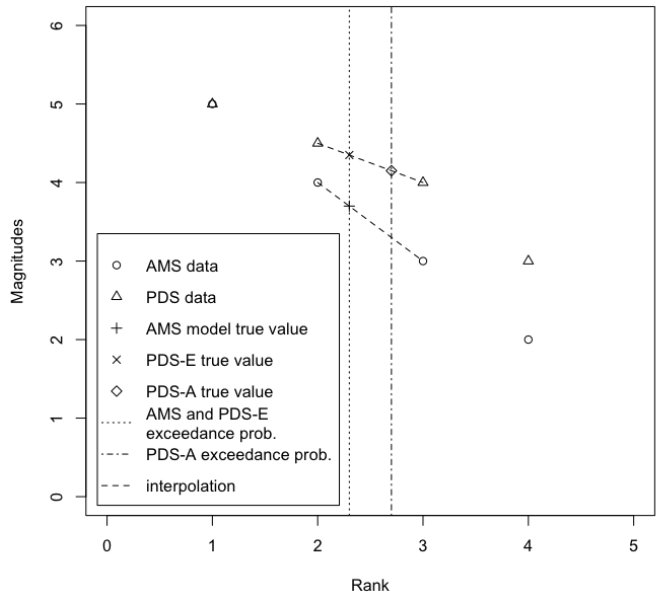

Figure 5.1: Relationships of True Values of PDS-E, PDS-A, and AMS Model

5.5 PDS Event-based Model Development

The development of PDS-E includes treatment of gaps in data records, test of independence and identically distributed assumptions, selection of the exceedance threshold and probability distributions, and estimates of distribution parameters and quantiles. The exceedance threshold determines data values in PDS, and further affects the distribution fitting and quantile estimation. Therefore, the exceedance threshold will be selected with considerations of distribution fitting and quantile estimation.

5.5.1 Missing Values

In comparison with the AMS model, the PDS model may involve more extreme events from those years when records have considerable numbers of missing values; however, it also extends the record length, even when there are no extreme events occurred in those years. The side effect of increasing the length of record is the possibility of reducing the annual arrival rate (λ). Further, the non-exceedance probability of the true value of the design rainfall will be decreased, as Equation 5.1.

It is inappropriate to manually examine rainfall record of each year and to determine whether or not to include the record, because the work involved is substantial, but also the discrimination between rainfall records will result in subjective bias in the model estimates (i.e., a modeler can exclude all years that have no extreme events to get a very large estimate).

This study applies a threshold of missing percentage to clean rainfall records at each rain gauge. If the rainfall record of a year has a percentage of missing values more than the threshold, then the record of this year is excluded from subsequent analysis. The sensitivity of the true value of the design rainfall intensity in relation to the threshold for the missing percentage is analyzed. If there were too many missing values, it would be difficult to conduct any statistical analysis. Therefore, the maximum percentage of missing values considered in this study is arbitrarily set to 40%.

5.5.2 Assumption of Independence

The assessment of independence between rainfall events is required priori in subsequent steps. The models for dependent peaks are different and more complex than independent peaks (Rosbjerg, 1985). Ashkar and Rousselle (1983b) argue that certain restrictions (e.g. 24h cessation of rainfall between events) will interfere with the hypothesis of Poissonian peak arrival. Ashkar and Rousselle (1987) also claim that the statistical independence of flood peaks will be less important if the arrival of flood peaks follows a Poisson process at, or above, the threshold.

On the other hand, researchers have applied simple rules to separate rainfall events for independence. Ben-Zvi (2009) applied 24 hours of rainfall cessation between events as a sign of independence. Vasiljevic et al. (2012) required a minimum of two days between events. Gerold and Watkins (2005) set the expected number of exceedances as twice per year, and estimated the threshold from rainfall data. Madsen et al. (2002) separated rainfall events using dry periods that have the same duration as the rainfall events, and required at least one hour dry period for events that last shorter than one hour. Independence is assumed between rainfall events. The values in rainfall record are calculated as the average rainfall intensity over a given duration for each rainfall event.

This study maintains at least a 24h dry period between storms in sequence. Events happening in sequence with less than a 24h dry separation period will be treated as a single storm, and only the maximum rainfall amount over the assumed duration will be considered as the basis for extracting PDS data.

5.5.3 Assumption of Identically Distributed Data Series

Many investigators (e.g. Madsen et al., 1994, 1995; Rosbjerg and Madsen, 1996; Trefry et al., 2005) assume that the data in PDS are identically distributed; therefore, the exceedances are modeled directly without any pretreatments. The rainfall peaks occurring in different seasons are modeled as one sample set. Todorovic and Zelenhasic (1970); Todorovic and Rousselle (1971) and Ashkar and Rousselle (1981) all applied the Kolmogorov-Smirnov test to verify the homogeneity of flood peaks in different seasons. Long-term changes in rainfall intensities can violate the identically distributed assumption. The Mann-Kendall trend test is able to verify the stationarity of the record, or examine the slope in linear regression for the count of exceedance in each individual year, as in Trefry et al. (2005). Beguería et al. (2011) applied the Poisson distribution and GPA distribution with parameters linearly varying with time, in order to model the non-stationary rainfall record.

The test of the assumption of identically distributed data is related to the selection of the threshold, since a high threshold will exclude more events than a low threshold, and the presence of these events will affect the results of a stationarity test. In this research, the Mann-Kendall trend test and the lag-1 autocorrelation tests are applied to each of the exceedance data series, to assess the presence of long-term trends or autocorrelations in the rainfall exceedances.

5.5.4 Exceedance Threshold Characterization

After the rainfall events are determined to be independent and identically distributed, a threshold is needed to extract the PDS data. However, there is no general consensus on procedures to select the threshold.

In the scope of flood frequency analysis, physical meaning is occasionally combined with the threshold, e.g. the flow rate of bankfull discharge (Kavvas, 1982). However, it is not physically meaningful to assign a threshold associated with rainfall intensities, since the rainfall-runoff process varies from one catchment to another.

Statistical techniques are also involved in selecting the threshold by focusing on the statistical characteristics of the extracted PDS series. To maintain the hypothesis of Poisson arrival peaks, Ashkar and Rousselle (1987) selected the threshold according to the ratio of the observed mean and the variance of the number of exceedances per year. They selected the threshold when the ratio is close to unity, and demonstrate a linear relationship with the average arrival rate. Ben-Zvi (2009) applied Anderson-Darling's test to identify the threshold. The general idea of the statistical perspective of threshold selection is to improve the confidence of not rejecting a hypothesis, to increase the goodness-of-fit of a distribution assumed to describe peak arrivals or peak magnitudes, and to improve the precision and accuracy of the rainfall intensity prediction.

Coles (2001) indicated that the asymptotic basis of the GPA model is likely to be violated if the threshold is too low and will lead to inaccuracy, while a high threshold will generate few exceedances leading to high variance in model estimates. Coles (2001) intro-

duced two methods to select exceedance threshold: by examining the mean of exceedances, or by assessing the stability of parameter estimation, both with the assumption of generalized Pareto distributed exceedances. The "Mean Residual Life Plot" plots the mean of all exceedances of a given threshold against that threshold to show linear relationship, and selects the threshold when the linear relationship appears stable. The other method is based on the fact that if all exceedances of x_T follow GPA, for any threshold greater than x_T, the exceedances will also follow GPA, with the same shape parameter κ. Therefore, the estimated κ is constant with respect to the threshold x_T. Similarly, the modified scale parameter ${\sigma_{x_T}}^* = \sigma_{x_T} - \kappa x_T$ is constant in respect to the threshold x_T.

To select the exceedance threshold, this study analyzes the Coles' mean residual life plot and the parameter estimates stability plot, along with the plot of design rainfall estimates and confidence limits against thresholds. The design rainfall estimate is expected to be a good approximation of the true value of design rainfall, and the confidence interval is expected to contain the true value at the selected threshold.

5.5.5 Frequency Distributions

To describe the magnitude of exceedances, the PDS data are usually modeled with the Generalized Pareto distribution (GPA), which was introduced as a heavy-tailed distribution to describe extreme values. It is a three-parameter distribution, including location parameter ξ, scale parameter α, and shape parameter κ. The cumulative distribution function is

given in Equation 5.6.

$$F(x) = 1 - [1 - \kappa\frac{x-\xi}{\alpha}]^{\frac{1}{\kappa}}, \begin{cases} \kappa < 0 & \xi < x < +\infty \\ \kappa > 0 & \xi \leq x \leq \xi + \frac{\alpha}{\kappa} \end{cases} \tag{5.6}$$

Other candidate probability distributions include the Pearson Type III distribution (PE3), Generalized Normal distribution (GNO), Generalized Logistic distribution (GLO), and Generalized Extreme value distribution (GEV). Shown in Fig. 5.2, these candidates are plotted on an L-moment ratio diagram according to the relationships of the 3rd and 4th L-moment ratios of each distribution. The L-moment ratios of PDS from all rain gauges are plotted as points as well. The candidate distribution plotted close to all PDS points is selected. In this study, the GPA curve is close to most of the PDS points and thus the GPA curve is selected as the probability distribution for subsequent analysis.

5.5.6 Estimation of Parameters, Design Rainfall, and Confidence Limits

In GPA, the location parameter (ξ) is estimated as the smallest value in the partial duration series, and the scale (α) and shape (κ) parameters are estimated with L-moments. Given the first and second sample L-moments as l_1 and l_2, the parameters are estimated as

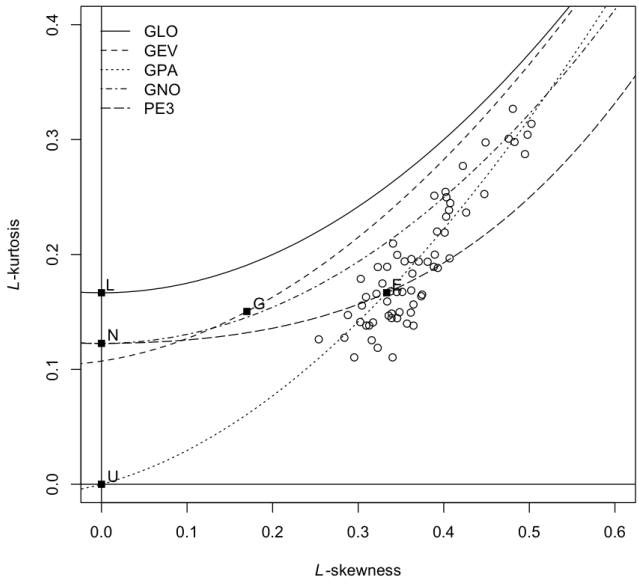

Figure 5.2: L-moment Ratio Diagram of PDS Data

given in Equation 5.7

$$\hat{\kappa} = \frac{l_1 - \hat{\xi}}{l_2} - 2, \hat{\alpha} = (l_1 - \hat{\xi})(1 + \hat{\kappa}) \tag{5.7}$$

For PDS-E, using the non-exceedance probability given by Equation 5.1, the design rainfall with return period T is estimated as Equation 5.8

$$\hat{x}_T = F^{-1}[1 - \frac{1}{\lambda T}] = [1 - (\frac{1}{\lambda T})\ \hat{\kappa}]\frac{\hat{\alpha}}{\hat{\kappa}} + \hat{\xi} \tag{5.8}$$

The precision of the estimated design rainfall is described by confidence limits, which are assessed by the resampling method. The original PDS data were resampled with replacement for N_sim times, and the design rainfall intensities of given return periods were

estimated by fitting GPA to the resampled data set. Given the confidence level of γ, the confidence limits were calculated as the $\gamma/2$ and $1-\gamma/2$ quantiles of N_sim resampled design rainfall intensities.

5.6 AMS Model Development

The AMS model uses the same rainfall records as PDS-E, but extracts rainfall data as annual maxima. AMS data are inherently independent since values are extracted as one event within each year and rainfall events in different years are independent. This is especially likely to be true in this study, since only rainfall events between April and October are considered. The identically distributed assumption is tested with the Mann-Kendall trend test and the lag-1 autocorrelation test tests the assumption of independence. Those records with significant Mann-Kendall trends or autocorrelations are excluded in subsequent assessment.

By using the L-moment ratio diagram, the Generalized Extreme Value distribution is selected as the probability distribution to model AMS data, as given in Equation 5.9.

$$F(x) = \exp\{-[1-\kappa(\frac{x-\xi}{\sigma})]^{\frac{1}{\kappa}}\}, \kappa \neq 0 \tag{5.9}$$

where κ is the shape parameter, α is the scale parameter, and ξ is the location parameter. Similar to the PDS-E model, the uncertainties of the AMS estimates are described with confidence limits, by resampling the original AMS data as well.

5.7 Model Application

5.7.1 Data Description

This study uses historical rainfall records at 21 stations in the Province of Ontario, Canada, all with 40 years or more of historical records. All of these records include daily maximum rainfall amounts for durations of 5, 10, 15, 30min, and 1, 2, 6, and 12h in a day, recorded by tipping bucket and quality-controlled by Environment Canada. The records between April 1st and October 31st are analyzed in this research, in order to focus on rainfall events.

The rainfall measurement methodologies used by Environment Canada have been modified several times, according to Mekis and Hogg (1999). Rain gauges were changed from Meteorological Service of Canada (MSC) gauge to Type-B at most stations in 1970s, and the inside container of MSC gauges were changed around 1965 resulting in non-homogeneity of the dataset. Compared to pit gauge measurements, Type-B gauge measurements are 1% lower on average, while MSC gauge measurements are 4% lower (Goodison and Louie, 1986). Non-homogeneity was also introduced when measuring instruments were relocated, in which case the station identifiers will be changed and records need to be combined.

The detailed information of instrument changes are not available to this study, and based on the consideration that all data have been corrected to the standard rain gauge by Environment Canada (Sandy Radecki, personal communication, 2013), the homogeneity

in data records are reasonably assumed.

5.7.2 PDS-E Model Application

The methodologies introduced in the model development section are applied to data described above, to develop a PDS-E model for each station in Ontario. The details of selecting missing percentages and exceedance thresholds are discussed in this section.

Missing Values Characterization

To explain the sensitivity test of true values of design rainfall intensities in respect to missing values, the 30min duration rainfall record at the City of Hamilton is shown as an example in Fig. 5.3. The estimated true values of design rainfall intensities for 2, 5, and 10-year return periods are plotted against the missing percentage (from 10 to 40%, with a step of 2%). The intensity threshold used to extract PDS data was set to the minimum of the corresponding AMS data, which was 18mm/hr.

The design rainfall intensities decreased (though fluctuations) about 5mm/h as the missing percentage increased from 10% to 30% and remained stable up to 40%. The record length increased from 33 years to 43 years (because those records having more than 10% missing values are included as the threshold is elevated), and increased especially rapidly with missing percentages between 14% and 24%. The design rainfall intensities are not sensitive with respect to the missing percentages while the record length is affected to some extent.

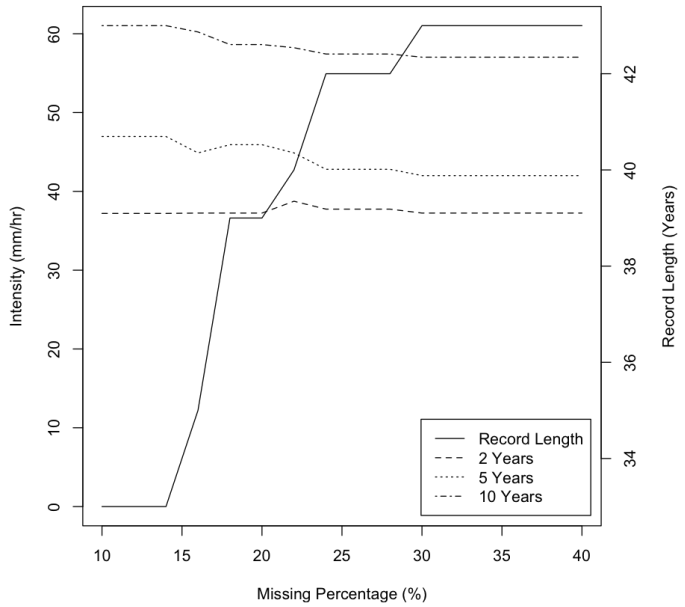

Figure 5.3: Changes of Observation Against the Missing Percentage For Hamilton 30min Duration Rainfall Record

The sensitivity test is conducted for all rainfall records among the 21 gauges. For most rainfall records, the design rainfall intensities are not sensitive to the missing percentage, especially when the missing percentage is greater than 20%. Therefore, records are removed if the missing percentage is greater than 20%, the same as for the AMS model, to facilitate comparison with the AMS model under the same circumstances.

Exceedance Threshold Characterization

The mean residual life plot, parameter estimates stability plot, and the design rainfall estimates stability plot are generated to characterize the sensitivity of PDS-E to the exceedance threshold. The extent of the exceedance threshold is set from the minimum of the AMS data to 90% of the 2-year return period estimate of the AMS model. This is based on

the consideration that the model will lead to bias if the threshold is too low, while too high a threshold will result in high variance in model estimates. Furthermore, the estimation of 2-year return period events will be impossible if the annual arrival rate is too small (if $\lambda < 0.5$, then the non-exceedance probability $1 - \frac{1}{2\lambda} < 0$).

The 30min rainfall record at Windsor is used as an example. Fig. 5.4 is a temporal plot of all independent events of intensities heavier than the minimum of AMS record (22.4 mm/hr). The rainfall records of years 1992 and 1996–1998 have considerable amounts of missing values and therefore are excluded in this analysis. The two dashed lines indicate the extent of potential exceedance threshold ($[22.4, 41.5]$). The mean residual life plot in Fig. 5.5 shows two segments: the mean residual fluctuates between 12 and 14 mm/h when the threshold increases until 52 mm/hr, and approximately linearly decreases to 6 mm/h until the threshold increases to 70 mm/hr. Note that the characterized extent of threshold is within the 1st segment, and this segment has some evidence of linearity. Therefore, the intended extent of threshold ($[22.4, 41.5]$) is accepted by the analysis of mean residual life plot. The plot of estimated distribution parameters and corresponding confidence limits (90%) are shown in Fig. 5.6 and 5.7. Both estimated parameters ($\hat{\alpha}^*, \hat{\kappa}$) gradually rise as the threshold increases, and the confidence intervals extend when threshold exceeds 28 mm/hr. Therefore, the intended extent of the threshold is set to $[22.4, 28]$. The model sensitivity to the threshold is further characterized in the design rainfall estimates stability plot, as per Fig. 5.8. Within the intended extent of threshold, the model estimates are relatively stable, and so are the confidence limits. Therefore, the exceedance threshold is

selected to be 28mm/h, as the upper limit of the intended extent. This procedure is

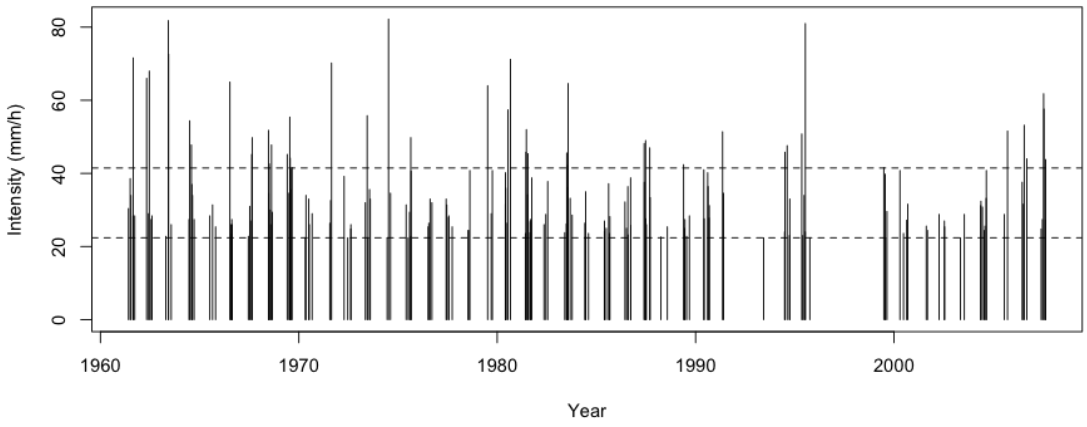

Figure 5.4: Thirty-minute Duration Rainfall Record at Windsor

applied to all records amongst the 21 gauges, to select thresholds for each PDS model. Some problems are apparent in this process. The parameter estimates are not constant with respect to exceedance thresholds in some cases, but the extent of the confidence interval of parameter estimates constantly expand as the threshold increases. Therefore, the threshold is selected at the value before the parameter estimates rapidly change, or the confidence intervals dramatically expand. In the design rainfall estimates stability plot, the confidence interval covers the true value of design rainfall in most rainfall records, and the thresholds are always selected to ensure the confidence intervals encompass the true values.

The Mann-Kendall trend test and the lag-1 autocorrelation test are used to assess the stationarity and independence of each extracted PDS. New thresholds are selected for those

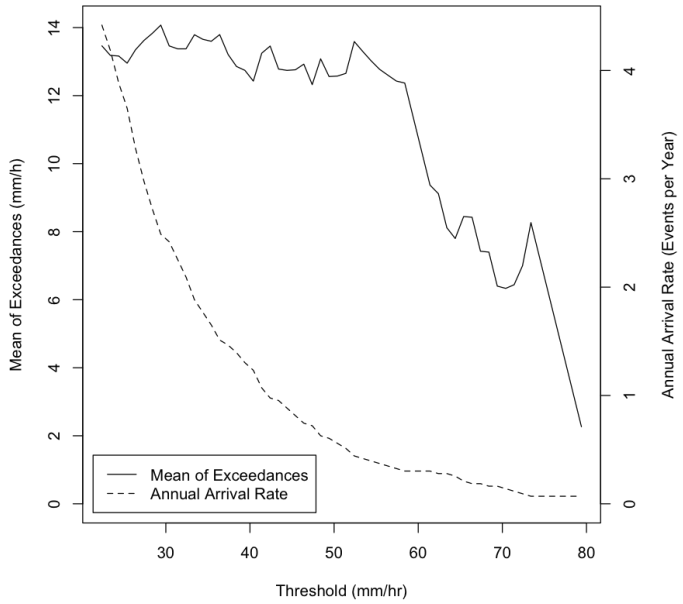

Figure 5.5: Mean Residual Life Plot For Windsor 30min Duration Rainfall Record

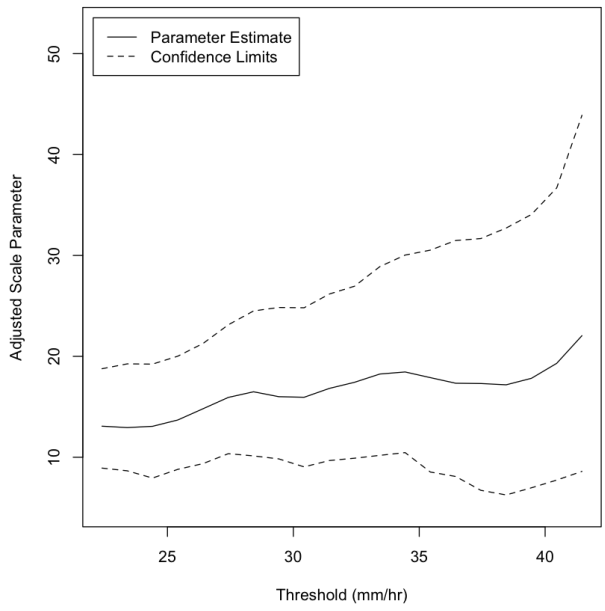

Figure 5.6: Stability Plot For The Adjusted Scale Parameter Estimate From 30min Duration Rainfall Record At Windsor

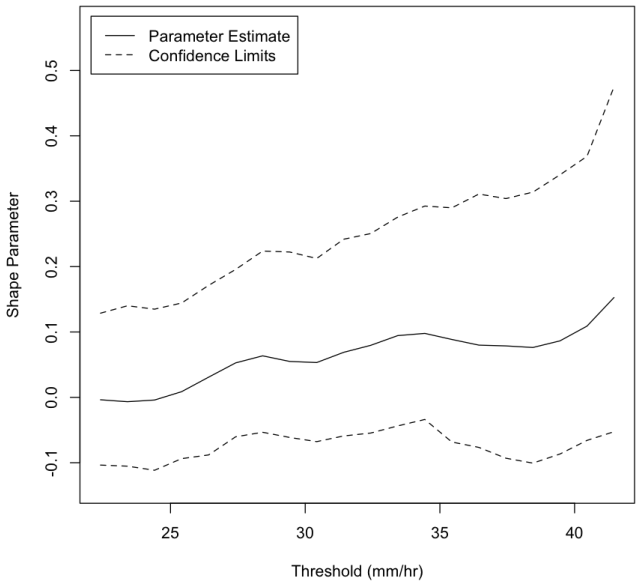

Figure 5.7: Stability Plot For The Shape Parameter Estimate From 30min Duration Rainfall Record At Windsor

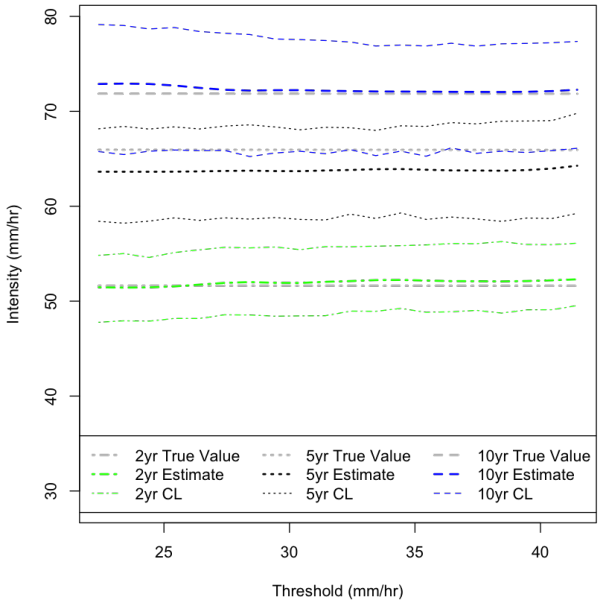

Figure 5.8: Design Rainfall Estimates Stability Plot For Windsor 30min Duration Rainfall Record

records showing significant Mann-Kendall trends or autocorrelations, and the new extracted PDS will be tested again, until stationarity is achieved.

Quantiles and Variances

The parameters and quantiles are finally estimated based on data extracted using the threshold determined as per above, and the confidence limits are estimated with 1000 re-sampled sample sets (with replacement) of same length as the original PDS.

5.7.3 AMS Model Application

The AMS data are extracted from the same rainfall records as the partial duration series, and tested with Mann-Kendall trend test and lag-1 autocorrelation test. All records at Toronto Pearson Airport rainfall station are excluded, due to both decreasing trends ($p < 0.05$) and lag-1 autocorrelation (95% confidence level, two-sided). The 30 min and 1 h rainfall records at Windsor are excluded for decreasing trends. The 2h rainfall record at Sioux Lookout and the 1h rainfall record at North Bay are both excluded due to significant autocorrelation.

The rest of the rainfall records are all fitted with the Generalized Extreme Value (GEV) distribution, The selection of GEV is also based on the L-moment ratio diagram, as per Fig. 5.9, which shows the GEV curve is the closest to the center of sample L-moment ratios. The design rainfall intensities are estimated at non-exceedance probability of $1 - 1/T$, and the confidence limits are estimated with resampling methods.

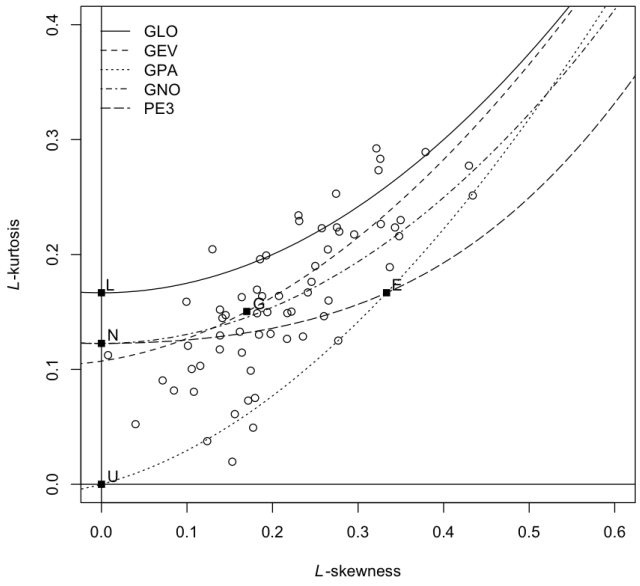

Figure 5.9: L-moment Ratio Diagram of AMS Records

5.8 Results

5.8.1 Comparison of The True Value of Design Rainfall in PDS-E and AMS Model

The estimated true values of design rainfall are compared between the PDS-E model and the AMS model. The differences are calculated as the percentages of the PDS-E estimates greater than the corresponding AMS estimates, for return periods of 2, 5, 10 years, over durations of 30 min, 1 and 2 h. The boxplots in Fig. 5.10 depict all percentages of differences of various rainfall records. The 2-year return events are showing the largest differences, up to 29% larger for the 1 h duration design rainfall at Windsor. The averaged differences are close to 10% for all rainfall durations. The 5-year return events show con-

siderable differences as well, with average differences around 3%. The average differences of 10-year return events are all close to zero, indicating small difference between estimates of the PDS-E and the AMS model.

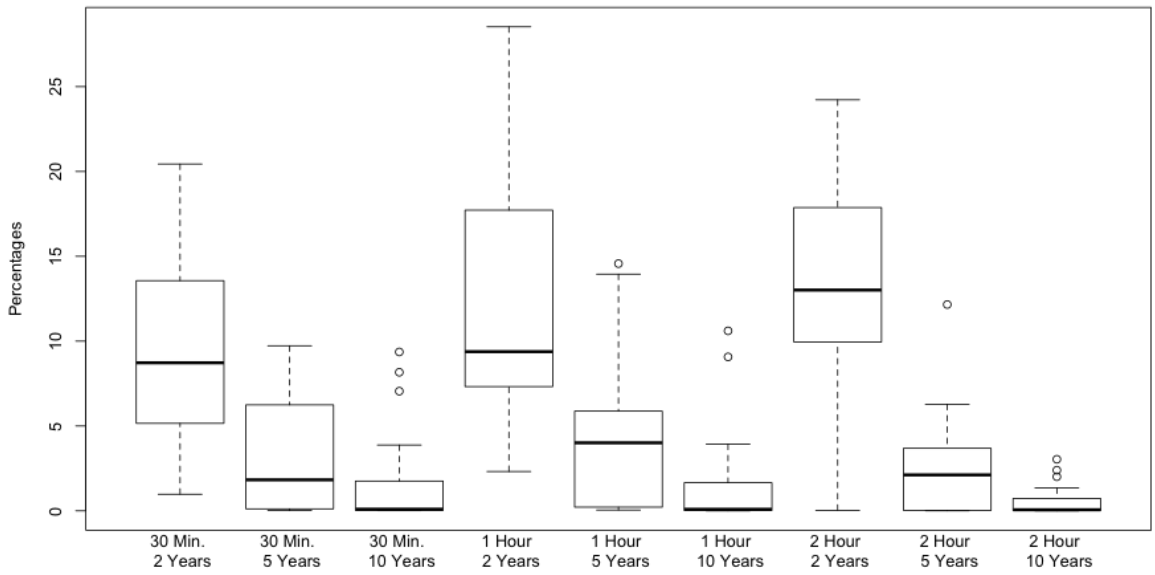

Figure 5.10: Percentage of True Values of PDS-E Greater Than True Values of AMS Model For Durations From 30min To 2h and Return Periods of 2, 5, and 10 Years

The PDS event-based model focuses on the probability of an intensity threshold being exceeded in an individual event, rather than being exceeded in a particular year, which is the annual scheme. Within different meanings of return periods, simply comparing the PDS event-based model estimates with AMS estimates is meaningless. However, it is interesting to identify conditions when this difference is substantial. One important factor determining the magnitudes of the event observations is the data series itself. Given 40 years of record, a 10-year return period event is approximately the 4^{th} largest of the extreme events. The

possibility of having more than one event exceed this 4^{th} largest event in a single year is small but not negligible. Therefore, considering a PDS event-based model in engineering design is appropriate.

5.8.2 Comparison of the PDS-E and the AMS Model Estimates

The PDS models and the AMS model are compared with respect to the magnitudes and the width of confidence intervals of predictions for 2, 5, and 10-year events. The 2-year event estimates are greater in the PDS-E model than in the AMS model, but the 5 and 10-year events estimates are not showing substantial difference.

Fig. 5.11 shows the difference between the PDS-E estimates and the AMS model estimates in percentages, which is calculated as $[(\text{PDS-E estimate}/\text{AMS Model estimate}) - 1] \times 100\%$. The 2-year return events estimated in PDS-E are constantly greater than in the AMS model. However, the 5 and 10-year return event estimates of PDS-E are less than those of the AMS model. This is due to the design rainfall which is underestimated by PDS-E model. A simple comparison of the estimates to the true values of design rainfall intensities shows an average of 5.6% underestimation on 5-year return events and 10.6% underestimation on 10-year return events. In the mean time, the AMS model underestimates design rainfall intensities by an average of 0.9% and 2.2% respectively.

To improve the accuracy of PDS-E estimates, a different set of thresholds was tried by assessing design rainfall estimates stability plot directly and selecting the exceedance threshold where the 5-year return event estimate is closest to true value, with a reasonable

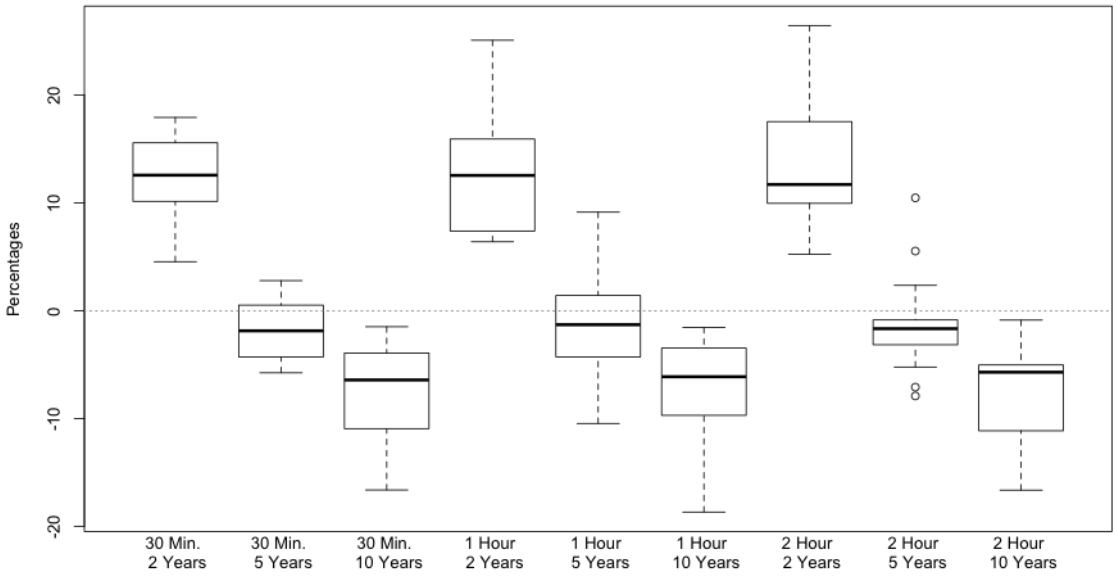

Figure 5.11: Difference Between the PDS-E Estimates And the AMS Model Estimates

number of exceedances and range of confidence intervals. This set of thresholds was applied to extract PDS data, and the estimates were compared again with the AMS estimates, as shown in Fig. 5.12. The averaged differences of 5-year return events estimated from the two models are close to zero, which is closer to, but still different from, the estimated true value comparison results.

To compare the models' precision, width of confidence intervals (90%) are assessed. In Fig. 5.13, the percentages of differences in confidence intervals are depicted as box plots. It shows that the PDS-E estimates have smaller width of confidence intervals compared to AMS model estimates, for most rainfall records. This is partially due to the sample sizes in PDS model being larger than in AMS model, more than tripled on average ($\bar{\lambda} = 3.27$),

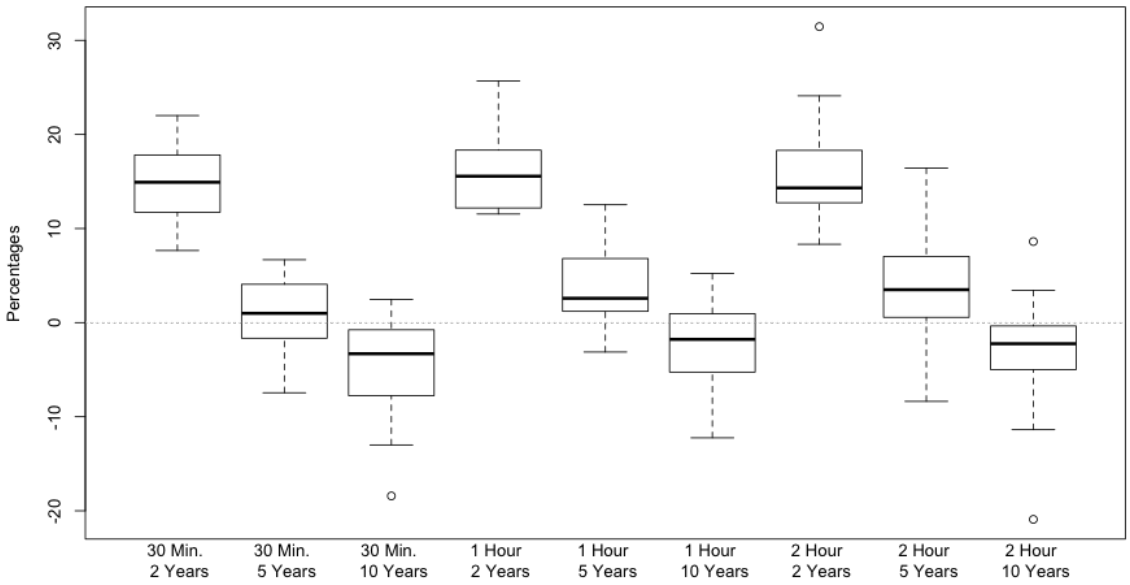

Figure 5.12: Percentage of Estimates of PDS-E Greater Than Estimates of AMS Model, Using Alternative Thresholds

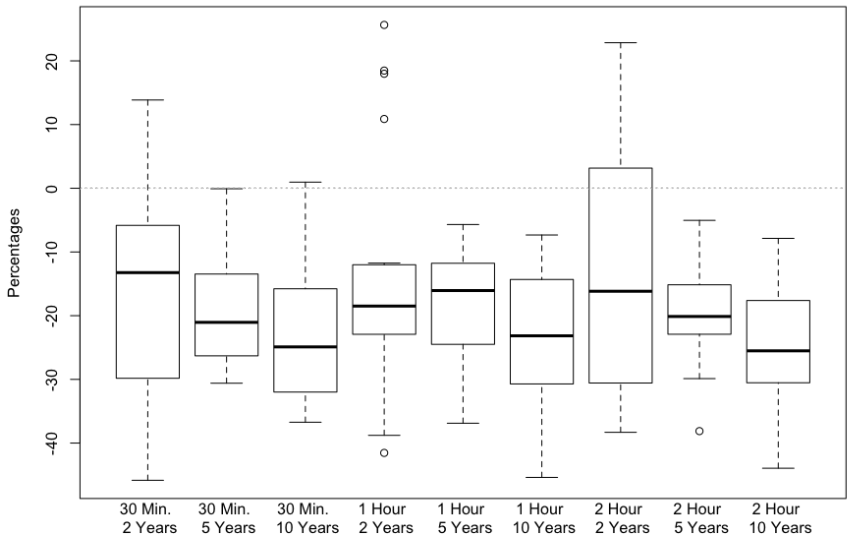

Figure 5.13: Percentage of Confidence Interval Widths of PDS-E Greater Than Those of AMS Model

which reduces sampling errors.

5.9 Discussion

The argument made by Laurenson (1987), which advocates the use of partial duration series in assessing frequent events, is supported by both theoretical derivation and analysis of true values of design rainfall intensities with real rainfall records. The design rainfall in partial series is on average 11.9% greater than in annual series for 2-year return period, and 3.5% for 5-year return period. The reciprocal of PDS recurrence interval was claimed as "not the probability of anything" in Laurenson (1987). It is acknowledged that the reciprocal is not a probability since it has a dimension (events per year); however, in this study, it is explained as the occurrence frequency of events exceeding a given threshold, and related to the exceedance probability used in statistical distributions by applying a conversion factor — the annual arrival rate (λ).

The threshold selection procedures introduced by Coles (2001) are applied in the model development process. These procedures focus on stability of model parameter estimates, and linearity between exceedance thresholds and mean residuals of exceedances. The thresholds selected are usually low, which result in large annual arrival rates, and eventually affect the accuracy of design rainfall estimates. It is shown that use of thresholds beyond the stable range of parameter estimates can improve the design rainfall estimates in some cases. Further, there is not always a range of thresholds that have stable parame-

ter estimates. This study assesses the stability and accuracy of design rainfall estimates in addition to Coles (2001)'s procedures. This additional procedure provides insights directly on the modeling objective — to provide accurate design rainfall estimates.

The selection of exceedance thresholds is related to the modeling objectives, and the procedures used in this study are recommended for modeling for frequent events using partial series. It is suggested the stability of event estimates be assessed along with stability of parameter estimates. The threshold that produces accurate event estimates should be considered as long as the parameter estimates stability is not severely deteriorated.

The width of confidence intervals, as an indicator of the precision of the design rainfall estimate, is shown to be smaller for PDS-E than in the AMS model. This advantage of PDS-E is a result of the large sample size in partial series, which is brought by using low thresholds. Additionally, it is possible to ensure stationarity of the data series by altering exceedance thresholds, as used in this study, which is impossible in AMS modeling. Nevertheless, the lack of accuracy in PDS-E estimates comparing to the AMS model limits the application of PDS-E in design rainfall assessment. It is important to assess the PDS-E model accuracy, and make improvement, if necessary.

5.10 Conclusion

The PDS event-based model (PDS-E), focusing on the average probability of a rainfall intensity being exceeded in a single event, is more pertinent to stormwater infrastructure

design objectives. Besides, the PDS-E generally provides estimates greater than the AMS model. The PDS-E also has advantages in association with the modeling objectives, by altering the thresholds during data series extraction.

In engineering design, infrastructure is designed with the capacity to carry a heavy storm, for example, once in five years on average. This design objective is in fact one exceedance expected in every five years. However, the AMS model predicts event magnitudes which are exceeded in one year in every five years, despite the number of exceedances in any single year. Therefore, for frequent events, using AMS model predictions in stormwater infrastructure design is misleading. Use of the PDS event-based model to estimate the design rainfall for stormwater system design is more appropriate.

Chapter 6

Identification of Design Rainfall Changes Using Regional Frequency Analysis — A Case Study in Ontario, Canada

Chapter 5 analyzes the advantages of the PDS model in comparison with the AMS model, and points out the need to reduce the uncertainties implicit in the PDS model. Hence, this paper demonstrates the application of the regional frequency analysis approach and the improvement with respect to model uncertainties. In addition, the changes in design rainfall intensities are identified from both the regional frequency analysis model and the PDS model using at-site rainfall records, and compares the consistency of changes iden-

tified from the two models. The climate stations used in this paper are different from the preceding papers. They include 32 climate stations from southern Ontario. These climate stations all have longer than 10 years of rainfall record both pre and post 1983. In addition, the high density of climate stations in southern Ontario can benefit the regionalization.

This paper modifies the original algorithms of the regional frequency analysis methods to accommodate the partial duration series. This is a major contribution in this thesis. The paper shows a complete procedure to develop a regional frequency analysis model using partial duration series data, including grouping gauges into homogeneous regions, selecting regional frequency distributions, and using a regional L-moment algorithm to predict rainfall intensities.

The paper indicates that the regional frequency analysis approach significantly reduces uncertainties involved in rainfall intensity estimates. The consistency of changes identified further confirms that design rainfall intensities have been changing over the last few decades with statistical significance, in several areas in southern Ontario, Canada.

6.1 Abstract

Providing design rainfall intensities appropriate for stormwater system design under climate change conditions requires a comprehensive understanding of changes in heavy rainfall events, which may have occurred over the past few decades. Historical rainfall records of 32 gauges are analyzed to assess if changes in design rainfall intensities in

southern Ontario are evident. To assess whether changes in rainfall intensity are occurring, rainfall records are split into two time periods and design rainfalls of 2, 5, and 10-year return periods are estimated; however, due to limited record lengths, uncertainties in design rainfall estimates are substantial. To reduce uncertainties, the potential for regionalization involving grouping the gauges into regions and a regional L-moment algorithm (a method combining at-site L-moment statistics via the weighted average to estimate a regional frequency distribution) is applied to each region.

The procedure used to develop the regional frequency analysis model employs Partial Duration Series data, and includes selecting regional frequency distributions, and using a regional L-moment algorithm to predict rainfall intensities. The result shows that the regional L-moment algorithm produces more accurate rainfall estimates (i.e. reduces RMSE and decreases the width of confidence intervals) in comparison with an at-site model. For 10-year return storms, 26% reduction in RMSE in the regional model was obtained for the first time period (1960-1983), and 35% for the second time period (1984-2007).

Comparing error bounds between the two time periods shows that design rainfall intensities have been changing over the last few decades with statistical significance, in several areas in southern Ontario, Canada.

6.2 Introduction

Climate change research has been catapulted to the fore in recent years. As a result of increased energy present in the hydrologic cycle, more intense precipitation events are expected, and are evident (Alexander et al., 2006; Burn and Taleghani, 2013; Adamowski et al., 2010). The changes expected in the mean value and variation of precipitation intensities are expected to be evident through changes in the extreme rainfall recurrence frequency. In response, challenges exist in the design and management of urban stormwater systems, where infrastructure is, for example, designed to prevent the flooding of road systems during a 5-year event. Developing design rainfall intensities appropriate for system design under changing climate conditions is challenging, i.e. conditions may be non-stationary. Further, estimating design rainfall intensities for the future requires a comprehensive understanding of changes that have been observed in relation to extreme rainfall events over the past few decades, and prediction of future changes based on changes identified in the past (although one can argue with the rationale to assume the continuance of any changes identified).

Types of temporal changes can be characterized as step change and gradual change. A step change describes the "jump" of a statistic between two non-overlapping time periods, and indicates possible changes in fundamental climate-driven forces. A gradual change is identified when a statistic has increased or decreased over a period of time. In frequency analysis, especially when the objective is to assess the design rainfall intensity, an independent and identically distributed record is normally assumed, and gradual changes

are removed (de-trended) if identified. Therefore, in frequency analysis, identifying step changes rather than gradual changes over time is more beneficial to the assessment of design rainfall.

Regarding extreme rainfall frequency analysis, statistics used for identifying changes over time include expected values and variances of design rainfalls, for a particular return period and duration. Cumulative density functions of extreme rainfall records may also be analyzed to discover step changes. Descriptive indices of extremes have been used to describe changes as well (WMO, 2009), e.g. the number of days with rainfall above the 95th percentile of daily accumulations, denoted as R95p.

At-site analysis is the frequency analysis focused on characteristics or changes in storm events at a particular site/rain gauge. A statistical model using only the rainfall record at a particular gauge is referred to as an 'at-site model', while a statistical model using regional frequency analyses for gauges with limited rainfall records is referred to as a 'regional model'. Both the at-site model and the regional model can perform the at-site analysis. Spatial variability of changes in a region can be illustrated by comparing changes identified at several gauges within the region.

A variety of assessments of changes in precipitation rates have been identified across Canada. Groisman et al. (1999) observed a 50% increase in mean summer precipitation over the past century, based on daily precipitation records. Zhang et al. (2001) characterized heavy precipitation events for the period of 1900–1998, and found increasing trends of spring heavy rainfall in eastern Canada. Vincent and Mekis (2006) analyzed daily pre-

cipitation records for periods of 1950–2003 and 1900–2003 separately, and found that in the latter half of the 20th century the number of days with precipitation has increased, while the daily intensity and maximum number of consecutive dry days have both decreased. Burn and Taleghani (2013) identified more increasing trends than decreasing trends based on records of 51 stations across Canada. In addition, Burn and Taleghani (2013) found that the design rainfall values of various return periods have increased in the most recent 20 years, compared to the entire record.

Rainfall patterns in southern Ontario, Canada have also been studied. Stone et al. (2000) grouped the Great Lakes and St. Lawrence area as one homogenous region when analyzing daily precipitation events across Canada. Stone et al. (2000) identified seasonally increasing trends in total precipitation in southern Ontario, and also concluded that more extreme precipitation events in autumn and winter are related to the negative Pacific/North American teleconnection pattern (PNA). Adamowski and Bougadis (2003) discovered both increasing and decreasing trends of extreme rainfall events in various rainfall stations in Ontario. Adamowski et al. (2010) demonstrated that with the presence of increasing trends, a given design storm may occur more frequently in the future.

Changes occurring in design rainfall values are discovered by comparing estimates of design rainfall values from records of two different time periods. Burn and Taleghani (2013) compared the estimate of the most recent 20 years to the estimate of the entire timeframe. Vasiljevic et al. (2012) compared estimates of 1970 – 1984 and 1985 – 2003. Since the record lengths of stations in Ontario are usually short (mostly starting from the

1960s), splitting the record into two segments results in even shorter records (approximately 20 years in each segment). A short record will entail more uncertainties in the estimates of design rainfall values. To solve this problem, Burn and Taleghani (2013) used resampling techniques to improve the accuracy of quantile estimates. On the other hand, regional frequency analysis can use rainfall records from adjacent rainfall stations in a statistically homogeneous region to improve the accuracy of design rainfall intensity estimates (Hosking and Wallis, 1997).

Regional frequency analysis is based on the assumption that sites in a statistically homogeneous region have identical frequency distributions except for site-specific scale factors. Hosking and Wallis (1997) introduce several comprehensive measures to delineate homogeneous regions and select frequency distributions, the regional L-moment algorithm, and the methods to assess the accuracy of estimated quantiles.

Research using regional frequency analysis techniques includes Madsen et al. (1998, 2002) who analyzed regional variability of extreme rainfall statistics by using linear regression between site statistics (e.g. index flood) and site characteristics (e.g. mean annual precipitation), and developed a regional estimation model for precipitation in Denmark. Trefry et al. (2005) updated Intensity–Duration–Frequency (IDF) curve estimates for Michigan, U.S., using regional frequency analyses based on both Annual Maximum Series (AMS, data series consisting of the maximum value in each year) and Partial Duration Series (PDS, data series consisting of all values exceeding a threshold) data. Results show that regional analysis can provide reliable rainfall IDF estimates. For 23 rainfall stations in

Malawi, Ngongondo et al. (2011) compared the accuracy of design rainfall estimates between at-site and regional analysis, and concluded that the regional-based estimates have smaller uncertainties and better accuracy. Sveinsson et al. (2002) analyzed regional extreme precipitation frequencies in northeastern Colorado, U.S., and focused specifically on an extraordinary storm which occurred in 1997. It shows that design values at the site of interest, are underestimated with regional analysis when the region is not statistically centered at the site.

Most research documents using regional frequency analysis techniques are based on AMS. Laurenson (1987) states the advantage of using PDS instead of AMS in at-site analyses: the rainfall model using PDS data evaluates rainfall intensity of average recurrence interval between storm events, instead of between two hydrologic years, in which a given rainfall intensity is exceeded regardless of the number of exceedances. The difference between rainfall intensity models based on PDS and AMS is discussed in Wang and McBean (2013).

This paper uses a regional frequency analysis approach to improve the accuracy of heavy event estimates, based on partial duration series data, and identifies regional changes of extreme rainfall values by comparing estimates of two consecutive time periods. The accuracies of rainfall intensity estimates will be measured herein as relative Root Mean Square Error (rRMSE) and computed using Monte-Carlo simulation.

6.3 Development of Regional Frequency Analysis Model

6.3.1 Differences Between Use of PDS and AMS Data

The simulation algorithms in the *lmomRFA* package in R project (Hosking, 2012; R Core Team, 2013) need to be modified when using PDS data in regional frequency analyses. This is required when using PDS data, since the record length is not the same as the number of years of the rainfall record. An average annual arrival rate (λ) is calculated as the number of values in the record divided by the number of years of the record. In the original regional L-moment algorithm, the annual maximum series was applied, and storms of the same return period have the same non-exceedance probability (F) for all gauges. This consistency of F is not preserved when using PDS data, due to the different λ between gauges. In this case, the projection from the regional frequency distribution to the at-site storm estimate is dependent on both the scale factor (l_1, mean rainfall intensity at gauge) and λ; that is, $\hat{Q}_i(T) = {l_1}^{(i)}\hat{q}(1 - 1/\lambda T)$ for the design rainfall intensity with T-year return period, and the non-exceedance probability is calculated as $F = 1 - 1/\lambda T$.

The PDS data are extracted with thresholds (x_T) specific to rainfall gauges. The sensitivity of distribution parameters (using Generalized Pareto distribution parameters) and design rainfall estimates with respect to the thresholds is analyzed, following Coles (2001). The threshold is selected in a range where the distribution parameters are relatively stable and rainfall intensity estimates are close to the interpolated values of ranked rainfall records using Gringorten's plotting position formula (Gringorten, 1963). Wang and McBean (2013)

discussed the selection of intensity thresholds.

6.3.2 Screening the Data

Data screening is one of the most important processes in frequency analyses. Gross errors introduced by instrument malfunction or mistakes in transcription need be eliminated. Hosking and Wallis (1997) suggest a discordancy measure to identify gauges that are discordant with other gauges in a group. This measurement compares statistics (L-moment ratios) from records of all gauges in a group to find out if any gauge has statistics deviating from the group average. Let $t^{(i)}, t_3^{(i)}, t_4^{(i)}$ be denoted as L-CV, L-skewness, and L-kurtosis for the record at the i-th gauge (N gauges in total), and a vector $\mathbf{u_i} = [t^{(i)} \quad t_3^{(i)} \quad t_4^{(i)}]^T$ consists of these three values. The unweighted group average of $\mathbf{u_i}$ is represented as Equation 6.1

$$\bar{\mathbf{u}} = N^{-1} \sum_{i=1}^{N} \mathbf{u_i} \tag{6.1}$$

The discordance measure for the i-th gauge is computed as given in Equation 6.2

$$D_i = \frac{1}{3} N (\mathbf{u_i} - \bar{\mathbf{u}})^T A^{-1} (\mathbf{u_i} - \bar{\mathbf{u}}) \tag{6.2}$$

Where A is the matrix of sums of squares and cross-products as in Equation 6.3

$$A = \sum_{i=1}^{N} (\mathbf{u_i} - \bar{\mathbf{u}})(\mathbf{u_i} - \bar{\mathbf{u}})^T \tag{6.3}$$

This discordance measure (D_i) is compared with critical values (Table 3.1 in Hosking and Wallis, 1997) to determine if the historical record from the i-th gauge is discordant with other records in the group. Records with a large discordancy measure need to be investigated carefully to decide whether to include these records in the group, or shift to other groups.

6.3.3 Identify Homogeneous Regions

The regional frequency analysis algorithms are based on assumptions that records of gauges within a homogeneous region have similar frequency distributions, apart from scale factors. The homogeneity of a region is in relation to the similarity of frequency distributions between records (in a statistical, not a geographical perspective), which indicate gauges within a homogeneous region are not necessarily close in proximity. If the rainfall pattern of an area is highly affected by geographical factors such as oceans, lakes, or mountains, then geographical characteristics should be considered in the grouping of gauges. Other site characteristics (e.g. the Mean Annual Precipitation (MAP), or time of year at which extreme events mostly occur) are widely used as well (e.g. Adamowski et al., 1996; Trefry et al., 2005; Ngongondo et al., 2011).

In the present paper, the storms being considered are located in southern Ontario which has a continental climate "markedly modified by the Great Lakes" (Hare and Thomas, 1979, pp105). Therefore, the gauge distances to the three lakes, including Lake Huron, Lake Erie, and Lake Ontario, are employed as site characteristics in the grouping of gauges.

To divide gauges into homogeneous regions, several grouping methods are described in Hosking and Wallis (1997). Subjective partitioning methods investigate site characteristics and define groups accordingly. Adamowski et al. (1996) assumed that all rain gauges across Canada belong to one homogeneous region, after finding that the at-site L-skewness and L-kurtosis are invariant to MAP, and rejected this hypothesis later when objective partitioning measures were applied. Objective partitioning methods measure "within group heterogeneity" of a site statistic, and determine the homogeneity of the group as to whether the heterogeneity measure exceeds a given threshold. Objective partitioning methods usually consider "within group variation" of the sample statistics such as coefficient of variation, skewness, or kurtosis.

Clustering methods are practical when dealing with large data sets. Gauges are partitioned or aggregated into groups based on similarities of their at-site characteristics or statistics. Trefry et al. (2005) used a k-means clustering method to group gauges, and Ngongondo et al. (2011) used k-means and Ward's hierarchical method to cluster rain gauges in southern Malawi. This study uses Ward's hierarchical clustering method to initially group rain gauges, and then uses a k-means clustering algorithm to adjust clusters.

Regional homogeneity is assessed using a measurement of the degree of heterogeneity in a group of gauges. This measurement compares two components, the "between gauge dispersion of the sample L-moment ratios", and the 'between gauge dispersion if it was a homogeneous group of gauges". The "between gauges dispersion" is the averaged difference between gauge statistics and group-averaged statistics, weighted by the length of

record (in years) at each gauge. The dispersion of a homogeneous region is calculated using Monte Carlo simulation. In each realization, records are simulated with the same length as their real world counterparts, using a parent frequency distribution (usually a four-parameter Kappa distribution).

The between gauge dispersion of sample L-CVs is calculated as in Equation 6.4

$$V = \{\sum_{i=1}^{N}(n_i(t^{(i)} - t^R)^2)/\sum_{i=1}^{N} n_i\}^{1/2} \tag{6.4}$$

where t^R is the group-averaged L-CVs, weighted by record length n_i, and $t^{(i)}$ is the L-CV at the i-th site.

The heterogeneity measure (H) is calculated as Equation 6.5

$$H = \frac{V - \mu_V}{\sigma_V} \tag{6.5}$$

Where μ_V and σ_V are the mean and standard deviation of the dispersions calculated from Monte Carlo simulations. The critical values for H are: acceptable homogeneity when $|H| < 1$, possible heterogeneity when $1 \leq |H| < 2$, and definite heterogeneity when $|H| \geq 2$. At least 500 replications in the Monte Carlo simulation are recommended by Hosking and Wallis (1997).

6.3.4 Selection of A Frequency Distribution

The regional frequency analysis algorithm is based on the assumption of identically distributed data from records of all gauges within a homogeneous region, apart from a scale factor at each gauge. This does not create the necessity to identify a true frequency distribution to apply to each gauge; any frequency distribution that can produce good quantile estimates is plausible. Therefore, it is not always necessary to choose the best-fit distribution; it makes sense to choose a robust distribution, i.e., a distribution that can provide a good quantile estimate even when future data may come from a distribution different from the fitted distribution, due to the changes in background mechanisms.

The Goodness-of-Fit measure introduced in Hosking and Wallis (1997), is designed to select between candidate frequency distributions. It assumes that the variation of L-moment ratios in a homogeneous region are due to sampling variability; therefore, the candidate distributions are evaluated by how well the fitted L-skewness and L-kurtosis match the regional average L-skewness and L-kurtosis of the observed data. For three-parameter candidate distributions, the L-skewness is fitted to regional average; thus, only the difference of L-kurtosis between fitted distribution (τ_4^{DIST}) and regional average (t_4^R) is evaluated, as in Equation 6.6

$$Z^{\text{DIST}} = \frac{t_4^R - \tau_4^{\text{DIST}}}{\sigma_4} \tag{6.6}$$

The 'DIST' refers to the candidate distribution, and σ_4 denotes the standard deviation of t_4^R.

The same as the heterogeneity measure, the Monte Carlo simulation is used here to quantify the variability (σ_4) and the bias (B_4) of t_4^R, as in Equation 6.7 and 6.8.

$$B_4 = N_{sim}^{-1} \sum_{m=1}^{N_{sim}} (t_4^{[m]} - t_4^R) \tag{6.7}$$

$$\sigma_4 = [(N_{sim} - 1)^{-1} \sum_{m=1}^{N_{sim}} (t_4^{[m]} - t_4^R)^2 - N_{sim} B_4^2]^{1/2} \tag{6.8}$$

As usual, m denotes the index in N_{sim} replications. With the bias of t_4^R, the Goodness-of-Fit measure is modified as given in Equation 6.9.

$$Z^{\text{DIST}} = \frac{\tau_4^{\text{DIST}} - t_4^R + B_4}{\sigma_4} \tag{6.9}$$

A criterion of $|Z^{\text{DIST}}| \leq 1.64$ is suggested to judge if Z^{DIST} is sufficiently close to zero (a 0.10 level test), i.e., the L-kurtosis of the fitted distribution is close to the regional average L-kurtosis of the observed data.

6.3.5 Regional L-moment Algorithm

The regional L-moment algorithm is based on the index-flood method, which averages the statistics of data at the gauge to form the regional estimates. Instead of using conventional moments in the index flood method, the regional L-moment algorithm uses L-moment ratios of data. The regional L-moment algorithm assumes no serial correlation

for data observed at the same gauge, and no dependence between observations at different gauges. The index flood at the i-th gauge, or scale factor, is estimated by the sample mean of the record, and denoted as $l_1^{(i)}$. Data at each gauge are divided by this index flood; therefore, the regional average mean rainfall intensity is unity.

The L-moment ratios at the i-th gauge are denoted as $t^{(i)}, t_3^{(i)}, t_4^{(i)}$, the record length is denoted as n_i, and the regional average L-moment ratios are denoted by t^R, t_3^R, t_4^R, calculated as Equation 6.10 and 6.11.

$$t^R = \sum_{i=1}^{N} n_i t^{(i)} / \sum_{i=1}^{N} n_i \tag{6.10}$$

$$t_r^R = \sum_{i=1}^{N} n_i t_r^{(i)} / \sum_{i=1}^{N} n_i, r = 3, 4, \cdots \tag{6.11}$$

The parameters of the chosen frequency distribution are estimated based on the regional average L-moment ratios, and the quantile function with non-exceedance probability F is calculated from Equation 6.12

$$\hat{Q}_l(F) = l_i^{(i)} \hat{q}(F) \tag{6.12}$$

6.3.6 Assessment of Accuracy of Estimated Quantile

The accuracy of the estimated quantile in the regional L-moment algorithm is estimated with Monte Carlo simulation. The simulated samples should have the same statistical characteristics as that of the observed data — to keep the heterogeneity, dependence and other

statistical characteristics in the observed data. The possibility when the frequency distribution is mis-specified should be considered as well.

Hosking and Wallis (1997) provide a detailed introduction of the assessment procedure; therefore, only the modifications applied for using partial duration series are demonstrated herein.

A correlation matrix $\mathbf{R}$ is used to indicate the between site dependencies. It is originally calculated as Equation 6.13

$$r_{ij} = \frac{\sum_k (Q_{ik} - \bar{Q}_i)(Q_{jk} - \bar{Q}_j)}{[\sum_k (Q_{ik} - \bar{Q}_i)^2 \sum_k (Q_{jk} - \bar{Q}_j)^2]^{1/2}} \tag{6.13}$$

Where $\bar{Q}_i = n_{ij}^{-1} \sum_k Q_{ik}$, and Q_{ik} is the data value for the gauge i at the time point k. The time point k extends over all time points for which both gauges i and j have values. Equation 6.13 works well for AMS data, since there is only one value in each year (as a time point); however, PDS data may have situations when several values are recorded in the same year. Thus, Q_{ik} is redefined as the maximum data value for the gauge i at the time point k.

It is noted that in Equation 6.13, those data values recorded in a year at one gauge without counterparts at the other gauge are excluded from the calculation of the between-site dependence. Still, in the simulation algorithm, these data values are generated together with those data values included in the dependence calculation, by using the correlation matrix $\mathbf{R}$. When using PDS data, the second largest values in a year are excluded when

calculating between site dependence; likewise, these data values are generated with the correlation matrix $\mathbf{R}$.

The correlation matrix $\mathbf{R}$ needs to be positive definite, to generate correlated variables using Cholesky decomposition. Non-positive definite correlation matrices are modified by changing negative eigenvalues to small positive values (1×10^{-8}) and normalized (Brissette et al., 2007).

Over a large number (N_{sim}) of repeated simulations, the rRMSE is approximated as Equation 6.14.

$$R_i(F) = [N_{sim}^{-1} \sum_{m=1}^{N_{sim}} (\frac{Q_i^{[m]}(F) - Q_i(F)}{Q_i(F)})]^{1/2} \tag{6.14}$$

where $Q_i^{[m]}(F)$ is the quantile estimate at the non-exceedance probability F of the m-th replication, and $Q_i(F)$ is the estimated quantile based on observed data, at the i-th gauge. The at-site rRMSE can be averaged over the N gauges within a region to obtain a regionally averaged rRMSE, as in Equation 6.15.

$$R_R(F) = N^{-1} \sum_{i=1}^{N} R_i(F) \tag{6.15}$$

The rRMSE introduced in Equation 6.14 is useful to quantify variances in estimates of the regional model, and compare to its counterpart in estimates of the at-site model. However, confidence intervals of design rainfall estimates are needed to identify step changes in the design rainfall intensity over time. As discussed in Wang et al. (2013), a step change is statistically significant if the confidence intervals of design rainfall estimates for different

time periods are not overlapping, with a significance level less than α, where α is used to construct the confidence intervals.

The calculation of the confidence interval requires assumptions such as independence between data from different rainfall gauges, statistically homogeneous regions, and properly selected regional statistical distributions. However, these assumptions can hardly all be satisfied in reality. The rainfall data usually present some extent of violation. Instead, the empirical quantiles of the distribution of estimates are useful assessments of errors. In Monte Carlo simulation, the ratio of the estimated value to the true value $[\hat{Q}_i(F)/Q_i(F)]$ at site i are accumulated over each realization, and the upper and lower 5$^{\text{th}}$ percentiles are found and denoted as $U_{.05}(F)$ and $L_{.05}(F)$. The true value $Q_i(F)$ is expressed as

$$\frac{\hat{Q}_i(F)}{U_{.05}(F)} \leq Q_i(F) \leq \frac{\hat{Q}_i(F)}{L_{.05}(F)} \tag{6.16}$$

Hosking and Wallis (1997) referred to these bounds as "90% error bounds" for $\hat{Q}_i(F)$, and indicated that they can be confidence intervals only if the distribution of $\hat{Q}_i(F)/Q_i(F)$ is independent of the at-site means and the regional average L-moment ratios. In practice, "the independence does not hold, and confidence statements are at best approximate" (Hosking and Wallis, 1997). The error bounds can be accurate estimates of the magnitude of errors when the number of repetitions (N_{sim}) is large, e.g. $N_{sim} = 1000$ or $N_{sim} = 10000$.

6.4 Application of A Regional Frequency Model

6.4.1 Data Description and Screening

Records for two hundred and seventy rainfall gauges located in the Province of Ontario were obtained from Environment Canada. The gauges have daily maximum one-hour rainfall amounts recorded for various time spans, from as early as 1937, to as late as 2009. Records of 44 gauges are combined with records from other gauges, since these gauges are at the same or very close locations, and have consecutive rainfall records. The research time span is set to 1960–2007, and split by the end of the year 1983 to identify step changes in extreme rainfall intensities by comparing estimates from rainfall records pre-/post-1983. The rainfall records between April 1st and October 31st are extracted, and any yearly record that has more than 20% missing values within the seven month period (Apr. – Oct.) is excluded in the analyses described below. In the present research, 32 gauges in southern Ontario are analyzed (shown in Figure 6.1 and details are listed in Table 6.1), due to the high density of gauges in southern Ontario. All of these gauges have records longer than 10 years for both pre- and post-1983. The data have already undergone quality control at Environment Canada; therefore, any gross errors are not expected to be present. The rain gauges were changed from Meteorological Service of Canada (MSC) gauge to Type-B at most locations in the 1970s (Mekis and Hogg, 1999). Around 1965, the inside container of the MSC gauge was changed from copper to soft plastic. These modifications are sup-

Table 6.1: Information of 32 Gauges in Southern Ontario

No.	Climate ID	Record Length (Years)		Region
		-1983	1984-	
1	6100971	16	17	1
2	6104027	13	17	1
3	6104175	22	23	1
4	6105978	20	20	1
5	6106000	14	20	1
6	6127514	16	21	3
7	6131415	17	17	3
8	6131983	19	20	4
9	6133362	16	12	3
10	6136606	16	14	4
11	6137287	11	18	4
12	6137362	20	21	3
13	6139148	13	10	4
14	6139525	23	20	3
15	6140954	22	11	4
16	6142400	20	21	3
17	6143090	20	14	5
18	6144478	23	23	3
19	6146714	10	12	3
20	6148105	16	17	3
21	6149387	13	18	3
22	6150689	17	24	1
23	6150830	14	17	2
24	6151042	13	16	2
25	6153194	13	19	4
26	6153301	17	22	4
27	6155878	12	16	2
28	6158355	24	24	2
29	6158665	13	11	2
30	6158733	24	22	2
31	6158875	17	15	1
32	6166418	11	18	2

*The name and location of climate stations are listed in Table 8.1

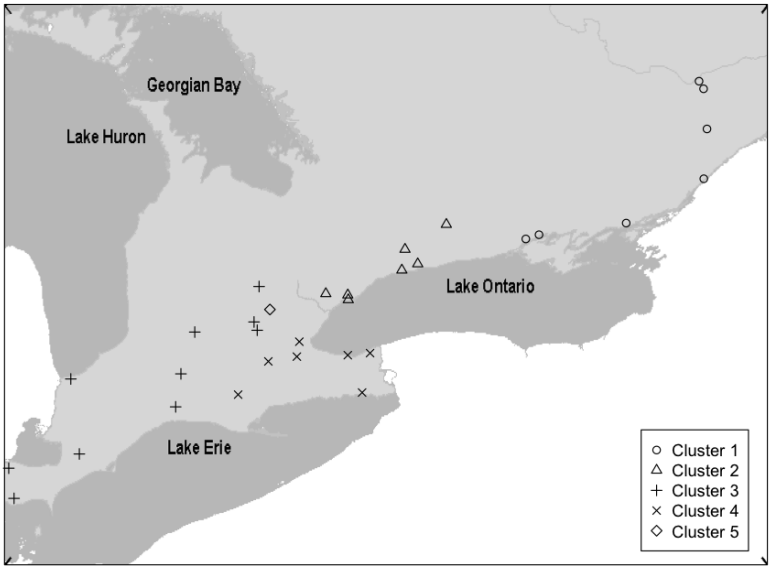

Figure 6.1: Thirty-two Gauges in Five Clusters Located in Southern Ontario

posed to introduce non-homogeneity in rainfall records and may lead to detection of false significant changes from the record (Groisman and Legates, 1995). It is reasonable to assume homogeneity in rainfall records, since all data are quality-controlled by Environment Canada.

6.4.2 Identification of Regions

The regions are formed by clustering site characteristics, which include distances to Lake Huron, Lake Erie, and Lake Ontario. The selection of these site characteristics is based on considerations of rainfall formation in southern Ontario. One-hour duration storms are too long to compare to convective storm durations, and mostly should be of the frontal rainfall type. In southern Ontario, sources of wet and warm air could be as close

as the Great Lakes, or as far as the Atlantic Ocean. The distances of gauges to the Atlantic Ocean are not sufficiently distinct to be clustering variables; therefore, the distances to three of the Great Lakes are used herein.

Using Ward's hierarchical clustering method and the k-means clustering algorithm, five regions are initially formed. However, some regions either include few gauges, or are statistically heterogeneous. According to Hosking and Wallis (1997), the heterogeneity measure tends to indicate false homogeneity for small size regions. Thus, regions are adjusted to obtain bigger regions and to achieve statistical homogeneity. The rainfall record (1984 – 2007) at the Guelph gauge has a negative L-kurtosis ratio and a small L-skewness ratio, which is statistically distinct from any other gauges; therefore, this gauge is split off as a single-site region. Four regions are distinguished and the numbers of gauges in each region and corresponding values of heterogeneity measure are listed in Table 6.2. Notice that regions 2 and 4 show some extent of heterogeneity; therefore, the regenerated samples should preserve equivalent heterogeneity.

Table 6.2: Number of Gauges in Each Region and Related Heterogeneity Measures

Region ID	# of Gauges	Heterogeneity Measure (Pre 1983)	Heterogeneity Measure (Post 1983)
1	7	0.58	-0.54
2	7	1.66	1.25
3	10	-0.07	0.28
4	7	1.23	1.68

6.4.3 Choice of Distribution

For the partial duration series of one hour daily maximum rainfall record, candidate frequency distributions are selected on the L-moment ratio diagram. Figures 6.2 and 6.3 show separate diagrams for each region, for the periods of pre- and post-1983. In each diagram, a frequency distribution is selected as a candidate if it is proximate to the center of at-site L-moment ratios. The five frequency distributions under consideration include: Generalized Logistic (GLO), Generalized Extreme Value (GEV), Generalized Pareto (GPA), Generalized Normal (GNO), and Pearson Type III (PE3). From both Figures 6.2 and 6.3, it is noted that all of the five distributions are potentially to be selected. The goodness-of-fit measure Z^{DIST} defined in Equation 6.9 is computed for each of the 5 candidate distributions for each region, as per Table 6.3. The bias of regionally averaged L-kurtosis is considered since all regions have less than twenty gauges. For both time periods, PE3 is chosen for use in regions 1 and 2, and GPA is chosen for use in regions 3 and 4.

Table 6.3: Measures of Goodness-of-fit for Candidate Distributions in Each Region

	1960 – 1983					1984 – 2007				
	GLO	GEV	GNO	PE3	GPA	GLO	GEV	GNO	PE3	GPA
Region 1	4.44	3.56	2.58	0.69	0.82	3.97	3.29	2.13	0.18	0.92
Region 2	3.28	2.50	1.70	0.17	0.44	3.23	2.43	1.58	0.09	-0.12
Region 3	3.07	2.33	0.92	-1.34	-0.31	4.16	3.20	1.77	-0.83	0.09
Region 4	3.70	2.54	1.78	0.53	-0.01	2.41	1.67	0.80	-0.67	-0.37

*Values underlined are moduli less than 1.64.

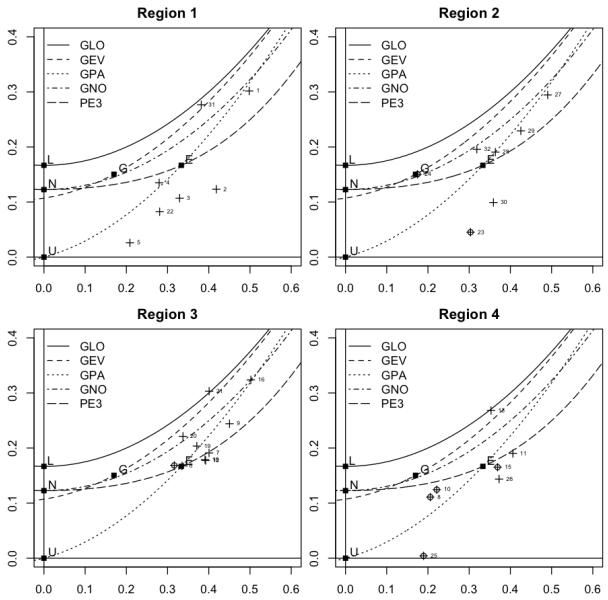

Figure 6.2: L-moment Ratio Diagrams of 1 h Partial Duration Seires in Each Region (1960 – 1983)

*Crosses with circles indicate gauges have less accurate estimates from the regional model in comparison with the at-site model

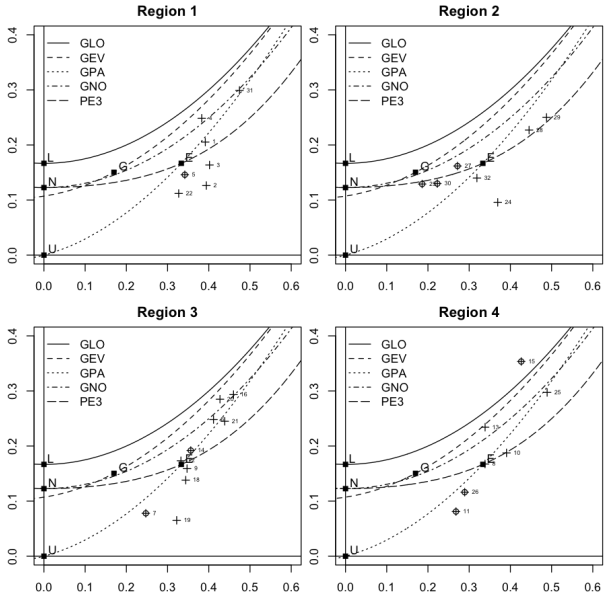

Figure 6.3: L-moment Ratio Diagrams of 1 h Partial Duration Seires in Each Region (1984 – 2007)

*Crosses with circles indicate gauges have less accurate estimates from the regional model in comparison with the at-site model

6.4.4 Assessment of Quantile Estimate Accuracy

In Monte Carlo simulation, a series of steps are applied to reproduce regions with the same statistical characteristics as the original region. The heterogeneity is preserved by arbitrarily assigning a range of L-CV values to gauges in the region. The range of L-CV values assigned is usually less than the range of sample L-CV values. The L-skewness ratios are all replaced with the regionally averaged L-skewness ratio. For example, Region 1 of period 1960–1983 has seven gauges with L-CVs varying over the range from 0.134 to 0.205, and the heterogeneity measure is $H = 0.58$. The simulated gauges have L-CV varying from 0.137 to 0.202, with a heterogeneity measure of 0.55.

Shown in Figures 6.4 and 6.5, between-gauge correlations are relatively low in all regions, with average values ranging from -0.02 to 0.21. Therefore, the samples generated in Monte Carlo simulation are not correlated. For each time period, 1000 replications of each region are simulated, and rRMSE and error bounds (90%) are calculated.

6.5 At-site PDS model

The design rainfall intensity estimates based on at-site PDS data are also calculated, to compare with estimates from the regional model. Statistical distributions used for at-site PDS models are consistent with the distribution used for the region in which the gauge was associated. The rRMSE and 90% error bounds are estimated in the same way as

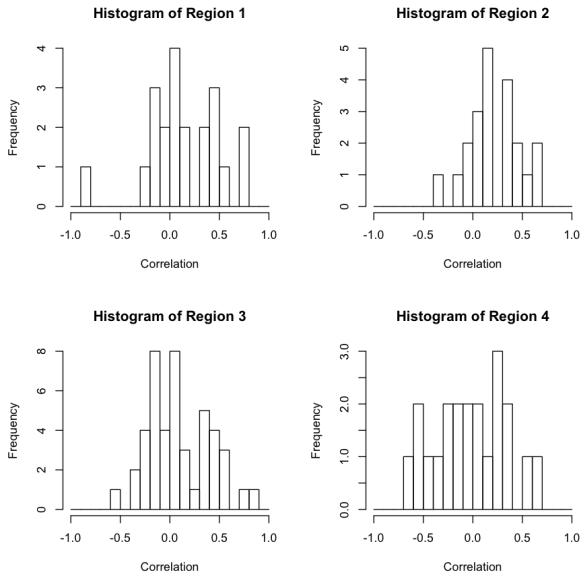

Figure 6.4: Histograms of Correlation between Gauges in Each Region (1960 – 1983)

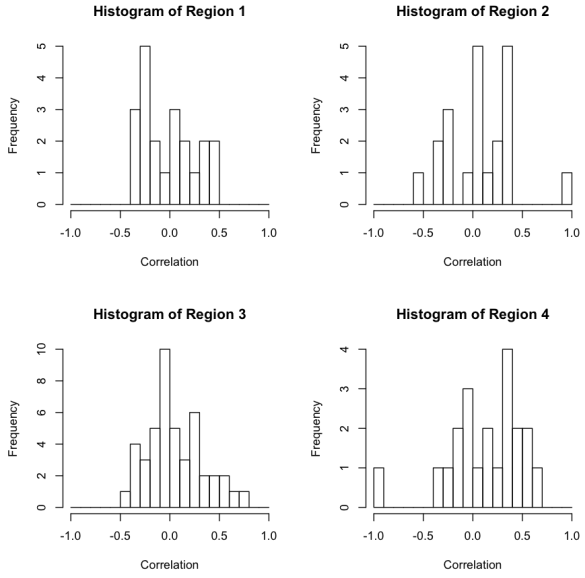

Figure 6.5: Histogram of Correlation between Gauges in Each Region (1984 – 2007)

the regional L-moment algorithm in Equation 6.14 and 6.16, apart from the use of at-site estimates instead of regional estimates.

6.6 Results of Accuracy Improvement

The comparison between the regional model and the at-site model shows improvement in the accuracy of the design rainfall intensity estimates. Table 6.4 shows the comparison of regionally averaged rRMSE between two models. The regionally averaged rRMSE is calculated using Equation 6.15, and the ratios in Table 6.4 are

$$[R^R(F) \text{ for at-site model})/R^R(F) \text{ for regional model}] \tag{6.17}$$

The reduction of rRMSE is demonstrated in all regions, for rainfall intensity estimates of all return periods.

Table 6.4: Ratio of Regionally Averaged RMSE of the Regional Model Against the At-site Models

Region	1960 – 1983			1984 – 2007		
	2 Year	5 Year	10 Year	2 Year	5 Year	10 Year
1	0.82	0.75	0.69	0.78	0.66	0.61
2	0.88	0.85	0.81	0.86	0.78	0.71
3	0.88	0.79	0.68	0.83	0.74	0.64
4	0.87	0.88	0.81	0.91	0.90	0.81

Amongst 32 gauges analyzed, 22 gauges have smaller rRMSE in the regional model in comparison with the at-site model, for the time period of 1960 – 1983, and 22 gauges (not the same set of gauges as referred to above) for the time period of 1984 – 2007, as

shown in Table 6.5. Figure 6.6 shows the histogram of ratios of extent of rRMSE between two models for both time periods. Comparisons of error bounds between two models show almost identical results.

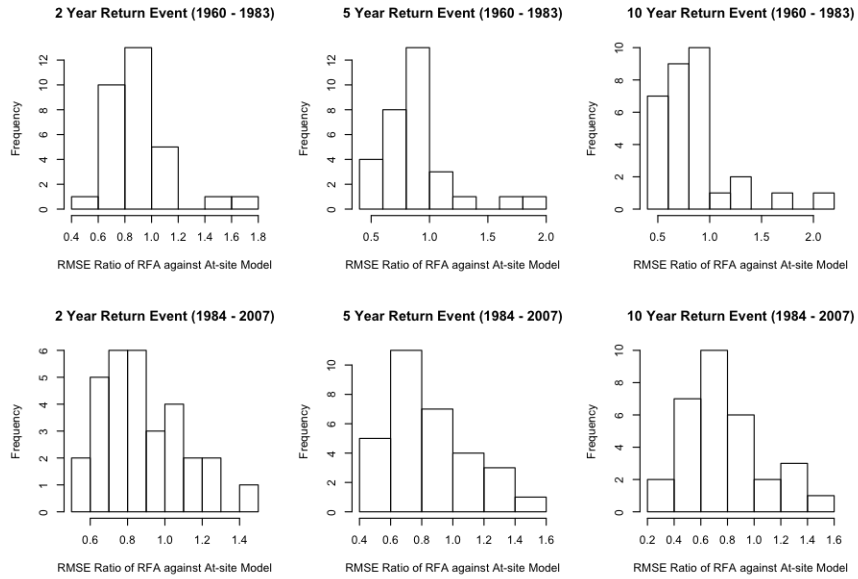

Figure 6.6: Histograms of Ratio of Error Bound Extent between the Regional Model and the At-site Model

The gauges that didn't show improvement of accuracy in the regional model are mostly in regions with possible heterogeneities. In Table 6.5, regions 2 and 4, which both have $H > 1$, have a substantial number of gauges that have larger rRMSE for the regional model than for at-site models. These gauges are indicated as symbols consisting of crosses and circles on the L-moment ratio diagrams in Figures 6.2 and 6.3, respectively for the two time periods. In the L-moment ratio diagram of the region 2 in Figure 6.3, the L-moment ratios of three gauges (No. 23, 27, 30) are all plotted close to the regional distribution

Table 6.5: Ratio of Regionally Averaged RMSE of the Regional Model Against the At-site Models

Gauge ID	1960 – 1983			1984 – 2007		
	2 Year	5 Year	10 Year	2 Year	5 Year	10 Year
6100971	0.59	0.54	0.47	0.68	0.63	0.62
6104027	0.80	0.64	0.50	0.82	0.65	0.56
6104175	0.93	0.93	0.89	0.76	0.65	0.63
6105978	0.77	0.75	0.75	0.96	0.81	0.74
6106000	0.89	0.89	0.87	1.01	0.84	0.80
6150689	0.93	0.90	0.89	0.76	0.79	0.79
6158875	1.01	0.85	0.80	0.58	0.46	0.37
6150830	1.09	1.05	0.94	1.13	1.14	1.12
6151042	1.69	1.76	1.70	0.84	0.73	0.68
6155878	0.78	0.67	0.60	1.00	1.02	1.02
6158355	0.85	0.88	0.87	0.69	0.63	0.58
6158665	0.72	0.66	0.63	0.58	0.43	0.36
6158733	0.79	0.84	0.84	1.25	1.32	1.26
6166418	0.75	0.76	0.74	0.95	0.93	0.91
6127514	0.92	0.94	0.87	0.66	0.57	0.47
6131415	0.66	0.58	0.52	1.07	1.23	1.23
6133362	0.87	0.71	0.55	0.75	0.69	0.62
6137362	0.83	0.82	0.71	0.83	0.80	0.75
6139525	1.14	1.19	1.13	1.13	1.02	0.90
6142400	0.68	0.54	0.42	0.81	0.66	0.51
6144478	0.87	0.81	0.74	1.0	0.98	0.89
6146714	1.09	0.96	0.85	0.87	0.83	0.75
6148105	0.87	0.83	0.79	0.73	0.59	0.49
6149387	0.98	0.81	0.69	0.70	0.54	0.45
6131983	1.45	1.93	2.08	0.77	0.86	0.82
6136606	0.98	1.20	1.30	0.69	0.69	0.62
6137287	0.61	0.54	0.44	1.09	1.38	1.36
6139148	0.74	0.69	0.61	0.82	0.83	0.80
6140954	1.10	0.94	0.81	1.42	1.13	0.91
6153194	0.95	1.25	1.34	0.77	0.64	0.53
6153301	0.80	0.73	0.68	1.21	1.48	1.53
6143090	1	1	1	1	1	1

* Horizontal lines separate regions.

curve (PE3); contrarily, the No. 24 gauge, which was plotted apart from the PE3 curve, was estimated more accurately in the regional model. This shows that closeness to the regional distribution curve on the L-moment ratio diagram is not an indicator of more accurate estimates.

6.7 Changes Identified in Design Rainfall Intensities

As discussed in Wang et al. (2013), a step change is identified if the confidence intervals of design rainfall estimates for two time periods are not overlapping, with a significance level less than α, where α is used to construct the confidence intervals.l. In addition, the 90% error bounds are good approximations of the confidence interval when the number of simulations is large ($N_{sim} = 1000$ in this analysis). Therefore, the error bounds are used to identify changes in the design rainfall intensity herein.

For the 1-hour design rainfall, based on the at-site PDS model, changes are identified at five gauges in southern Ontario. In detail, the gauges located at Ottawa Macdonald-Cartier Int'l A and Toronto Pearson Airport show statistically significant decreases; while the Delhi, Belleville, and Bowmanville gauges have increased significantly. The changing rate is calculated as Equation 6.18

$$\frac{(i_2 - i_1)/i_1}{t_2 - t_1} \times 100\% \tag{6.18}$$

Where i_1 and i_2 are design rainfall intensities estimated from the 1st and 2nd periods, sep-

arately; and t_1 and t_2 are the mid point year of these two periods. A complete result of changes identified based on the at-site PDS model is listed in Table 6.6, including statistically insignificant changes.

Five gauges are identified with statistically significant changes in the regional model. The difference in comparison with the at-site model results are: no changes identified at Delhi or Toronto Pearson Airport gauges, but changes identified at the Toronto Island Airport Gauge (2-year return storm, decreased), Waterloo Wellington Airport (2-year return storm, increased), and Belleville (5-year return storm, increased). The rainfall estimates and error bounds of these five gauges are listed in Table 6.7.

6.8 Discussion

To discuss the different changes identified in the regional model estimates, consider the view of the regional L-moment algorithm. The rainfall intensities at gauges in the same region are assumed statistically identically distributed apart from scale factors (defined as the sample means at each gauge). This assumption implicitly states that storms observed at one gauge are as likely to be observed at other gauges in the same region, both historically, and in the future. Therefore, the between-site variations of the occurrences of heavy storms, which substantially determine the at-site model estimates, are averaged over all gauges in the regional model, except the variation of scale factors. For regions that are not acceptably homogeneous, the heterogeneity between gauges is preserved in the Monte

Table 6.6: Changes of Design Rainfall Intensity in Southern Ontario

Gauge ID	1960 – 1983			1984 – 2007		
	2 Year	5 Year	10 Year	2 Year	5 Year	10 Year
6100971	-0.23	-0.48	-0.63	0.12	0.32	0.44
6104027	0.79	0.92	0.96	0.62	0.80	0.93
6104175	0.01	0.27	0.43	-0.04	0.11	0.20
6105978	-0.73	-0.69	-0.64	-0.50	-0.37	-0.28
6106000	-1.29*	-1.09	-0.94	-1.18*	-0.95	-0.81
6150689	1.15*	1.29	1.38	1.02*	1.06*	1.10
6158875	1.01	1.81	2.31	0.71	0.89	1.00
6150830	1.81*	1.35	1.08	1.88*	1.41	1.17
6151042	0.51	1.29	1.86	0.83	0.51	0.34
6155878	1.22	0.37	-0.15	0.94	0.61	0.42
6158355	-0.56	-0.43	-0.34	-0.53	-0.61	-0.65
6158665	-2.11	-1.69	-1.39	-1.79*	-1.82	-1.84
6158733	-0.66	-1.05*	-1.26*	-0.54	-0.62	-0.66
6166418	-0.64	-1.02	-1.20	-0.43	-0.73	-0.89
6127514	0.64	1.02	1.36	0.43	0.35	0.27
6131415	-0.50	-1.10	-1.52	-0.17	-0.25	-0.31
6133362	0.66	0.49	0.29	0.42	0.36	0.30
6137362	0.20	0.06	-0.08	0.18	0.16	0.13
6139525	-0.61	-0.52	-0.43	-0.54	-0.52	-0.52
6142400	0.03	-0.15	-0.30	0.05	-0.02	-0.08
6144478	0.02	-0.16	-0.31	0.12	0.04	-0.02
6146714	2.62	2.81	2.78	2.14	1.93	1.77
6148105	0.35	0.60	0.89	0.42	0.28	0.17
6149387	1.63	2.00	2.30	1.47*	1.23	1.07
6131983	0.97*	1.75*	2.38*	0.46	0.52	0.58
6136606	-0.06	0.44	0.96	0.01	-0.02	-0.01
6137287	-0.46	-1.19	-1.72	-0.46	-0.47	-0.45
6139148	-0.62	-0.67	-0.72	-0.62	-0.54	-0.48
6140954	-0.07	-0.27	-0.32	0.08	0.04	0.05
6153194	-0.43	0.40	1.41	0.05	0.06	0.09
6153301	0.00	-0.37	-0.63	0.05	0.01	0.02
6143090	0.65	-0.45	-1.26	0.65	-0.45	-1.26

* Horizontal lines separate regions. Unit: Percentages Per Year. Use At-site Partial Duration Series Model
* Values with asterisks are statistically significant changes (90%).

Table 6.7: Changes of Design Rainfall Intensity in Southern Ontario (Percentages per year, using at-site PDS model)

Gauge ID	T	Model	1960 – 1983				1984 – 2007			
			L-CV	Q(F)	0.05	0.95	L-CV	Q(F)	0.05	0.95
6131983	5yr	regional	0.11	29.71	26.66	33.36	0.11	33.89	29.69	38.59
		at-site*	0.12	27.17	25.10	28.99	0.20	36.70	31.64	42.35
	10yr	regional	0.11	33.20	29.08	38.05	0.11	39.10	33.43	46.23
		at-site*	0.12	28.95	26.47	31.43	0.20	42.73	35.19	51.01
6158733	5yr	regional	0.21	34.96	30.68	39.94	0.18	30.01	26.93	33.68
		at-site*	0.20	36.59	31.25	42.14	0.12	27.77	25.35	30.70
	10yr	regional	0.21	40.71	34.78	47.72	0.18	34.53	30.14	39.72
		at-site*	0.20	43.21	35.87	51.04	0.12	30.65	27.44	34.63
6158665	2yr	regional*	0.19	28.09	24.84	31.66	0.17	22.05	19.63	24.76
		at-site	0.20	28.26	24.02	33.01	0.20	21.11	17.08	25.96
6149387	2yr	regional*	0.24	24.77	21.64	27.47	0.23	30.41	27.93	33.61
		at-site	0.17	24.25	20.97	27.77	0.22	30.36	26.28	34.93
6150689	5yr	regional*	0.19	25.51	22.62	28.63	0.20	31.60	28.67	35.02
		at-site	0.16	24.63	21.43	28.13	0.19	31.78	27.99	35.93

* Models with asterisks are identified statistically significant changes (90%). Unit: Percentages Per Year.

Carlo simulations, by means of assigning L-CV values for replications of rainfall records. The re-assigned L-CV values vary over a range not the same as the original L-CV values. The consequence is that the new variations between gauges may not be the same amount as in the original rainfall records.

For the gauges at Delhi CS and Toronto Pearson Airport, the rearrangement of sample variation changed the design rainfall intensity estimate in a direction reversed to the direction of changes identified in the at-site model (as listed in Table 6.7); therefore, the differences between estimates from the two time periods are substantially reduced, and no statistically significant differences can be identified in the regional model. The gauge at Delhi CS has an original L-CV of 0.20 over the time period 1984 – 2007, but was simulated with a value of 0.11 in the regional model. The reassignment of L-CV values results

in the reduced rainfall intensity estimates in the regional model. The Toronto Pearson Airport gauge has an original L-CV = 0.12 and a regional simulated L-CV = 0.18 over the 2nd time period; therefore, the estimates are substantially increased for 5 and 10 years return events. The 2-year event estimates at Toronto Island airport are changed as L-CV values changed as well. The error bounds at Waterloo Wellington Airport and Belleville gauges were only slightly overlapping in the at-site model, and the changes of L-CV values lead to completely unconnected error bounds. The correlation coefficients between $\frac{\hat{Q}(F)_{\text{regional}}}{\hat{Q}(F)_{\text{at-site}}}$ and $\frac{\text{L-CV}_{\text{simulated}}}{\text{L-CV}_{\text{regional}}}$ amongst all gauges are calculated, where F is the non-exceedance frequency of 2, 5, and 10-year return events. The correlation coefficients are all statistically significant (0.95, using Student's t-test), for both time periods, which support the relationship between intensity estimates and simulated L-CV values.

The regional L-moment algorithm was expected to improve the accuracy of the rainfall intensity estimate in this study, especially for gauges with limited rainfall records, and this is partially supported by the results of accuracy improvement. It shows that for region 1, which is statistically homogeneous, the 10-year storm estimates rRMSE are reduced by 26% (ranging from 11% to 53%) in the regional model on average, for the 1st time period, and 35% (ranging from 20% to 63%) reduced for the 2nd time period. Given that the record lengths are approximately 20 years, which is definitely inadequate to estimate 10-year return storm, this reduction in rRMSE is very impressive. The performances of the regional model on the 5-year return storm estimates are promising as well — 22% and 31% rRMSE reduction on average. For regions with statistical heterogeneity (e.g. regions 2 and

4), many gauges with record lengths shorter than 15 years show reduced rRMSE in the regional model, while gauges with relatively longer records have increased rRMSE in the regional model. The accuracy improvement of rainfall intensity estimates with the regional model has considerable merit.

6.9 Conclusion

This study explores the use of a regional L-moment algorithm combined with partial duration series to identify changes in design rainfall intensity. The results show that:

- The regional L-moment algorithm is capable of reducing the uncertainty involved in rainfall intensity estimates, especially at gauges with limited records and within statistically homogeneous regions.

- The rainfall intensity estimates for the regional model are subject to the simulated L-CV values, which determine the between-site variation in a region.

- The design rainfall intensity changes identified in the regional model can be different from at-site PDS model, due to the reassignment of between-site variations (L-CV values) in the regional model.

- The regional L-moment algorithm using PDS data, as introduced in this study, can develop a regional model with respect to PDS extracted with different annual arrival rate (λ). This enables the benefits of using PDS in heavy rainfall models, including

greater and more practical design rainfall estimates, in comparison with the AMS model.

Chapter 7

The Sensitivity of Changes in Design Rainfall Intensities

7.1 The Rate of Change of Design Rainfall Intensity

In chapter 6, to analyze changes in design rainfall intensities with respect to the time-frame of the rainfall record, design rainfall intensities estimated from records of two consecutive time periods (1960 –1983 and 1984 – 2007) are compared, based on 1 h rainfall records from 32 climate stations in southern Ontario. The confidence intervals are computed using the resampling method. If the confidence intervals for the design rainfall intensity of the same return period do not overlap, then a step change in the design rainfall intensity is identified, with a significance level less than α, where α is used to construct the confidence intervals. Further, the rate of change of the design rainfall intensity are

calculated, as given in Equation 7.1.

$$\frac{(i_2 - i_1)/i_1}{t_2 - t_1} \times 100\% \tag{7.1}$$

where i_1 and i_2 are design rainfall intensities estimated from two time periods, separately; and t_1 and t_2 are the mid-point years of these two time periods.

7.2 The Sensitivity of the Rate of Change

In addition, it is of interest to determine how the selection of the split year affects the design rainfall intensity changes identified. Therefore, in this chapter the sensitivities of the changes with respect to the split year are assessed using the split year changing, enumerated from 1975 to 1990, using the PDS model with at-site rainfall data. The result of the 1 h daily maximum rainfall record at Delhi, ON (climate station ID: 6131983) is shown in Figure 7.1. The rate of change of 25-year return rainfall is the largest for all split years, while that of the 2-year return rainfall is the smallest. The rate of change of the 2-year return rainfall is insensitive in response to the split year, fluctuating between 1 and 1.5% per year. Most changes identified at Delhi are statistically significant, except the two split years of 1989 and 1990. This provides strong evidence of increasing design rainfall intensities at Delhi, ON.

Another example at the Toronto Pearson Airport gauge (climate station ID: 6158733)

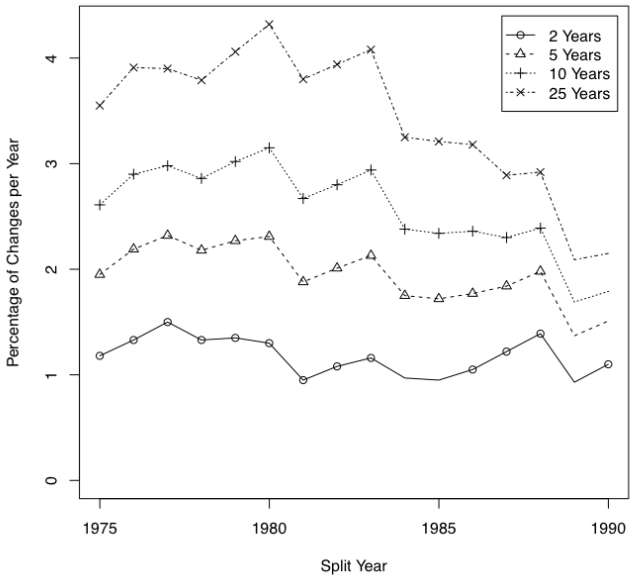

Figure 7.1: Sensitivity of Rate of Change and Significance in respect to Split Year at Delhi CS, ON (1 h Duration Rainfall)

demonstrates a different pattern of sensitivities of the rate of change, as shown in Figure 7.2. The 25-year design rainfall intensity estimate shows high decreasing rates for all split years, and is the least sensitive amongst all four return periods; the rate of change of 2-year design rainfall intensity exhibits large sensitivity to the split year, and is always the smallest decreasing rate amongst all four return periods. The statistical significances of the changes are sensitive to the split years as well. For the 5, 10, and 25-year event, changes are significant when the rainfall record is split from early 1980s until 1990, while the changes for the 2-year event are only statistically significant if split the record from the late 1980s. The sensitivity results of the statistical significance demonstrates the emergence of changes in the 1980s, and provides insights on which period of record should be used to estimate design rainfall intensities.

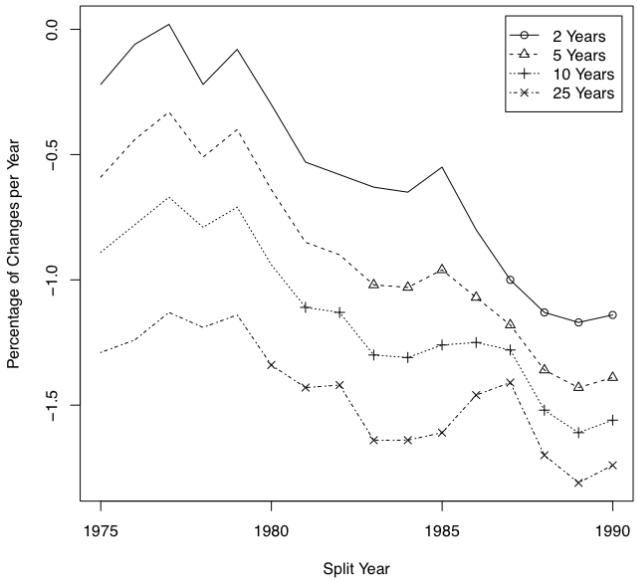

Figure 7.2: Sensitivity of Rate of Change and Significance in respect to Split Year at Toronto Lester B. Pearson INT'L A, ON (1 h Duration Rainfall)

Examining sensitivity analysis results at all 32 stations shows that changes in design rainfall intensity between records of two consecutive time periods are sensitive to the split year. However, the analyses of 32 stations found no consistent pattern, in terms of the trends of the rate of change or the statistical significance of changes. To conclude, the design rainfall intensity varies over time (and substantially, sometimes). Therefore, the sensitivity of the design rainfall intensity should be analyzed in relation to the timeframe of the rainfall record being used, as an alternative to the use of the entire historical rainfall record.

Chapter 8

Conclusions and Future Work

8.1 Synthesis Conclusion

8.1.1 Conclusion for Rainfall Intensity Changes

The changes in heavy rainfall intensities have been analyzed using three different models, and the changes identified are consistent between models. It is appropriate to conclude that rainfall intensities have been changing during the last few decades in Ontario. Spatially, changes are occurring mostly in southern Ontario, along the coasts of both Lake Erie and Lake Ontario from Windsor to Ottawa. There are no conclusive regional changes identified, although several climate stations with geographical closeness show the same direction of changes. For example, the Toronto area and the area from Windsor to London show decreased changes. Temporally, changes are occurring during the 1980s and 1990s, from the sensitivity analyses of the changes.

This study has been mostly using the 90% confidence limits to detect changes in rainfall intensities, and addressed that the actual significance level is 0.02. As shown in Table 3.2, there are 35 changes identified with significance level of 0.02, in the AMS model. However, by using a significance level of 0.05 (83.4% confidence limits), there are 56 significant changes identified in rainfall intensities, which is similar to the results listed in table 3.3, which is using 80% confidence limits. For the PDS models, when relaxing the significant level from 0.02 to 0.05, one significant change is identified at Delhi for the at-site model, and one significant change is identified at Belleville for the regional frequency analysis model.

8.1.2 Conclusion for Rainfall Intensity Models

The research developed three types of statistical models for heavy rainfall intensities: the at-site model using annual maximum series, the at-site model using partial duration series, and the regional frequency analysis model using partial duration series. The application of the Gumbel distribution in the AMS model is investigated and supported, which shows that the Gumbel distribution is as good as other three-parameter distributions in the modeling of rainfall values. In urban stormwater system design, the PDS model is more appropriate for heavy rainfall modeling when the return period is less than or equal to 10 years. It is also exhibited that the regional model using partial duration series can reduce uncertainties involved in the rainfall intensity estimates.

8.1.3 Conclusion for Rainfall Intensity Uncertainties

The uncertainties involved in rainfall intensity estimates can be substantial, due to limited rainfall records or temporal changes. In this research, the uncertainties are characterized using relative RMSE and confidence intervals. The currently used design rainfall intensities, either from the MSC IDF file or from the MTO IDF tool, are associated with considerable amounts of uncertainties in certain conditions. The rainfall intensity estimates derived from the EC data also have substantial amounts of uncertainties involved, including the large extent of confidence intervals, and the shift of the expected values. The extent of the confidence interval is linearly related to the log-transformed length of the rainfall record, which provides insights to understand the condition in Ontario — most climate stations do not have rainfall records long enough to provide accurate rainfall intensity estimates (e.g., less than 10% for 95% confidence level). The regional frequency analysis model is capable of reducing uncertainty substantially, and is recommended for use if rainfall records are available from adjacent climate stations.

To assess the rainfall intensity estimate for stormwater system design, the following recommendations are given based on the studies in this research:

- Use the partial duration series instead of the annual maximum series for the rainfall intensity model when the return period is no more than 10 years. This is because the AMS model will not use all the information available about heavy rainfall events. It is agreed that the difference is trivial when modelling for extreme events (e.g., 100-year return period).

- When extracting the partial duration series, use the mean residual life plot, parameter estimates stability plot, and the design rainfall estimates stability plot to select the rainfall intensity threshold.

- Analyze the sensitivity of the rainfall intensity estimate in relation to the missing values. The heavy events recoded in those years which have considerable numbers of missing values are valuable information for the statistic model.

- Try to split the record in two pieces, at different years, and develop models for each piece of the record, compare the estimate for given return period to identify if changes have occurred over time.

- Try use of different lengths of record (always use the most recent record) to examine the extent of the uncertainties involved in the rainfall intensity estimate, and use the appropriate time period of the rainfall record, which provides rainfall intensity estimates with small uncertainties, instead of always using the entire available rainfall record.

- Develop the regional frequency analysis model if rainfall records are available from adjacent climate stations, especially when the rainfall record is too short to provide accurate rainfall intensity estimates.

- When developing rainfall models using partial duration series, select the frequency distribution with the L-moment ratio diagram and examine the goodness-of-fit using relative RMSE, instead of the Probability Plot Correlation Coefficient (PPCC)

method.

- Estimate the distribution parameters with the L-moment method, instead of the conventional method of moments.

- In the regression of IDF curves, use non-linear regression instead of the linear regression, and use the upper confidence limit when the width of the confidence interval is large.

8.2 Contributions

This research has contributions to theories and methodologies in heavy rainfall frequency analysis, including theoretical explanation of the confidence interval comparison; clarification of the relationship between the event-based model and the annual-based model; and the application of regional frequency analysis using partial duration series.

This research theoretically validates the methodology for the identification of changes in heavy rainfall intensities by examining the confidence intervals for overlapping. It is proved that the two estimates are significantly different if the two confidence intervals are not overlapping, with a significance level less than that used for constructing confidence intervals. A previous master student, Ms. Branislava Vasiljevic, has applied this method in her master thesis. However, she did not validate the usage of this method, nor provide the reason for not using conventional tests, e.g. the Student's t-test. This research explains that the t-test is not directly applicable, but managed to relate the inequality of confidence

limits to the Student's t-test. It is shown that the significance level of the changes identified in the rainfall intensity is less than α, where α is used to construct the confidence intervals.

The difference between the partial duration series model and the annual maximum series model is clarified in this research. Previously, the estimates from the PDS model and the AMS model were compared directly, without consideration of the different concepts behind the two models. This research explains the difference between the event-based and the annual-based models. It is shown that a PDS model is related to the recurrence interval between individual events, while the AMS model is related to the return period between two hydrologic years, in which a given rainfall intensity is exceeded, regardless of the number of exceedances. The use of PDS model is not only attributed to the greater rainfall intensity estimates, but also more importantly, because of the more practical relationships with the urban stormwater management.

The application of regional frequency analysis (the regional L-moment algorithm) using partial duration theory is another contribution from this research. The original algorithm and codes in R-project were modified to handle the situations when the length of the record is different from the number of values in the data series. The algorithms for the discordance measure, the homogeneity measure, the goodness-of-fit measure, and the assessment of accuracy are all modified accordingly. The modified algorithms are tested with real data and the results show that the regional frequency analysis method can reduce uncertainties to a large extent.

8.3 Limitations and Future Work

While extensive work has been done, there are still limitations in this research, and suggestions for future work.

Only a few rainfall durations are discussed in this research (30 minutes to 2 hours, mostly). These design rainfall estimates are applied in a regression to generate IDF curves. The regression inevitably introduces uncertainties into an interpolated design rainfall estimate. Therefore, the uncertainty associated with, for example, 45 min duration rainfall intensity is dependent on both the uncertainties in 30 min and 1 h rainfall intensity estimates and the errors of the regression function inbetween. The relationship has not been clearly demonstrated, and it is of interest to quantify this relationship and test its sensitivity to all kinds of factors including record length, the duration time, the regression functions, etc. This research did not discuss this, because the research was focused on the rainfall intensities over given durations.

Besides the temporal interpolation, the spatial interpolation is another potentially fruitful direction. This research only developed regional models for gauged locations. It is needed to further develop these models to estimate design rainfall intensities for ungauged locations. In addition, the site characteristics used in this research are limited to the distances between climate stations and the Great Lakes, while there is more information capable to characterize the rainfall intensity pattern at a location, for example the mean annual precipitation, the time of the largest event in a year, the dominant wind direction in the rainy season, the land use, and the topography of adjacent area.

Further, the impact of an uncertain rainfall intensity estimate on a given urban stormwater system should be quantified. The accuracy of the rainfall-runoff model also depends on the uncertainties in other hydrologic parameters in the drainage area, e.g. the infiltration and abstraction rates, the imperviousness, and the roughness of the land surface. With all these parameters unchanged, the marginal improvement of the model accuracy will decrease and eventually become insensitive to the improvement of the accuracy of rainfall intensity estimates. In addition, the urban stormwater system is equipped with detention/retention facilities, which will lessen the effects of underestimated rainfall events. As well, the stormwater conduits are manufactured with specific diameters. It is not possible to bury a conduit of 566.7 mm in diameter that is just sufficient to handle the design storm; the conduit will be designed as 600 mm or even larger. Thus, the uncertainty in the design rainfall is not as critical because the stormwater conduit can handle larger rainfall runoff naturally. It is suggested to analyze the response of urban stormwater system with respect to design rainfall intensities and uncertainties involved.

Appendix

Table 8.1: Climate Stations In Southern Ontario

Station ID	Station Name	Latitude	Longitude	Altitude
6010738	BIG TROUT LAKE	53.83	-89.87	224.10

6011305	CENTRAL PATRICIA	51.50	-90.15	345.00
6012199	EAR FALLS (AUT)	50.63	-93.22	362.60
6014353	LANSDOWNE HOUSE (AUT)	52.20	-87.94	253.40
6016295	PEAWANUCK (AUT)	54.98	-85.43	52.70
6016525	PICKLE LAKE (AUT)	51.45	-90.22	390.80
6016527	PICKLE LAKE A	51.45	-90.21	386.20
6016975	RED LAKE A	51.07	-93.79	385.88
6020LPQ	ATIKOKAN (AUT)	48.76	-91.63	389.30
6034075	KENORA A	49.79	-94.37	409.65
6035190	MINAKI	49.98	-94.67	335.30
6036904	RAWSON LAKE	49.65	-93.72	358.10
6036907	RAWSON LAKE (AUT)	49.66	-93.73	435.00
6037775	SIOUX LOOKOUT A	50.12	-91.90	383.10
6040325	ARMSTRONG (AUT)	50.29	-88.91	322.50
6041110	CAMERON FALLS (AUT)	49.15	-88.34	232.60
6041221	CARIBOU ISLAND	47.33	-85.83	186.50
6042716	GERALDTON A	49.78	-86.93	348.40
6046770	PUKASKWA NATL PARK	48.60	-86.30	192.00
6047810	SLATE ISLAND	48.62	-87.00	185.90
6048145	STURGEON LAKE	49.88	-90.97	428.20
6048235	TERRACE BAY(AUT)	48.82	-87.10	289.60

6048268	THUNDER BAY CS	48.37	-89.33	199.40
6049095	UPSALA (AUT)	49.03	-90.47	488.50
6052259	ELLIOT LAKE A	46.35	-82.56	331.30
6055210	MISSISSAGI ONT HYDRO	46.43	-83.38	225.60
6056907	RAYNER	46.33	-83.50	243.80
6057592	SAULT STE MARIE A	46.48	-84.51	192.00
6059408	WAWA (AUT)	47.97	-84.78	287.10
6059475	WHITE RIVER	48.60	-85.28	378.90
6059D09	WAWA A	47.97	-84.78	287.10
605DJ25	KILLARNEY (AUT)	45.97	-81.48	196.30
6061361	CHAPLEAU A	47.82	-83.35	448.06
6068148	SUDBURY	46.48	-80.98	259.10
6068150	SUDBURY A	46.63	-80.80	347.50
6068158	SUDBURY SCIENCE NORTH	46.47	-81.00	263.00
6070027	ABITIBI CANYON	49.88	-81.57	204.20
6072183	DYMOND ONT HYDRO	47.52	-79.68	198.10
6073980	KAPUSKASING CDA ON	49.41	-82.44	218.00
6074211	KIRKLAND LAKE CS	48.15	-80.00	324.00
6075435	MOOSONEE RCS	51.29	-80.62	9.10
6075543	NAGAGAMI (AUT)	49.75	-84.16	264.00
6076540	PINARD	49.85	-81.60	231.60

6076572	PORCUPINE ONT HYDRO	48.47	-81.27	298.70
6078285	TIMMINS VICTOR POWER A	48.57	-81.38	294.70
6079068	UPPER NOTCH	47.25	-79.58	240.80
6080192	ALGONQUIN PARK EAST GATE	45.53	-78.27	397.00
6084278	LA CAVE	46.37	-78.73	172.20
6084307	LAKE TRAVERSE	45.95	-78.07	236.20
6085700	NORTH BAY A	46.36	-79.42	370.30
6093004	GREAT DUCK ISLAND	45.65	-82.97	182.90
6100285	APPLETON	45.19	-76.11	133.00
6100493	BARK LAKE DAM	45.42	-77.80	335.30
6100720	BELLROCK	44.48	-76.77	146.30
6100971	BROCKVILLE PCC	44.60	-75.67	96.00
6101335	CHALK RIVER AECL	46.05	-77.37	121.90
6101820	COMBERMERE	45.37	-77.62	286.50
6101874	CORNWALL	45.02	-74.75	64.00
6101901	CORNWALL ONT HYDRO	45.03	-74.80	76.20
6101986	DELTA	44.62	-76.13	97.50
6102839	GLOUCESTER DESJARDINS	45.33	-75.50	76.20
6103024	GRENADIER ISLAND	44.42	-75.85	82.00
6103367	HARTINGTON IHD	44.43	-76.69	160.00
6104027	KEMPTVILLE CS	45.00	-75.63	99.40

6104146	KINGSTON A	44.22	-76.60	93.00
6104175	KINGSTON PUMPING STATION	44.24	-76.48	76.50
6105061	MERIVALE CDA	45.30	-75.73	89.90
6105978	OTTAWA CDA RCS	45.38	-75.72	79.20
6105960	OTTAWA BRITANNIA	45.37	-75.80	57.60
6105980	OTTAWA CITY HALL	45.43	-75.70	56.40
6106000	OTTAWA MACDONALD-CARTIER INT'L A	45.32	-75.67	114.00
6106098	OTTAWA RIDEAU WARD	45.40	-75.63	71.30
6106400	PETAWAWA NAT FORESTRY	45.98	-77.43	183.00
6107836	SMITHS FALLS TS	44.88	-76.00	114.30
610F3Q0	PERTH	44.88	-76.20	133.20
610FC98	PETAWAWA HOFFMAN	45.88	-77.25	153.00
6110210	ALLAN PARK	44.17	-80.93	285.00
6110557	BARRIE WPCC	44.38	-79.69	221.00
6110606	BEATRICE 2	45.13	-79.40	297.20
6110607	BEATRICE CLIMATE	45.14	-79.40	297.20
6110617	BEAUSOLEIL	44.85	-79.87	183.00
6110827	BORDEN A	44.27	-79.93	227.40
6110854	BRACEBRIDGE ONT HYDRO	45.03	-79.30	266.70
6111792	COLLINGWOOD	44.50	-80.22	179.80
6112072	DORSET MOE	45.22	-78.93	323.10

6113490	HONEY HBR BEAUSOLEIL	44.85	-79.87	182.90
6114295	LAGOON CITY	44.55	-79.22	220.70
6115525	MUSKOKA A	44.97	-79.30	281.90
6115811	ORILLIA BRAIN	44.60	-79.44	250.00
6116132	OWEN SOUND MOE	44.58	-80.93	178.90
6116254	PARRY SOUND	45.33	-80.00	193.50
6116257	PARRY SOUND CCG	45.34	-80.04	176.30
6116843	RAGGED RAPIDS	45.02	-79.68	228.60
6117700	BARRIE-ORO	44.48	-79.55	289.00
6119115	UTTERSON ONT HYDRO	45.20	-79.35	297.20
61191LK	VANKOUGHNET	45.03	-79.00	304.80
6119500	WIARTON A	44.75	-81.11	222.20
6.11E+03	EGBERT CS	44.23	-79.78	251.00
61210K7	BRUCE ONTARIO HYDRO	44.33	-81.58	179.80
6121275	CENTRALIA A	43.30	-81.52	253.00
6121499	CHESLEY	44.28	-81.13	251.50
6121912	COVE ISLAND	45.33	-81.73	179.80
6121940	CYPRUS LAKE CS	45.23	-81.53	190.00
6122079	DOUGLAS POINT	44.33	-81.60	179.80
6122456	FORMOSA	44.07	-81.28	304.80
6122847	GODERICH	43.77	-81.72	213.70

6127518	SARNIA CHRIS HADFIELD A	43.00	-82.31	181.00
6127514	SARNIA AIRPORT	42.99	-82.30	180.60
6128323	TOBERMORY CYPRUS LAKE	45.23	-81.53	190.00
6129660	WROXETER	43.86	-81.15	335.00
6131415	CHATHAM WPCP	42.39	-82.22	180.00
6131983	DELHI CS	42.87	-80.55	231.70
6133362	HARROW CDA AUTO	42.03	-82.90	191.00
6134344	LANGTON	42.73	-80.58	228.60
6134610	LONG POINT	42.55	-80.05	175.30
6135638	NIAGARA FALLS	43.13	-79.08	182.90
6135642	NIAGARA FALLS CHIPPAWA	43.07	-79.05	175.00
6136606	PORT COLBORNE	42.88	-79.25	175.30
6136699	PORT WELLER (AUT)	43.25	-79.22	79.00
6137154	RIDGETOWN RCS	42.45	-81.88	205.70
6137287	ST CATHARINES A	43.20	-79.17	97.80
6137362	ST THOMAS WPCP	42.77	-81.21	209.10
6137401	ST WILLIAMS ACS	42.70	-80.45	213.40
6137730	SIMCOE	42.85	-80.27	240.50
6139148	VINELAND STATION RCS	43.18	-79.40	79.20
6139525	WINDSOR A	42.28	-82.96	189.60
6139538	WINDSOR UNIVERSITY	42.30	-83.07	179.80

613KLLM	ERIEAU (AUT)	42.25	-81.90	178.00
613P001	POINT PELEE CS	41.95	-82.52	176.80
6140818	BLUE SPRINGS CREEK	43.63	-80.12	373.40
6140954	BRANTFORD MOE	43.13	-80.23	196.00
6141095	CAMBRIDGE GALT MOE	43.33	-80.32	268.20
6142286	ELORA RCS	43.65	-80.42	376.40
6142400	FERGUS SHAND DAM	43.73	-80.33	417.60
6142627	FULLARTON	43.38	-81.20	335.30
6142803	GLEN ALLAN	43.68	-80.71	400.00
6142991	GRAND VALLEY WPCP	43.88	-80.33	464.80
6143070	GUELPH ARKELL FARM	43.53	-80.18	335.30
6143073	GUELPH EDINBURGH ROAD T	43.52	-80.23	333.80
6143074	GUELPH EDINBURGH ROAD W	43.52	-80.23	333.80
6143075	GUELPH ERAMOSA TWP	43.57	-80.17	349.00
6143087	GUELPH SMALLFIELD FARM	43.53	-80.30	344.40
6143090	GUELPH TURFGRASS CS	43.55	-80.22	325.00
6144240	KITCHENER CITY ENG 1	43.45	-80.48	320.00
6144241	KITCHENER CITY ENG 2	43.45	-80.48	320.00
6144478	LONDON CS	43.03	-81.15	278.00
6145504	MOUNT FOREST (AUT)	43.98	-80.75	414.50
6145516	MOUNTSBERG	43.47	-80.03	304.80

6146714	PRESTON WPCP	43.38	-80.35	272.80
6146745	PROSPECT HILL	43.22	-81.23	312.40
6148105	STRATFORD MOE	43.37	-81.00	345.00
6148212	TAVISTOCK	43.32	-80.83	343.20
6149380	WATERLOO FIRE HALL	43.47	-80.52	317.00
6149387	WATERLOO WELLINGTON A	43.45	-80.38	317.00
6149625	WOODSTOCK	43.14	-80.77	281.90
614B2H4	ELORA ACS	43.65	-80.42	376.40
6150100	ALBION	43.93	-79.83	274.30
6150689	BELLEVILLE	44.15	-77.39	76.20
6150825	BOLTON SPS	43.88	-79.73	213.10
6150830	BOWMANVILLE MOSTERT	43.92	-78.67	99.10
6150863	BRADFORD MUCK RESEARCH	44.03	-79.60	221.00
6151042	BURKETON MCLAUGHLIN	44.03	-78.80	312.40
6151057	BURLINGTON ELIZABETH GDN	43.37	-79.73	83.80
6151059	BURLINGTON FIRE HQ'S	43.35	-79.82	114.30
6151137	CAMPBELLFORD	44.30	-77.80	146.30
61515DE	CLAREMONT FIELD CENTRE	43.95	-79.08	182.90
6151684	COBOURG (AUT)	43.95	-78.17	77.70
6153020	GREENWOOD MTRCA	43.90	-79.07	128.00
6153194	HAMILTON A	43.17	-79.93	237.70

6153301	HAMILTON RBG CS	43.29	-79.91	102.00
6153410	HEART LAKE	43.73	-79.78	259.10
6153545	HORNBY	43.57	-79.85	198.10
6154611	LONG SAULT IHD	44.05	-78.72	342.90
6154820	MAIN DUCK ISLAND	43.93	-76.63	75.00
6154950	MAPLE	43.87	-79.48	244.10
6154990	MARKHAM MTRCA	43.87	-79.28	167.60
6155187	MILTON KELSO	43.50	-79.95	243.80
6155496	MORVEN IHD	44.25	-76.85	106.70
6155619	NEWMARKET WPCP	44.07	-79.43	245.00
6155790	ORANGEVILLE MOE	43.92	-80.09	411.50
6155878	OSHAWA WPCP	43.87	-78.83	83.80
6156518	PICKERING FIRE HALL #5	43.83	-79.08	83.80
6156533	PICTON	44.02	-77.13	76.20
6156559	POINT PETRE (AUT)	43.83	-77.15	78.60
6157015	RICHMOND HILL 2	43.90	-79.40	233.00
6157832	SMITHFIELD CDA ACS	44.08	-77.67	119.00
6158084	STOUFFVILLE WPCP	43.97	-79.25	266.70
6158355	TORONTO CITY	43.67	-79.40	112.50
6158385	TORONTO BERMONDSEY	43.72	-79.32	138.40
61583FL	TORONTO AMESBURY	43.70	-79.48	153.90

6158406	TORONTO BOOTH	43.65	-79.35	77.10
6158418	TORONTO DISCO	43.70	-79.62	160.00
6158443	TORONTO DOWNSVIEW A	43.75	-79.48	198.10
6158520	TORONTO ELLESMERE	43.77	-79.27	164.00
6158525	TORONTO ETOBICOKE	43.63	-79.53	118.90
6158575	TORONTO GREENWOOD	43.67	-79.32	99.10
6158665	TORONTO ISLAND A	43.63	-79.40	76.50
6158712	TORONTO JANE-WILSON	43.72	-79.52	129.50
6158718	TORONTO KEELE-FINCH	43.77	-79.48	199.90
6158732	TORONTO LESLIE EGLINTON	43.72	-79.35	133.30
6158733	TORONTO LESTER B. PEARSON INT'L A	43.68	-79.63	173.40
6158740	TORONTO MET RES STN	43.80	-79.55	193.50
6158748	TORONTO NASHDENE	43.82	-79.25	177.40
6158749	TORONTO NEW INT'L A	43.95	-79.13	262.70
615874R	TORONTO NEW INT'L A 2	43.95	-79.15	245.40
6158764	TORONTO OLD WESTON RD	43.65	-79.47	121.90
61587D9	TORONTO NEW INT'L A 3	43.95	-79.22	260.60
61587P6	TOR SCARBOROUGH COLLEGE	43.78	-79.18	129.50
61587PG	TORONTO SENECA HILL	43.78	-79.35	189.00
6158875	TRENTON A	44.12	-77.53	86.30
6159010	TWEED	44.50	-77.28	144.80

6159127	VALENS	43.38	-80.13	281.90
6159510	WILCOX LAKE	43.95	-79.43	289.60
615HHDF	TORONTO YORK MILLS	43.75	-79.38	153.30
615HMAK	TORONTO BUTTONVILLE A	43.86	-79.37	198.10
615N619	NEWMARKET 2	44.03	-79.40	292.00
615N745	OAKVILLE SOUTHEAST WPCP	43.48	-79.63	86.90
615S001	TORONTO NORTH YORK	43.78	-79.47	187.00
6163171	HALIBURTON 3	45.03	-78.53	330.00
6164432	LINDSAY FILTRATION PLANT	44.35	-78.73	251.50
6166418	PETERBOROUGH A	44.23	-78.37	191.40
6166450	PETERBOROUGH STP	44.28	-78.32	192.00
6166456	PETERBOROUGH TRENT U	44.35	-78.30	216.00
6169453	WEST GUILFORD	45.10	-78.68	327.70
616I001	BANCROFT AUTO	45.07	-77.88	330.70

References

Jan Adamowski, Kaz Adamowski, and John Bougadis. Influence of trend on short duration design storms. *Water Resources Management*, 24:401–413, 2010. ISSN 0920-4741. URL http://dx.doi.org/10.1007/s11269-009-9452-z. 10.1007/s11269-009-9452-z.

Kaz Adamowski and John Bougadis. Detection of trends in annual extreme rainfall. *Hydrological Processes*, 17(18):3547–3560, 2003. ISSN 1099-1085. doi: 10.1002/hyp.1353. URL http://dx.doi.org/10.1002/hyp.1353.

Kaz Adamowski, Younes Alila, and Paul J. Pilon. Regional rainfall distribution for canada. *Atmospheric Research*, 42(1–4):75 – 88, 1996. ISSN 0169-8095. doi: 10.1016/0169-8095(95)00054-2. URL http://www.sciencedirect.com/science/article/pii/0169809595000542.

L. V. Alexander, X. Zhang, T. C. Peterson, J. Caesar, B. Gleason, A. M. G. Klein Tank, M. Haylock, D. Collins, B. Trewin, F. Rahimzadeh, A. Tagipour, K. Rupa Kumar, J. Revadekar, G. Griffiths, L. Vincent, D. B. Stephenson, J. Burn, E. Aguilar, M. Brunet, M. Taylor, M. New, P. Zhai, M. Rusticucci, and J. L. Vazquez-Aguirre. Global observed changes in daily climate extremes of temperature and precipitation. *Journal of Geophysical Research: Atmospheres*, 111:22, 2006. ISSN 2156-2202. doi: 10.1029/2005JD006290. URL http://dx.doi.org/10.1029/2005JD006290.

Giuseppe Aronica, Gabriele Freni, and Elisa Oliveri. Uncertainty analysis of the influence of rainfall time resolution in the modelling of urban drainage systems. *Hydrological Processes*, 19(5):1055–1071, 2005. ISSN 1099-1085. doi: 10.1002/hyp.5645. URL http://dx.doi.org/10.1002/hyp.5645.

Fahim Ashkar and Jean Rousselle. Design discharge as a random variable: A risk study. *Water Resour. Res.*, 17(3):577–591, 1981. doi: 10.1029/WR017i003p00577. URL http://dx.doi.org/10.1029/WR017i003p00577.

Fahim Ashkar and Jean Rousselle. Some remarks on the truncation used in partial flood series models. *Water Resour. Res.*, 19(2):477–480, 1983a. doi: 10.1029/WR019i002p00477. URL http://dx.doi.org/10.1029/WR019i002p00477.

Fahim Ashkar and Jean Rousselle. The effect of certain restrictions imposed on the inter-arrival times of flood events on the poisson distribution used for modeling flood counts. *Water Resour. Res.*, 19(2):481–485, 1983b. doi: 10.1029/WR019i002p00481. URL http://dx.doi.org/10.1029/WR019i002p00481.

Fahim Ashkar and Jean Rousselle. Partial duration series modeling under the assumption of a poissonian flood count. *Journal of Hydrology*, 90(1-2):135 – 144, 1987. ISSN 0022-1694. doi: 10.1016/0022-1694(87)90176-4. URL http://www.sciencedirect.com/science/article/pii/0022169487901764.

Santiago Beguería, Marta Angulo-Martínez, Sergio M. Vicente-Serrano, J. Ignacio López-Moreno, and Ahmed El-Kenawy. Assessing trends in extreme precipitation events intensity and magnitude using non-stationary peaks-over-threshold analysis: a case study in northeast spain from 1930 to 2006. *International Journal of Climatology*, 31(14):2102–2114, 2011. ISSN 1097-0088. doi: 10.1002/joc.2218. URL http://dx.doi.org/10.1002/joc.2218.

Arie Ben-Zvi. Rainfall intensity-duration-frequency relationships derived from large partial duration series. *Journal of Hydrology*, 367(1-2):104 – 114, 2009. ISSN 0022-1694. doi: 10.1016/j.jhydrol.2009.01.007. URL http://www.sciencedirect.com/science/article/pii/S0022169409000122.

G. Blom. *Statistical estimates and transformed beta-variables*. Wiley, New York, 1958. URL http://books.google.ca/books?id=ujAKAQAAIAAJ.

F.P. Brissette, M. Khalili, and R. Leconte. Efficient stochastic generation of multi-site synthetic precipitation data. *Journal of Hydrology*, 345(3–4):121 – 133, 2007. ISSN 0022-1694. doi: http://dx.doi.org/10.1016/j.jhydrol.2007.06.035. URL http://www.sciencedirect.com/science/article/pii/S002216940700385X.

T.A. Buishand. The partial duration series method with a fixed number of peaks. *Journal of Hydrology*, 109(1-2):1–9, 1989. ISSN 0022-1694. doi: 10.1016/0022-1694(89)90002-4. URL http://www.sciencedirect.com/science/article/pii/0022169489900024.

D H Burn and M A Hag Elnur. Detection of hydrologic trends and variability. *Journal of Hydrology*, 255(1-4):107–122, 2002. URL http://linkinghub.elsevier.com/retrieve/pii/S0022169401005145.

Donald H. Burn and Amir Taleghani. Estimates of changes in design rainfall values for canada. *Hydrological Processes*, 27(11):1590–1599, 2013. ISSN 1099-1085. doi: 10.1002/hyp.9238. URL http://dx.doi.org/10.1002/hyp.9238.

David A. Chin. *Water-Resources Engineering*. Pearson Education, 2nd edition, 2006.

V. T. Chow, D.R. Maidment, and L.W. Mays. *Applied Hydrology*. McGraw-Hill Series in Water Resources and Environmental Engineering. McGraw-Hill, 1988. ISBN 9780071001748. URL http://books.google.ca/books?id=cmFuQgAACAAJ.

S. Coles. *An Introduction to Statistical Modeling of Extreme Values*. Springer Series in Statistics. Springer-Verlag, 2001. ISBN 1852334592. URL http://books.google.ca/books?id=2nugUEaKqFEC.

Stuart Coles, Luis Raul Pericchi, and Scott Sisson. A fully probabilistic approach to extreme rainfall modeling. *Journal of Hydrology*, 273(1-4):35 – 50, 2003. ISSN 0022-1694. doi: 10.1016/S0022-1694(02)00353-0. URL http://www.sciencedirect.com/science/article/pii/S0022169402003530.

C. Cunnane. A particular comparison of annual maxima and partial duration series methods of flood frequency prediction. *Journal of Hydrology*, 18(3-4):257 – 271, 1973. ISSN 0022-1694. doi: 10.1016/0022-1694(73)90051-6. URL http://www.sciencedirect.com/science/article/pii/0022169473900516.

C. Cunnane. Unbiased plotting positions - a review. *Journal of Hydrology*, 37(3-4):205 – 222, 1978. ISSN 0022-1694. doi: 10.1016/0022-1694(78)90017-3. URL http://www.sciencedirect.com/science/article/pii/0022169478900173.

C. Cunnane. A note on the poisson assumption in partial duration series models. *Water Resour. Res.*, 15(2):489–494, 1979. doi: 10.1029/WR015i002p00489. URL http://dx.doi.org/10.1029/WR015i002p00489.

E.M. Douglas, R.M. Vogel, and C.N. Kroll. Trends in floods and low flows in the united states: impact of spatial correlation. *Journal of Hydrology*, 240(1-2):90 – 105, 2000. ISSN 0022-1694. doi: 10.1016/S0022-1694(00)00336-X. URL http://www.sciencedirect.com/science/article/pii/S002216940000336X.

B. Efron. Bootstrap methods: Another look at the jackknife. *The Annals of Statistics*, 7 (1):pp. 1–26, 1979. ISSN 00905364. URL http://www.jstor.org/stable/2958830.

Heinz D. Fill and Jery R. Stedinger. L moment and probability plot correlation coefficient goodness-of-fit tests for the gumbel distribution and impact of autocorrelation. *Water Resour. Res.*, 31(1):225–229, 1995. doi: 10.1029/94WR02538. URL http://dx.doi.org/10.1029/94WR02538.

James J. Filliben. The probability plot correlation coefficient test for normality. *Technometrics*, 17(1):111–117, 02 1975. URL http://www.jstor.org/stable/1268008.

H. J. Fowler and C. G. Kilsby. A regional frequency analysis of united kingdom extreme rainfall from 1961 to 2000. *International Journal of Climatology*, 23(11):1313–1334, 2003. ISSN 1097-0088. doi: 10.1002/joc.943. URL http://dx.doi.org/10.1002/joc.943.

Christoph Frei, Regina Scholl, Sophie Fukutome, Jurg Schmidli, and Pier Luigi Vidale. Future change of precipitation extremes in europe: Intercomparison of scenarios from regional climate models. *J. Geophys. Res.*, 111(D6), 03 2006. doi: 10.1029/2005JD005965. URL http://dx.doi.org/10.1029/2005JD005965.

P. Frich, L.V. Alexander, P. Della-Marta, B.Gleason, M. Haylock, A. M. G. Klein Tank, and T. Peterson. Observed coherent changes in climatic extremes during the second half of the twentieth century. *Climate Research*, 19:193–212, January 2002.

J. M. García-Ruiz, J. Arnáez, S. M. White, A. Lorente, and S. Beguería. Uncertainty assessment in the prediction of extreme rainfall events: an example from the central spanish pyrenees. *Hydrological Processes*, 14(5):887–898, 2000. ISSN 1099-1085. doi: 10.1002/(SICI)1099-1085(20000415)14:5⟨887::AID-HYP976⟩3.0.CO;2-0. URL http://dx.doi.org/10.1002/(SICI)1099-1085(20000415)14:5<887::AID-HYP976>3.0.CO;2-0.

L. Gerold and D. Watkins. Short duration rainfall frequency analysis in michigan using scale-invariance assumptions. *Journal of Hydrologic Engineering*, 10(6):450–457, 2005. doi: 10.1061/(ASCE)1084-0699(2005)10:6(450). URL http://ascelibrary.org/doi/abs/10.1061/%28ASCE%291084-0699%282005%2910%3A6%28450%29.

B.E. Goodison and P.Y.T. Louie. Canadian methods for precipitation measurement and correction. In *Proc. International Workshop of Correction of Precipitation Measurements*, pages 141–145, Zürich, Switzerland, 1986.

Irving I. Gringorten. A plotting rule for extreme probability paper. *J. Geophys. Res.*, 68(3):813–814, 1963. doi: 10.1029/JZ068i003p00813. URL http://dx.doi.org/10.1029/JZ068i003p00813.

Pavel Ya. Groisman, Thomas R. Karl, David R. Easterling, Richard W. Knight, Paul F. Jamason, Kevin J. Hennessy, Ramasamy Suppiah, Cher M. Page, Joanna Wibig, Krzysztof Fortuniak, Vyacheslav N. Razuvaev, Arthur Douglas, Eirik Førland, and Pan-Mao Zhai. Changes in the probability of heavy precipitation: Important indicators of climatic change. *Climatic Change*, 42(1):243–283, 1999. doi: 10.1023/A:1005432803188. URL http://dx.doi.org/10.1023/A:1005432803188.

PavelYa. Groisman and DavidR. Legates. Documenting and detecting long-term precipitation trends: Where we are and what should be done. *Climatic Change*, 31

(2-4):601–622, 1995. ISSN 0165-0009. doi: 10.1007/BF01095163. URL http://dx.doi.org/10.1007/BF01095163.

F. Kenneth Hare and Morley K. Thomas. *Climate Canada*. John Wiley and Sons, Ltd., Toronto, Canada, 2nd edition, 1979.

W. D. Hogg, D.A. Carr, and B. Routledge. *Rainfall Intensity-Duration Frequency Values for Canadian Locations*. Environment Canada, Atmospheric Environment Service, 1989.

J. R. M. Hosking. *Regional frequency analysis using L-moments*, 2012. URL http://CRAN.R-project.org/package=lmomRFA. R package, version 2.4.

J. R. M. Hosking. *Regional frequency analysis using L-moments*, 2013. URL http://CRAN.R-project.org/package=lmomRFA. R package, version 2.5.

J. R. M. Hosking and J. R. Wallis. Parameter and quantile estimation for the generalized pareto distribution. *Technometrics*, 29(3):pp. 339–349, 1987. ISSN 00401706. URL http://www.jstor.org/stable/1269343.

J. R. M. Hosking, J. R. Wallis, and E. F. Wood. Estimation of the generalized extreme-value distribution by the method of probability-weighted moments. *Technometrics*, 27 (3):pp. 251–261, 1985. ISSN 00401706. URL http://www.jstor.org/stable/1269706.

J.R.M. Hosking and J.R. Wallis. *Regional Frequency Analysis: An Approach Based on L-Moments*. Cambridge University Press, 1997. ISBN 9780521019408. URL http://books.google.ca/books?id=gurAnfB4nvUC.

IPCC. *Climate Change 2013: The Physical Science Basis. Contribution of Working Group I to the Fifth Assessment Report of the Intergovernmental Panel on Climate Change*. Cambridge University Press, Cambridge, United Kingdom and New York, NY, USA, 2013.

Thomas R. Karl, Robert G. Quayle, and Pavel Ya Groisman. Detecting climate variations and change: New challenges for observing and data management systems. *Journal of Climate*, 6(8):1481–1494, 1993. doi: 10.1175/1520-0442(1993)006⟨1481:DCVACN⟩2.0.CO;2. URL http://dx.doi.org/10.1175/1520-0442(1993)006<1481:DCVACN>2.0.CO;2.

ThomasR. Karl, VernonE. Derr, DavidR. Easterling, ChrisK. Folland, DavidJ. Hofmann, Sydney Levitus, Neville Nicholls, DavidE. Parker, and GregoryW. Withee. Critical issues for long-term climate monitoring. *Climatic Change*, 31(2-4):185–221, 1995. ISSN 0165-0009. doi: 10.1007/BF01095146. URL http://dx.doi.org/10.1007/BF01095146.

M. L. Kavvas. Stochastic trigger model for flood peaks: 1. development of the model. *Water Resources Research*, 18(2):383–398, 1982. ISSN 1944-7973. doi: 10.1029/WR018i002p00383. URL http://dx.doi.org/10.1029/WR018i002p00383.

M.G. Kendall. *Rank correlation methods*. Charles. Griffin, London, 3 edition, 1978. URL http://books.google.ca/books?id=hiBMAAAAMAAJ.

E. M. Laurenson. Back to basics on flood frequency analysis. *Transactions of the Institution of Engineers, Australia Civil Engineering*, 29(2):47–53, 1987.

H. Madsen, D. Rosbjerg, and P. Harremoes. Pds-modelling and regional bayesian estimation of extreme rainfalls. *Nordic Hydrology*, 25(4):279–300, 1994. URL http://search.proquest.com/docview/16828115?accountid=11233.

H. Madsen, D. Rosbjerg, and P. Harremoöes. Application of the bayesian approach in regional analysis of extreme rainfalls. *Stochastic Hydrology and Hydraulics*, 9:77–88, 1995. ISSN 0931-1955. doi: 10.1007/BF01581759. URL http://dx.doi.org/10.1007/BF01581759.

H. Madsen, P.S. Mikkelsen, D. Rosbjerg, and P. Harremoës. Estimation of regional intensity-duration-frequency curves for extreme precipitation. *Water Science and Technology*, 37(11):29 – 36, 1998. ISSN 0273-1223. doi: 10.1016/S0273-1223(98)00313-8. URL http://www.sciencedirect.com/science/article/pii/S0273122398003138.

Henrik Madsen, Peter F. Rasmussen, and Dan Rosbjerg. Comparison of annual maximum series and partial duration series methods for modeling extreme hydrologic events: 1. at-site modeling. *Water Resour. Res.*, 33(4):747–757, 1997. doi: 10.1029/96WR03848. URL http://dx.doi.org/10.1029/96WR03848.

Henrik Madsen, Peter Steen Mikkelsen, Dan Rosbjerg, and Poul Harremoës. Regional estimation of rainfall intensity-duration-frequency curves using generalized least squares regression of partial duration series statistics. *Water Resources Research*, 38(11):21–1–21–11, 2002. ISSN 1944-7973. doi: 10.1029/2001WR001125. URL http://dx.doi.org/10.1029/2001WR001125.

Alain Mailhot, Sophie Duchesne, Daniel Caya, and Guillaume Talbot. Assessment of future change in intensity-duration-frequency (idf) curves for southern quebec using the canadian regional climate model (crcm). *Journal of Hydrology*, 347(1-2):197 – 210, 2007. ISSN 0022-1694. doi: 10.1016/j.jhydrol.2007.09.019. URL http://www.sciencedirect.com/science/article/pii/S0022169407005045.

Alain Mailhot, Ahmadi Kingumbi, Guillaume Talbot, and Audrey Poulin. Future changes in intensity and seasonal pattern of occurrence of daily and multi-day annual maximum

precipitation over canada. *Journal of Hydrology*, 388(3-4):173 – 185, 2010. ISSN 0022-1694. doi: 10.1016/j.jhydrol.2010.04.038. URL http://www.sciencedirect.com/science/article/pii/S0022169410002374.

Lasse Makkonen. Plotting positions in extreme value analysis. *Journal of Applied Meteorology and Climatology*, 45(2):334–340, 2006. doi: 10.1175/JAM2349.1. URL http://dx.doi.org/10.1175/JAM2349.1.

Henry B. Mann. Nonparametric tests against trend. *Econometrica*, 13(3):245–259, 07 1945. URL http://www.jstor.org/stable/1907187.

A. I. McLeod. *Kendall: Kendall rank correlation and Mann-Kendall trend test*, 2011. URL http://CRAN.R-project.org/package=Kendall. R package version 2.2.

E. Mekis and W. D. Hogg. Rehabilitation and analysis of canadian daily precipitation time series. *ATMOSPHERE-OCEAN*, 37(1):53–85, 1999. URL http://www.atmos-chem-phys.net/6/5261/2006/acp-6-5261-2006.pdf.

B. Mladjic, L. Sushama, M. N. Khaliq, R. Laprise, D. Caya, and R. Roy. Canadian rcm projected changes to extreme precipitation characteristics over canada. *Journal of Climate*, 24(10):2565 – 2584, 2011. ISSN 08948755.

Cosmo Ngongondo, Chong-Yu Xu, Lena Tallaksen, Berhanu Alemaw, and Tobias Chirwa. Regional frequency analysis of rainfall extremes in southern malawi using the index rainfall and l-moments approaches. *Stochastic Environmental Research and Risk Assessment*, 25:939–955, 2011. ISSN 1436-3240. URL http://dx.doi.org/10.1007/s00477-011-0480-x. 10.1007/s00477-011-0480-x.

R Core Team. *R: A Language and Environment for Statistical Computing*. R Foundation for Statistical Computing, Vienna, Austria, 2013. URL http://www.R-project.org/.

W. Rauch and S. de Toffol. On the issue of trend and noise in the estimation of extreme rainfall properties. *Water Science and Technology*, 54(6/7):17 – 24, 2006. ISSN 02731223.

Dan Rosbjerg. Estimation in partial duration series with independent and dependent peak values. *Journal of Hydrology*, 76(1-2):183 – 195, 1985. ISSN 0022-1694. doi: 10.1016/0022-1694(85)90098-8. URL http://www.sciencedirect.com/science/article/pii/0022169485900988.

Dan Rosbjerg and Henrik Madsen. The role of regional information in estimation of extreme point rainfalls. *Atmospheric Research*, 42(1-4):113 – 122, 1996. ISSN 0169-8095. doi: 10.1016/0169-8095(95)00057-7. URL http://www.sciencedirect.com/science/article/pii/0169809595000577. ¡ce:title¿Closing the gap between theory and practice in urban rainfall applications¡/ce:title¿.

Annette Semadeni-Davies, Claes Hernebring, Gilbert Svensson, and Lars-Goran Gustafsson. The impacts of climate change and urbanisation on drainage in helsingborg, sweden: Combined sewer system. *Journal of Hydrology*, 350(1-2):100 – 113, 2008. ISSN 0022-1694. doi: 10.1016/j.jhydrol.2007.05.028. URL http://www.sciencedirect.com/science/article/pii/S0022169407002910.

J. R. Stedinger, R. M. Vogel, E. Foufoula-Georgiou, and D. R. Maidment. *Frequency analysis of extreme events*. McGraw-Hill, 1993.

Daithi A. Stone, Andrew J. Weaver, and Francis W. Zwiers. Trends in canadian precipitation intensity. *Atmosphere-Ocean*, 38(2):321–347, 2000. doi: 10.1080/07055900.2000.9649651. URL http://www.tandfonline.com/doi/abs/10.1080/07055900.2000.9649651.

O. Sveinsson, J. Salas, and D. Boes. Regional frequency analysis of extreme precipitation in northeastern colorado and fort collins flood of 1997. *Journal of Hydrologic Engineering*, 7(1):49–63, 2002. doi: 10.1061/(ASCE)1084-0699(2002)7:1(49). URL http://dx.doi.org/10.1061/(ASCE)1084-0699(2002)7:1(49).

L.Valadares Tavares and J.Evaristo Da Silva. Partial duration series method revisited. *Journal of Hydrology*, 64(1-4):1–14, 1983. ISSN 0022-1694. doi: 10.1016/0022-1694(83)90056-2. URL http://www.sciencedirect.com/science/article/pii/0022169483900562.

P. Todorovic and J. Rousselle. Some problems of flood analysis. *Water Resour. Res.*, 7(5):1144–1150, 1971. doi: 10.1029/WR007i005p01144. URL http://dx.doi.org/10.1029/WR007i005p01144.

P. Todorovic and E. Zelenhasic. A stochastic model for flood analysis. *Water Resour. Res.*, 6(6):1641–1648, 1970. doi: 10.1029/WR006i006p01641. URL http://dx.doi.org/10.1029/WR006i006p01641.

Christopher M. Trefry, David W. Watkins, and Dennis Johnson. Regional rainfall frequency analysis for the state of michigan. *Journal of Hydrologic Engineering*, 10(6):437–449, 2005.

B. Vasiljevic, E. McBean, and B. Gharabaghi. Trends in rainfall intensity for stormwater designs in ontario. *Journal of Water and Climate Change*, 3(1):1–10, 2012.

Lucie A. Vincent and Éva Mekis. Changes in daily and extreme temperature and precipitation indices for canada over the twentieth century. *Atmosphere-Ocean*, 44(2):177–193, 2006. doi: 10.3137/ao.440205. URL http://www.tandfonline.com/doi/abs/10.3137/ao.440205.

Q.J. Wang. The pot model described by the generalized pareto distribution with poisson arrival rate. *Journal of Hydrology*, 129(1-4):263–280, 1991. ISSN 0022-1694. doi: 10.1016/0022-1694(91)90054-L. URL http://www.sciencedirect.com/science/article/pii/002216949190054L.

Yi Wang and E. McBean. Performance comparisons of partial duration and annual maxima series models for rainfall frequency analyses of selected rain gauge records ontario, canada. *Hydrology Research*, 2013.

Yi Wang, E. McBean, and Philip Jarrett. Improving the efficiency of quantile estimates to identify changes in heavy rainfall events. *Canadian Journal of Civil Engineering*, 2013.

WMO. Guidelines on analysis of extremes in a changing climate in support of informed decisions for adaptation. Technical report, Geneva, 2009.

V.M. Yevjevich. *Probability and statistics in hydrology*. Water Resources Publications, Fort Collions, Colorado, 1972. URL http://books.google.ca/books?id=_fFOAAAAMAAJ.

Panmao Zhai, Anjian Sun, Fumin Ren, Xiaonin Liu, Bo Gao, and Qiang Zhang. Changes of climate extremes in china. *Climatic Change*, 42:203–218, 1999. ISSN 0165-0009. URL http://dx.doi.org/10.1023/A:1005428602279. 10.1023/A:1005428602279.

Xuebin Zhang, W. D. Hogg, and Éva Mekis. Spatial and temporal characteristics of heavy precipitation events over canada. *Journal of Climate*, 14(9):1923–1936, 2001. doi: 10.1175/1520-0442(2001)014⟨1923:SATCOH⟩2.0.CO;2. URL http://dx.doi.org/10.1175/1520-0442(2001)014<1923:SATCOH>2.0.CO;2.